# SURFACE PROPERTIES OF POLY(ε-CAPROLACTONE) - POLY(DIMETHYLSILOXANE) - POLY(ε-CAPROLACTONE) TRIBLOCK COPOLYMERS

by

Şehri Banu (Boz) Yaşar

B.S. in Ch.E., Boğaziçi University, 1994

Submitted to the Institute for Graduate Studies in Science and Engineering in partial fulfillment of the requirements for the degree of Master of Science

in

Chemical Engineering

# ACKNOWLEDGEMENTS

I would like to express my deep appreciation to my thesis supervisor, Prof. Dr. Bahattin Baysal for his invaluable supervision, guidance and encouragement through out this work.

I am also grateful to Ass. Prof. Yıldırım Erbil for his kind help, interest and especially his constructive suggestions throughout the work.

I wish to thank to Prof. Dr. Şefik Süzer for his help in ESCA studies.

Special thanks are due to Ass. Prof. Mehmet Çamurdan and Ass. Prof. Turgut Nugay for the time they devoted to reading and commenting on my thesis.

I wish to thank all my friends in Chemical Engineering Department, especially, Saybil Ercan and my friends in Tübitak Marmara Research Center, especially, Okşan Karal and Nilhan Kayaman for their encouragement and support throughout my thesis.

Financial support of Boğaziçi University Research Fund (Project No: 95A05351) is gratefully appreciated.

Finally, I am also deeply indebted to my husband, Hakan Yaşar and my family for their confidence, patience and support. Therefore I dedicated my thesis to them.

# ABSTRACT

Surface properties of polymers are of very much importance in many application fields such as adhesion, wettability, coating, printing and biocompatibility. In this industrial areas polydimethylsiloxanes are materials of broad applicability because of their well-known surface modifying properties. In this work, the surfaces of two grades of commercial triblock polycaprolactone-polydimethylsiloxane- polycaprolactone (PCL-PDMS-PCL) copolymers differing only in the molecular weights of PCL end-blocks and homopolymer polycaprolactone were characterized by contact angle measurements and by Electron Spectroscopy for Chemical Analysis (ESCA) technique.

Contact angle measurements give information about the surface energetics on the gross structure of the immediate outer boundary of a polymer. Measurements were made with different polar liquids, and with apolar liquid paraffin. Measurements according to the two-liquid method (a three phase system of two immiscible liquids and a solid surface) were also made. Contact angles of water, formamide, ethylene glycol, glycerol drops in paraffin bulk phase and contact angles of paraffin drop in water, formamide, ethyleneglycol, glycerol bulk phases were determined. Surface energy parameters of the polymers were calculated using different approaches.

Drop size and time dependence of contact angles of liquid drops on polymer samples and the effect of evaporation on time dependence of contact angles were investigated.

Surface enrichment of the copolymers by PDMS segments was also shown quantitatively from the evaluation of relative binding energies and peak areas of ESCA spectra.

# ÖZET

Polimerlerin yüzey özellikleri, yapışma, ıslanabilme, kaplama, baskı ve biyolojik uyumluluk gibi birçok uygulama alanında önem taşır. Bu endüstriyel uygulamalarda polidimetilsiloksanlar, iyi bilinen yüzey değiştirici özellikleri nedeniyle geniş ölçüde kullanılan materyal olarak bilinir. Bu çalışmada, polikaprolakton son bloklarının molekül ağırlığı farklı olan iki çeşit ticari üç bloklu polikaprolakton-polidimetilsiloksan-polikaprolakton kopolimerleri ile saf polikaprolaktonun yüzeyleri, değme açısı ölçümleri ve kimyasal analiz için elektron spektroskopisi (ESCA) teknikleri ile karakterize edilmiştir.

Değme açısı ölçümleri, bir polimerin en dış yüzey yapısı üstündeki yüzey enerjileri hakkında bilgi verir. Bu çalışmada, ölçümler çeşitli polar sıvılar ve polar olmayan sıvı parafin ile yapıldı. Ayrıca, iki sıvı yöntemi (birbirine karışmayan iki sıvı ve bir yüzeyin üçlü sistemi) ile de ölçüm yapıldı. Su, formamid, etilenglikol, gliserin damlalarının parafin fazı içindeki değme açıları ve parafin damlasının su, formamid, etilenglikol, gliserin fazları içindeki değme açıları belirlendi. Polimerlerin yüzey enerji parametreleri farklı yaklaşımlar kullanarak hesaplandı.

Polimer örnekleri üzerindeki sıvı damlalarının değme açılarının damla büyüklüğü ve zamana bağlı olarak değişmesi, ayrıca buharlaşmanın değme açıları üzerindeki etkisi araştırıldı.

Kopolimerlerdeki polidimetilsiloksan segmanlarının yüzeyde toplanması, ESCA spektralarının bağıl bağlanma enerjilerinin ve tepe alanlarının belirlenmesi ile nicel olarak kanıtlanmıştır.

# TABLE OF CONTENTS

# LIST OF FIGURES

# LIST OF TABLES

# LIST OF SYMBOLS

| | |
|---|---|
| a | Capillarity constant |
| A | Area |
| b | Radius of curvature |
| BE | Binding energy |
| d | Thickness of surface layer |
| E | Energy gained |
| f | Converting factor |
| $f_i$ | Fraction of surface |
| F | Free energy |
| g | Acceleration due to gravity |
| h | height |
| hv | Photon energy |
| I | Intensity |
| $I^n$ | Dispersive interaction component of surface tension |

| | |
|---|---|
| KE | Kinetic energy |
| Kgs | Geodesic curvature of three phase contact line |
| L | Length of triple junction |
| n | Number of bonds per unit area |
| p | Perimeter |
| r | Radius |
| S | Solid phase |
| T | Temperature |
| V | Volume |
| W | Weight |
| WA | Work of adhesion |
| $\Delta G$ | Change in surface free energy |
| $\Delta H$ | Enthalpy of interaction |
| $\Delta P$ | Pressure difference |
| $\gamma$ | Surface tension |
| $\rho$ | Density |

| | |
|---|---|
| $\theta$ | Contact angle |
| $\Lambda$ | Escape depth of photoemitted electron |
| $\phi$ | Correction parameter |

Superscripts

| | |
|---|---|
| AB | Acid-base interactions |
| d | London dispersion force |
| h | Hydrogen bonding |
| I | Debye induction force |
| LW | Liftshitz-van der Waals forces |
| n | Nondispersion forces |
| p | Keasom dipole-dipole force |

# 1. INTRODUCTION

The interaction of a polymer with its surroundings occurs at the surface. Therefore, many properties of a polymer are determined by the composition and structure of its surface. Surface properties of solid polymers are of very much importance in many application fields such as adhesion, corrosion, wettability, printing, friction and wear, biocompatibility and many others. In most of the cases, they are controlled by the overlayer materials on surfaces. [1,2]

Surfaces of polymer solids are decidedly different from those of more rigid materials such as metals and ceramics, because polymer molecules have much greater freedom for rearrangement in the bulk and at the surface, therefore, they may orient themselves differently at the surface than in the bulk. Accordingly, the surface properties of a polymer may not be the same as the properties of the solid in the bulk. [3,4]

A desired polymer surface sometimes cannot be obtained from the material itself but through modification. Modification of a polymer surface can be achieved by means of various chemical or physical processes. The most common surface modification techniques include plasma treatment, surface grafting and chemical reaction.

Polysiloxanes, especially, polydimethylsiloxanes (PDMS) are materials of broad applicability in a variety of industrial areas because of their well-known surface-modifying properties. Due to their very large molar volumes combined with the very low cohesive energy densities (intermolecular interactions) and high flexibilities, polydimethylsiloxanes have extremely low surface tension and

surface energies which is around 16-22 dynes/cm changing according to the MW of PDMS. This value is at least 10 dynes/cm lower than that of many other polymers. Hydrophobicity (water repellancy), biocompatibility, high gas permeability, surface activity, excellent atomic oxygen and oxygen plasma resistance, very high chain flexibility are the unique combination of properties of polydimethylsiloxanes which are not shown by any other polymeric material. Some of the most interesting properties of polydimethylsiloxanes are associated with their surface activity and related surface properties, therefore they are very attractive materials for modification of other surfaces and interfaces. However, their low solubility parameters cause it to be highly immiscible with most other materials. Therefore, PDMS has in practice only little use for surface modification by blending, since it tends to be rejected from the matrix. Also pure polydimethylsiloxanes are mechanically too weak to be used directly as a polymer and they show cold flow even at very high molecular weights. An effective way to overcome these difficulties and to increase the compatibility of PDMS in blends is to form multiphase, block, segmented or graft copolymers of siloxanes with carbon based polymers. [5-7]

Surface modification of conventional polymers through the addition of small amounts of siloxane containing copolymers was first in 1960's. In polymer modification through blending, siloxane containing copolymers have been shown to be particularly useful when compared with siloxane homopolymers. The organic component of the siloxane containing copolymers is usually chosen to be compatible with the base polymer in order to provide specific interactions to the system to obtain permanent surface modification.

In multicomponent polymer systems, copolymers and polymer blends, the surface composition may differ greatly from the composition in the bulk since components of lower surface energy

always tend to enrich the surface to minimize the free energy of the system. The surface segregation occurs at very low concentrations which allows an efficient modification of the surface sensitive properties to be accomplished without significant change in the bulk properties.

As a result of low surface tension and surface energies of polydimethylsiloxanes, the air-polymer surfaces of siloxane containing copolymers, as well as their blends with other polymers are substantially enriched in the lower surface energy siloxane. The thermodynamic driving force behind this process is the minimization of the interfacial and surface energy. It is known that surface and interfacial tensions vary with both temperature and molecular weight of the active component and probably to some extent with the copolymer architecture. [8-17]

The surface free energy of solids is a characteristic parameter that determines most of the surface properties such as adsorption, wetting, adhesion etc. This characteristic of solid cannot be measured directly because of elastic and viscous restraints of bulk phase, which necessitate indirect methods.

The present study is related to the surface characterization of polycaprolactone (PCL) homopolymer in comparison with the two grades of triblock PDMS copolymer with polycaprolactone (PCL) ends differing only in the molecular lengths of the PCL end blocks. The aim of this work is to examine that the air-polymer surface of PCL-PDMS-PCL triblock copolymers are enriched in the lower surface energy siloxane by means of contact angle measurements and Electron Spectroscopy for Chemical Analysis (ESCA) technique. At the same time surface tensions of the copolymers were reported by measurements of contact angles of different liquids.

On the other hand, time and drop size dependency of the contact angles were investigated. The effect of evaporation on time dependence of contact angles of water on polycaprolactone was also studied.

# 2. SURFACE CHARACTERISTICS TERMS

## 2.1. Indirect Methods Measuring the Surface Tension

The term, surface free energy implies only that work is required to form more surface i.e. to bring molecules from the interior of the phase into the surface region. Classically, the surface energy of a solid is defined as half the energy required to separate unit area of two adjacent atomic planes and separate them to infinity in a vacuum. This definition, of course, assumes perfectly elastic behavior, thermodynamic equilibrium and the absence of any atmosphere. [18]

The surface free energy of solids is a characteristic parameter that determines most of the surface properties such as adsorption, wetting, adhesion etc. This characteristic of solid cannot be measured directly because of elastic and viscous restraints of bulk phase, which necessitate indirect methods.

The terms surface tension or surface free energy are fundamental concepts which are usually used interchangeably. The term surface tension is the earlier of the two, it goes back to early ideas that the surface of a liquid had some kind of contractile skin. More subtly, it can convey the erroneous impression that extending a liquid surface somehow stretches the molecules in it.

### 2.1.1. Capillary Rise Method

If the liquid wets the wall of the capillary, the liquid surface is thereby constrained to lie parallel with the wall and the complete surface must therefore be concave in shape. The pressure difference across the interface is related to the surface tension as follows:

$$\Delta P = 2\gamma / r \qquad (2.1)$$

where $\gamma$ is the surface tension of the liquid and r is the radius of the capillarity. The pressure difference is also given by:

$$\Delta P = \Delta\rho g h \qquad (2.2)$$

where $\Delta\rho$ denotes the difference in density between the liquid and gas phase, g is the acceleration due to gravity, h is the height of the meniscus. (liquid meets the circularly cylindrical capillary wall at some angle $\theta$)

$$\Delta\rho g h = 2\gamma \cos\theta / r \qquad (2.3)$$

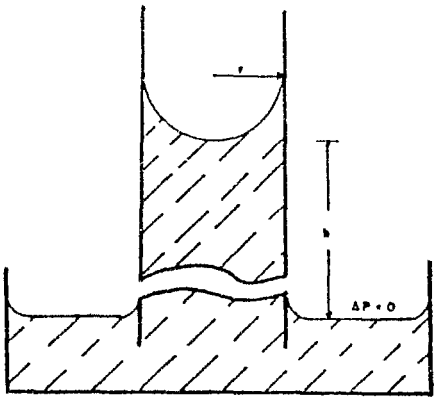


FIGURE 2.1. Capillary rise (capillary much magnified wrt. dish) [18]

It is considered to be the one of the best and most accurate absolute methods. On the other hand, as zero contact angle is needed for practical reasons fairly large volume of liquids are needed.

### 2.1.2. The Maximum Bubble Pressure Method

The procedure is to blow slowly bubbles of an inert gas in the liquid by means of an tube projecting below the surface. The equation for capillary rise method is used to find surface tension.

As it does not depend on contact angle, it is easy to handle and can be used to measure surface tensions of not easily accessible liquids such as molten metals.

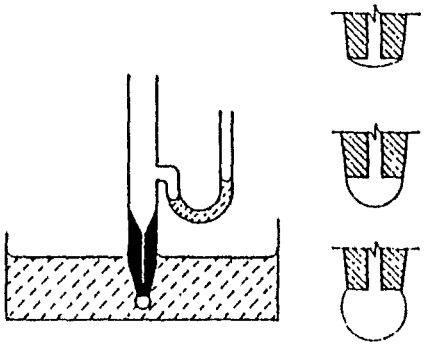

FIGURE 2.2. Maximum Bubble Pressure Method [18]

### 2.1.3. The Drop Weight Method

This is a fairly accurate method and perhaps the most convenient laboratory one for measuring the surface tension of a liquid-air or a liquid- liquid interface. The procedure is to form drops of the liquid at the end of a tube, allowing them to fall into a container until enough have been collected so that the weight per drop can be determined accurately.

$$W = 2\pi r\gamma \qquad (2.4)$$

Equation can be considered as the maximum force available to support the weight of the drop is given by the surface tension per centimeter times the circumference of the tip. Empirical correction factors are needed for weight.

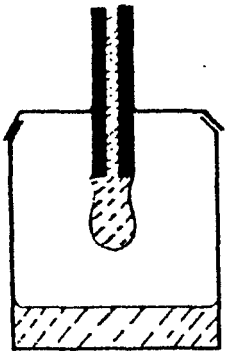

FIGURE 2.3. Drop Weight Method (drop and tip enlarged) [18]

### 2.1.4. The Ring Method

A method that has been widely used involves the determination of the force to detach a ring or loop of wire from the surface of a liquid. Empirical correction factors are needed.

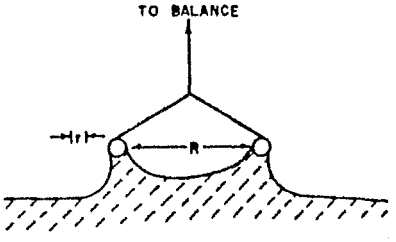


FIGURE 2.4. Ring Method [18]

$$W_{tot} = W_{ring} + 4\pi R\gamma \qquad (2.5)$$

### 2.1.5. Wilhelmy Slide Method.

The basic observation is that a thin plate, such as a microscope cover glass or piece of a platinum foil, will support a meniscus whose weight is measured either statically or by detachment is given very accurately by the ideal equation (assuming zero contact angle)

$$W_{tot} = W_{plate} + \gamma_p \qquad (2.6)$$

where p is perimeter.

Another procedure is to suspend the plate so that it is partly immersed and to determine from the dry and immersed weights the meniscus weight and hence surface tension. A general equation is:

$$\gamma Cos\theta = \frac{W_{tot} - (W_{plate} - b)}{P} \qquad (2.7)$$

Where $W_{tot}$ is the weight of the plate as partially immersed.
$W_{plate}$ is the weight of the plate suspended in the vapor phase.
b is the buoyancy correction for the immersed portion.

This method does not require any correction factor.

The experimental arrangement is shown below.

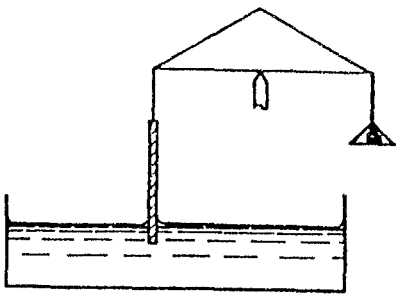

FIGURE 2.5. Wilhelmy Slide Method [18]

## 2.2. METHODS BASED ON THE SHAPE OF STATIC DROPS OR BUBBLES

Small drops of bubbles will tend to be spherical because surface forces depend on the area, which decreases as the square of the linear dimension, where as distortions due to gravitational effects depend on the volume, which decreases as the cube of linear dimension. Likewise, a drop of liquid in a second liquid of equal density will be spherical. However, when gravitational and surface tensional effects are comparable, then one can determine in principle the surface tension from measurements of the shape of the drop or bubble. Certain measurements of dimensions can be made from a taken photograph.

### 2.2.1. Sessile Drop (or Bubble) Method

Sessile drops are symmetrical as shown in the figure below:

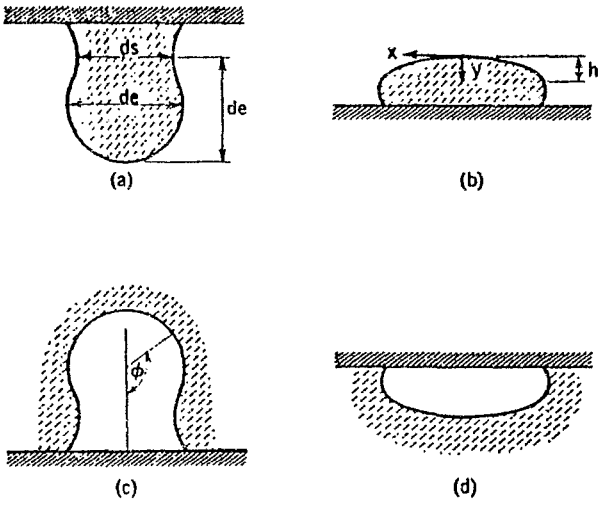


FIGURE 2.6. Shapes of sessile and hanging drops and bubbles: (a) hanging drop, (b) sessile drop, (c) hanging bubble, (d) sessile bubble

The equation of surface tension is:

$$\gamma = \Delta\rho g h^2 / 2 \qquad (2.8)$$

where h denotes the distance from the apex to the equatorial plane. The equation is independent of contact angle. The method is suitable for the observation of long-term changes in surface tension with time.

### 2.2.2. Pendant Drop Method

A drop hanging from a tip (or a clinging bubble) elongates as it grows longer because the variation in hydrostatic pressure $\Delta P$ eventually becomes appreciable in comparison with that given by curvature at the apex.

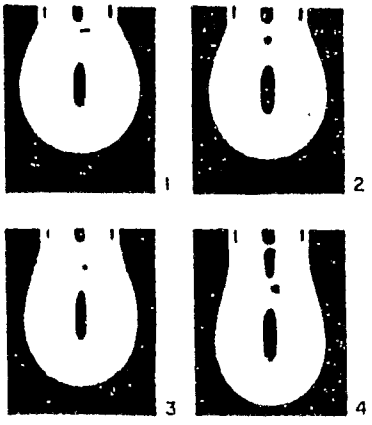


FIGURE 2.7. Shapes of pendant drops [18]

$$\gamma = -\Delta\rho g b^2 / \beta \tag{2.9}$$

where

$$\beta = 2b^2 / a^2 \tag{2.10}$$

b is radius of curvature, a is capillary constant ($a^2$=bh)

This method is very widely used, requires only small quantities of liquid and applicable to the experimentally difficult situation of measurements at high temperature or with reactive materials.

# 3. SOLID-LIQUID INTERFACE

A solid deforms in response to applied forces in an elastic manner and its shape will be determined more by its past history than by surface tensional forces. Surface atoms of solids are relatively immobile, although vibrating about equilibrium or quasi equilibrium positions, the surface is highly conditioned by its past history and cannot be studied by the usual methods of capillarity.

Solids at temperature near their melting points show surface mobility, in the form of traffic with the vapor phase and with the interior. Unlike the situation with liquids, in the case of a solid, the surface tension is not necessarily equal to the surface stress. Surface tension or surface free energy is the work spent in forming unit area of surface. Surface stress is the work spent in stretching the surface.

## 3.1.Contact Angle Phenomena

It is observed that in most instances a liquid placed on a solid will not wet it but remains as a drop having a definite angle of contact between the liquid and solid phases. The situation is illustrated in the following figure.

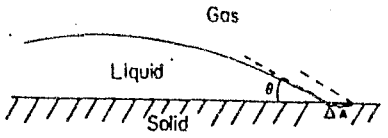


FIGURE 3.1 Contact Angle [18]

The change in surface free energy $\Delta G^s$, accompanying a small displacement of the liquid such that the change in area of solid covered $\Delta A$ is:

$$\Delta G^S = \Delta A(\gamma_{SL} - \gamma_{SV}) + \Delta A \gamma_{SL} \cos(\theta - \Delta\theta) \tag{3.1}$$

At equilibrium

$$\lim_{\Delta A \to 0} \Delta G^S / \Delta A = 0 \tag{3.2}$$

$$\gamma_{SL} - \gamma_{SV} + \gamma_{LV} \cos\theta = 0 \tag{3.3}$$

or

$$\gamma_{LV} \cos\theta = \gamma_{SV} - \gamma_{SL} \tag{3.4}$$

Work of adhesion, $W_{AB}$, between two phases A and B is given by

$$W_{AB} = \gamma_A + \gamma_B - \gamma_{AB} \tag{3.5}$$

By combination

$$W_{SLV} = \gamma_{LV}(1+\cos\theta) \tag{3.6}$$

Equation (3.4) was stated in qualitative form by Young [19] in 1805 and the equivalent equation, equation (3.6) was stated in more definite form by Dupre [20] in 1869 along with the definition of work of adhesion.

It is important to keep in mind what phases are supposed to be mutually in equilibrium and, in particular, the designation $\gamma_{SV}$ is a reminder that the solid surface near the liquid should have an equilibrium adsorbed film of vapor, of film pressure. Thus

$$\gamma_{LV}\cos\theta = \gamma_S - \gamma_{SL} - \pi \tag{3.7}$$

For practical purposes, if the contact angle is greater than 90° the liquid is said not to wet the solid, in such a case drops of liquid tend to move about easily on the surface and not to enter capillary pores. On the other hand, a liquid is considered to wet a solid only if the contact angle is zero.

The above definitions have been directed toward the treatment of the solid-liquid-gas contact angle. It is also quite possible to have a solid-liquid-liquid contact angle where two mutually immiscible liquids are involved. Thus, for a solid and liquids A and B the Young and Dupre equation becomes:

$$\gamma_{AB}\cos\theta_{SAB} = \gamma_{SB(A)} - \gamma_{SA(B)} \tag{3.8}$$

$\theta_{SAB}$ denotes the angle as measured in liquid A and the phases in parentheses have saturated the immediately preceding phase.

### 3.2. Measurement of Contact Angle

The tilting plate method, due to Adam and Jessop, has given the most reproducible and probably the most accurate contact angle values. The general arrangement is indicated schematically in the figure below:

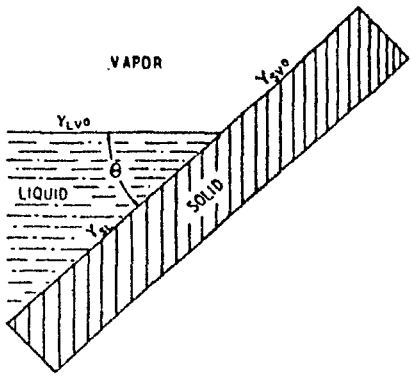


FIGURE 3.2. The Tilting Plate Method [18]

A several centimeter wide plate of the solid dips into the liquid, and its position is altered by means of an adjustable mount until the angle is such that the liquid surface appears to remain perfectly flat right up to the surface of solid. It is essential to appreciate that contact angle measurements require all the precautions against surface contamination that film pressure measurements do.

It is not generally convenient to have available both the large sample of solid and the large volume of liquid needed for the tilting plate method, and most contact angle measurements have been made by means of involving a liquid drop or a gas bubble. Illustrative arrangements are shown below:

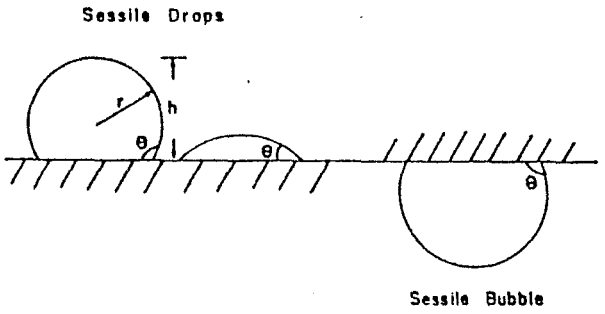


FIGURE 3.3. Use of Sessile Drops or Bubbles for Contact Angle Determination [18]

Zisman and coworkers simply viewed a sessile drop through a comparator microscope fitted with a goniometer scale, thus measuring the angle directly. [21]

It is possible to make use of a captive bubble method where in a bubble formed by manipulation of a micrometer syringe is made to contact the solid surface and the angle is then measured from a photograph.

The contact angle may also be obtained indirectly, from the measurements of a sessile drop. If a spherical shape can be assumed.

$$\tan\theta/2 = h/r \qquad (3.9)$$

An alternative procedure due to Bikerman requires the measurement of the diameter of a drop of known volume. [22]

The solid for which a contact angle measurement is desired may be available only in finely divided form, and it may not be possible to compact it to a smooth enough surface for one of the above methods to be used. An alternative procedure is to compress the material to a porous plug and to measure the capillary pressure toward the liquid in question. [18]

If the porous plug is regarded as equivalent to a bundle of capillaries of average radius r, then from the Laplace equation

$$\Delta P = 2\gamma_{LV} \cos\theta / r \qquad (3.10)$$

where, depending on the value of $\theta$, $\Delta P$ is the pressure required to force entry of the liquid or to restrain its entry. For a wetting liquid

$$\Delta P_0 = 2\gamma_{LV_0} / r \qquad (3.11)$$

The principle of the method is then to obtain the effective capillary radius r by measuring the pressure required to prevent a wetting liquid from entering. The measurement is then repeated with the nonwetting liquid, and by elimination of r

$$\cos\theta = (\Delta P / \Delta P_0)(\gamma_{LV_0} / \gamma_{LV}) \qquad (3.12)$$

### 3.3. Contact Angle Hysteresis

Contact angle measurement constitutes a sensitive method for the characterization of solid surface. While the simple theory describing the equilibrium of a small, axisymmetric sessile drop on a flat, horizontal, smooth, homogeneous, isotropic and rigid (ideal!) solid is straightforward with Young's equation defining the unique value of the contact angle ($\theta_o$) at the triple line; it is generally found in practice that a whole range of contact angles, $\theta$, is accessible experimentally. This effect of variability of $\theta$ is called wetting hysteresis. [23]

Understanding contact angle hysteresis is essential for mastering and controlling many wetting processes, such as coating, spraying, adhesion and printing. These processes may either rely on contact angle hysteresis or be hindered by it, depending on the specific underlying mechanism. Also, successful surface characterization by wettability depends on a correct interpretation of contact angle hysteresis. [24]

Recognized causes of wetting hysteresis fit basically into two classes: chemical and physical. In the former class, such effects as chemical heterogeneity of the solid surface and dissolution and / or swelling of the solid by the liquid should be included. As for the

latter, surface roughness, the existence of pores and asperities, molecular orientation and surface strain are to be taken into account.

Of the many possible equilibrium contact angles for a real surface, one represents the global minimum in free energy and therefore is the stable equilibrium state. The others are metastable equilibrium states. The system may or may not adopt a contact angle which is associated with a metastable state, depending on the free energy barriers around it, on the availability of sufficient energy to overcome such barriers and on geometrical constraints. [23]

The range of wetting hysteresis, generally corresponding to static measurements of contact angle, goes from the maximum, or advancing value, $\theta_A$ down to the minimum, or receding value, $\theta_R$ while $\theta_o$ being somewhere in between. Sometimes dynamic contact angles are considered, in which case $\theta_A$ is usually larger and $\theta_R$ smaller, thus increasing the hysteretic range. [24-25]

Some of the first theoretical efforts about contact angle hysteresis were aimed only at calculating the global minimum in free energy. These theories showed that the stable equilibrium state for a drop on a rough or heterogeneous surface is different from that predicted by the Young equation for an ideal surface. An important attempt to define hysteresis suggested that the range of hysteresis is determined by the range of apparent contact angles which correspond to metastable equilibrium states. In other words, the highest (advancing) contact angle which is experimentally observed was assumed to be the highest angle which is theoretically possible taking into account equilibrium requirements and geometrical constraints. Similar arguments were applied to the lowest (receding) contact angle. [26]

A refinement of this approach was based on the theoretical observation that the height of an energy barrier between successive metastable positions increases as the contact angle becomes closer to the stable equilibrium state.

It was concluded that the range of hysteresis depended also on the availability of energy to overcome such barriers. More recent theories have developed in two main directions: using sophisticated models for the solid surface and analyzing molecular mechanisms and non equilibrium jumps between metastable states.

### 3.3.1.Non-Uniform Surfaces

The derivation given for the contact angle equation can be adopted in an empirical manner to the case of a nonuniform solid surface.

First the surface may be rough:

Wenzel was the first to discuss the influence of surface roughness on the apparent or macroscopic contact angle. He introduced the roughness factor r, defined as the ratio of the true interfacial area to the area projected on the planar envelope of the surface.

$$\cos\theta_r = r\cos\theta_{true} \qquad (3.13)$$

This factor was incorporated into the Young equation in its original form resulting in the so-called Wenzel equation. Wenzel's treatment predicted a major effect of roughness on contact angle. Subsequent treatment of this subject mainly focused on the existence of energy barriers to the movement of the boundary of a liquid drop due to surface roughness and their implications on contact angle hysteresis. [27]

Good chose his surface geometry as a set of concentric circular grooves on the solid, in the middle of which a drop of liquid was placed. Johnson and Dettre [28] subsequently performed computer calculations to simulate the presence of energy barriers by assuming a sinusoidal cross section for the grooves. Eick [29] et al. developed a more general approach to the theory of hysteresis on rough surfaces by using a sawtooth surface. Huh and Mason [30] employed a mechanistic approach to relate contact angle and roughness due to various axisymmetric geometries of surfaces. If $\theta$ is less than 90°, it is decreased by roughness, while if $\theta$ is greater than 90° it is increased. [31]

The second nonuniformity is the surface heterogeneity:

The surface may be composite. If it may be assumed that contact angle equilibrium is in practice determined by sufficiently macroscopic fluctuations such that $\Delta A_{SL}$ and $\Delta A_{SV}$ effectively average the heterogeneties, then for the case of two kinds of patches occupying fractions $f_1$ and $f_2$ of the surface, it follows that [18]

$$\gamma_{LV}\cos\theta_c = f_1\left(\gamma_{s_1V} - \gamma_{s_1L}\right) + f_2\left(\gamma_{s_2V} - \gamma_{s_2L}\right) \qquad (3.14)$$

or

$$\cos\theta_c = f_1 \cos\theta_1 + f_2 \cos\theta_2 \qquad (3.15)$$

Equation (3.15) is known as the Cassie equation. But in this equation the three-phase contact angle, the concept and significance of the line-tension term was not appreciated. Therefore, wide scatter in contact angle data often observed for heterogeneous systems.

### 3.3.1.1. Modification of Cassie Equation

It should be noted that Cassie [32] only predicted the effect of surface heterogeneity on the interfacial free energy of a system. He did not describe the corrugation of the three-phase contact line. A portion of a hypothetical three-phase contact line is shown in the figure below:

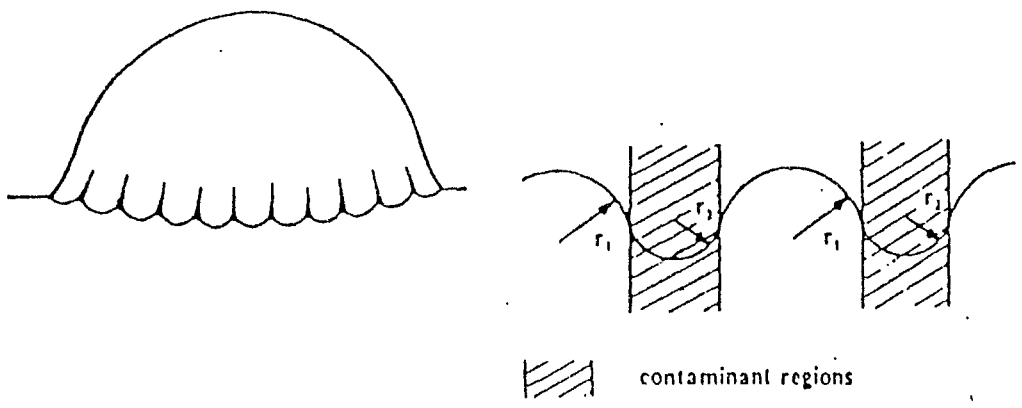


FIGURE 3.4 Corrugation of Three Phase Contact Line [33]

It is known that the excess energy associated with the triple junction has, in some cases, made a significant contribution to the

total energy of the three-phase system. In this regard, a better understanding of wetting phenomena was made possible after the generalized Young equation was derived by Boruvka. [34]

$$\gamma_{SV} - \gamma_{SL} = \gamma_{LV}\cos\theta + \gamma_{SLV}K_{gs} \qquad (3.16)$$

$\gamma_{SV}$, $\gamma_{SL}$, $\gamma_{LV}$ are the interfacial tensions for solid / vapor, solid / liquid and liquid / vapor interfaces respectively. $\theta$ is the contact angle. $\gamma_{SLV}$ is the line tension. $K_{gs}$ is the geodesic curvature of the three-phase contact line which is equal to the reciprocal of the drop base radius ($K_{gs}$=1/r) for a spherical drop sitting on a flat and homogeneous solid surface. The line tension $\gamma_{SLV}$ is associated with the three-phase contact line and can be defined thermodynamically as:

$$\gamma_{SLV} = (\delta F / \delta L)_{T,V,A} \qquad (3.17)$$

where F is the free energy of the system T, V, A and L are temperature, volume, interfacial area and length of the triple junction, respectively.

The Cassie equation was derived on the basis of the Young equation and thus modification of the Young equation (3.16) leads to modification of the Cassie equation including the line-tension term.

If E is the energy gained when the liquid spreads over a unit area of heterogeneous surface, composed i different energetic surface regions.

$$E = \Sigma f_i\left(\gamma_{SV_i} - \gamma_{SL_i}\right) \tag{3.18}$$

and the contact angle θ for the solid surface is

$$\cos\theta = E/\gamma_{LV} \tag{3.19}$$

If the generalized Young equation is taken into consideration, the modified Cassie equation is:

$$\cos\theta = \Sigma f_i \cos\theta_i - \left(1/\gamma_{LV}\right)\Sigma f_i \gamma_{SLV_i} K_{gs_i} \tag{3.20}$$

For systems with a uniform radius of curvature $K_{gsi}=1/ri$, therefore;

$$\cos\theta = \Sigma f_i \cos\theta_i - \left(1/\gamma_{SL}\right)\Sigma\left(f_i \gamma_{SLV_i}/r_i\right) \tag{3.21}$$

The line tension values ($\gamma_{SLV}$) predicted theoretically, on the basis of the energy excess at the triple junction, are very small (from $10^{-11}$ to $10^{-10}$ N as reported in the literature.) Experimental data show that the line tension can be even one order of magnitude larger (~$10^{-9}$ N) Thus, it is expected that the corrugation of the three-phase contact line with radii of local deformation of less than several micrometers can significantly contribute to the contact angle. On the

other hand, for systems with only the three-phase contact line corrugated at the macroscale with a radius of local curvature of hundreds of micrometers, generally the line-tension term has no significant contribution to the observed contact angle and no need for the modified Cassie equation.

When the dimension of impurities reaches the molecular dimension, the Cassie equation as well as the modified Cassie equation may not be valid and that the system should be described by the following equation [33]

$$\left(1+\cos\theta^2\right) = f_1\left(1+\cos\theta_1\right)^2 + f_2\left(1+\cos\theta_2\right)^2 \qquad (3.22)$$

Besides surface roughness and surface heterogeneity the third cause of hysteresis that appears to have emerged is surface immobility, on a macromolecular scale. [18]

### 3.3.2. Dependence of Contact Angles on Drop Size

It is generally known that the spherical shape of a drop can be deformed by gravity but for a long time there has been a controversy regarding the effect of drop size, for a small volume of liquid, on contact angle. The technical literature, has provided evidence that this effect exists and is significant. Nevertheless, the factors

affecting the contact angle/drop size relationship are not fully recognized. [25]

The Young equation describes a force balance in the plane of the solid surface for three phase systems in which the equilibrium contact angle is established in order to resolve the interfacial tensions. There can be no doubt, however, that the contact angle is also affected by the nature of the molecules near the contact line; the line common for the three phases. In this regard modification of the Young equation is required to account for the drop size effect and derivation of this modification is based on thermodynamic considerations. Only the simplest three-phase system being in thermodynamic equilibrium is considered with the following assumptions: [33]

- The surface free energy as well as the line free energy are constant and independent of drop size.
- The three-phase system is simplified to a spherical liquid drop resting on a homogeneous, horizontal, isotropic and flat solid surface.
- The temperature, pressure, volume, chemical potential and composition are constant.

The general equation for the free energy relationships can be simply expressed as follows:

$$dF = \left(\frac{\delta F_{SL}}{\delta A_{SL}}\right) dA_{SL} + \left(\frac{\delta F_{SV}}{\delta A_{SV}}\right) dA_{SV} + \left(\frac{\delta F_{LV}}{\delta A_{LV}}\right) dA_{LV} + \left(\frac{\delta F_{SLV}}{\delta L_{SLV}}\right) dL_{SLV} \quad (3.23)$$

where F is the free energy, A is the area of interface, L is the length of the three-phase contact line and subscripts S,L,V correspond to solid, liquid and vapor phase, respectively.

A change in the free energy with a change in the interfacial area leads to the surface free energy, whereas a change in the length of the three-phase contact line leads to the line free energy.

$$\left(\frac{\delta F_{SL}}{\delta A_{SL}}\right) = \gamma_{SL} \tag{3.24}$$

$$\left(\frac{\delta F_{SV}}{\delta A_{SV}}\right) = \gamma_{SV} \tag{3.25}$$

$$\left(\frac{\delta F_{LV}}{\delta A_{LV}}\right) = \gamma_{LV} \tag{3.26}$$

$$\left(\frac{\delta F_{SLV}}{\delta L_{SLV}}\right) = \gamma_{SLV} \tag{3.27}$$

For the model under consideration the following substitutions are valid:

$$dA_{SV} = -dA_{SL} \tag{3.28}$$

where $\theta$ is the contact angle, r is the drop base radius.

$$dA_{LV} = dA_{SL}\cos\theta \tag{3.29}$$

$$\frac{dL_{SLV}}{dA_{SL}} = \frac{1}{r} \tag{3.30}$$

Thus equation (3.30) leads to modification of Young equation for a spherical drop resting on a homogeneous, smooth solid surface.

$$\gamma_{SV} - \gamma_{SL} = \gamma_{LV}\cos\theta + \frac{\gamma_{SLV}}{r} \tag{3.31}$$

The generalized Young equation was derived by Boruvka and Neumann [34]

$$\gamma_{SV} - \gamma_{SL} = \gamma_{LV}\cos\theta + \gamma_{SLV}K_{gs} \tag{3.32}$$

where $K_{gs}$ is the geodesic curvature of the three phase contact line, which is equal to the reciprocal radius of the three-phase contact line for an axisymmetric drop on a smooth, homogeneous, isotropic and horizontal solid surface.

According to the modified Young equation - which was proposed to account for the drop size effect - the line tension phenomenon is responsible for the effect of drop size on contact angle. Line tension is attributed to the excess energy associated with the three phase contact line, it was predicted by Gibbs to be one dimensional analog

of the surface tension. In this regard a thermodynamically stable system can be characterized by only one value for the line tension.

The line tension is easy to determine from the slope of a plot of $\cos\theta$ vs. 1/r according to the dependence

$$\cos\theta = \cos\theta_{\infty} - \gamma_{SLV} / \gamma_{LV} r \qquad (3.33)$$

where $\theta=\theta_{\infty}$ for $r\rightarrow\infty$

Unfortunately, values of the line tension calculated from contact angle data for varying drop size are much larger, $10^{-6}$ - $10^{-5}$ N, than those expected from theoretical consideration of the excess energy at the triple junction, $10^{-12}$ - $10^{-10}$ N (Harkins [35], Rowlinson [36]) or obtained using other experimental approaches, $10^{-11}$ - $10^{-9}$N (Mingins and Scheludko [37], Schultze [38]). Only Wallace and Schurch obtained much lower values of the line tension, about $10^{-8}$ N, from the contact angle / drop size relationship.

Why such large values for the line tension as calculated from contact angle/drop size data for certain systems were obtained was not clear Leja and Poling [39]postulated that gravitational forces could contribute to the contact angle / drop size relationship. Shanahan theoretically analyzed the effect of solid microdeformation on contact angle and postulated that solid strain in the vicinity of the triple wetting line for a system with a deformable solid may explain a variation of contact angle with drop size. Good and Koo [40]stated that large changes in contact angle with drop size could be attributed to the solid surface heterogeneity. Furthermore, Good mentioned that

solid surface roughness would contribute to the effect of drop size on contact angle and this concept was supported theoretically by derivation of the modified Wenzel equation.

From the systematic examination of the effect of drop size on contact angle for several three phase systems, differing in physicochemical properties, it was concluded that the gravitational effect and the solid strain in the vicinity of the three - phase contact line are not the factors responsible for the large difference between the theoretical line tension and that calculated from $\cos\theta$ vs. $1/r$ data for rigid solids.

But the solid surface imperfections, heterogeneties and/or roughness are believed to be significant factors which cannot be ignored for the inconsistency between the line tension values calculated from contact angle/ drop size data and theoretical values. The commonly used Cassie equation (a modification of the Young equation for heterogeneous surfaces) and the Wenzel equation (a modification of Young equation for rough surfaces) do not take the line tension term into consideration. In both cases, the equations are incomplete and the line-tension term must be taken into consideration.

### 3.3.2.1. Modification of Wenzel Equation

For rough solid surfaces, Wenzel proposed the modification of Young Equation [27]

$$x = \left(\delta_{SV} - \delta_{SL}\right) = \delta_{LV}\cos\theta \tag{3.34}$$

$$x = \frac{q}{A} = \frac{da}{dA} \geq 1 \tag{3.35}$$

where a is the actual interfacial area and A is the apparent area of the geometrical interface. From thermodynamic consideration of three-phase systems the Wenzel equation can be modified with respect to the line tension term. When the solid surface is homogeneous but rough (shown in below figure) the general equation expressing the free energy relations of the three-phase system at equilibrium is as follows:

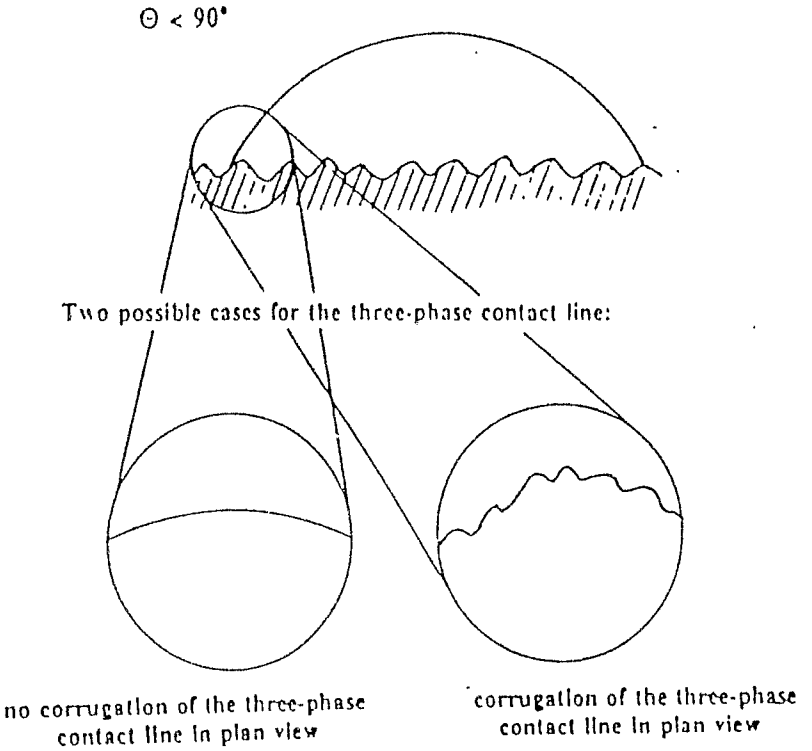


FIGURE 3.5 A Liquid Drop Resting on a Rough Solid Surface[33]

$$\frac{dF}{dA_{SL}} = 0 = \left(\frac{\delta F_{SL}}{\delta a_{SL}}\right)\left(\frac{da_{SL}}{dA_{SL}}\right) + \left(\frac{\delta F_{SV}}{\delta a_{SV}}\right)\left(\frac{da_{SV}}{dA_{SV}}\right)\left(\frac{dA_{SV}}{dA_{SV}}\right) + \left(\frac{\delta F_{LV}}{\delta a_{LV}}\right)\left(\frac{da_{LV}}{dA_{LV}}\right)\left(\frac{da_{LV}}{dA_{SL}}\right) + \left(\frac{\delta F_{SLV}}{\delta L_{SLV}}\right)\left(\frac{dl_{SLV}}{dL_{SLV}}\right)\left(\frac{dL_{SLV}}{dA_{SL}}\right) \tag{3.36}$$

Following substitutions can be used.

$$\frac{da_{LV}}{dA_{LV}} = 1 \tag{3.37}$$

$$\frac{dL_{SLV}}{dA_{SL}} = \frac{1}{r} \tag{3.38}$$

$$\frac{da_{SL}}{dA_{SL}} = \frac{da_{SV}}{dA_{SV}} = x \tag{3.39}$$

$$\frac{dl_{SLV}}{dL_{SLV}} = y \tag{3.40}$$

The modified Wenzel equation is as follows.

$$x(\gamma_{SV}-\gamma_{SL}) = \delta_{LV}\mathrm{Cos}\theta + \frac{y\delta_{SLV}}{r} \tag{3.41}$$

or

$$\cos\theta_r = x\mathrm{Cos}\theta_s - \frac{1}{r}\frac{y\gamma_{SLV}}{\gamma_{LV}} \tag{3.42}$$

where subscripts r and correspond to rough and smooth surface, respectively.

The surface roughness affects the length of the three-phase contact line and can also affect its horizontal corrugation. The theoretical background, expressed as the modified Wenzel equation indicates that the roughness of a solid surface can affect the contact angle / drop size relationship. Surface roughness can significantly contribute to the line tension term ($y\gamma_{SLV}K_{gs}$) and the slope of a plot of $\cos\theta$ vs. 1/r may be larger by a factor y for a rough surface when compared to that for smooth one. Also corrugation of the three-phase contact line can be affected by the surface irregularity ($_{Kgs}\neq 1/r$). For some systems ($\theta>90^{\circ}$) a layer of air or another fluid, depending on the system, may be entrapped inside pores, grooves. A more appropriate equation to describe a liquid drop on both porous and rough, heterogeneous surfaces was derived.

$$\cos\theta_r=fx_1\cos\theta_{s1}+(1-f)x_2\cos\theta_{s2}-(1/\gamma_{LV})(y_1\gamma_{SLV1}K_{gs1}-y_2\gamma_{SLV2}K_{gs2}) \qquad (3.43)$$

Equation (3.43) indicates that the relationship between $\cos\theta$ and 1/r may be very difficult to predict for such complex rough solids with surface heterogeneities. The surface roughness significantly affects the hysteresis in contact angle values measured for the same bubble size. Depending on the location of the drop on a rough heterogeneous solid surface and thus geometry in the vicinity of the three-phase contact line, several different contact angles can be measured.

### 3.3.3. Factors Affecting the Contact Angle/Drop Size Relationship

Gravitational Forces:

The effect of gravitational forces on contact angle / drop size data was considered and discussed by Leja and Poling [39]. Their theoretical analysis was found incorrect by Good[41] in 1979, Lucassen-Rynders [42] stated that gravitational effects play no part in the Young equation. They can alter the shape of bubbles and drops but not their contact angle. Drelich and Miller [25] also concluded from their results that gravitational forces are negligible.

Solid Surface Deformation:

It is generally known that the solid surface in the vicinity of the triple junction can be deformed due to the effect of solid strain. However, it is also true that the effect of solid strain should be important only for elastic solid surfaces as rubber, thin membranes or gels. From experimental observations it was concluded that other factors are of much greater significance for the contact angle / drop size relationship than solid surface deformation.

Surface Roughness:

The effect of roughness on contact angle can be explained based on the modified Wenzel equation.

Surface Heterogeneity:

It was shown, using a theoretical approach by Li et al. [43] in 1991 that corrugations of the three-phase contact line with local

contact angles, caused by the heterogeneity of the solid surface, play an important role in the effect of drop size on contact angle.

The effect of solid surface heterogeneity can be better understood when the modified Cassie equation is taken into consideration. The contact angle is affected by the fractional area of surface contaminants as well as by the shape of the contorted three-phase contact line. The shape of a contorted triple line changes with drop size but at the present time, a change in corrugation of the three phase contact line with a change in drop size is unpredictable and the literature does not provide any satisfactory analysis of a corrugated three-phase contact line in different regions of drop-solid contact can increase as well as decrease with decreasing drop size, depending on the system.

Thin Liquid Film:

Li and Neumann [41] considered a thermodynamic model for a liquid drop setting on a solid surface covered by a thin film and they concluded that the effect of the thin film on the contact angle / drop size dependence is negligibly small. However, a change in film thickness with drop size for liquid / gas / solid system is rather hard to believe.

It was found that for many systems there is a nonlinear relationship between $\cos\theta$ and $1/r$ for a wide range of drop size. The line tension being a thermodynamic property can not change over an entire drop size range. It is expected that the line tension will be dependent on the triple junction length when it reaches molecular dimensions as is the case for the surface tension. It is clear that a system in thermodynamic equilibrium can be characterized by only one value for the line tension. Thus the observed nonlinear

correlation between contact angle and drop size can only be explained based on the deviation of the system from the theoretically ideal case.

### 3.3.4. Pseudo Line Tension

The term line tension will be replaced by the term "pseudo line tension" as suggested by Good and Koo for use in the interpretation of the observed changes in contact angle with drop size.

The actual shape of the three-phase contact line ($K_{gs}$) is difficult to determine, hence, the true value of the line tension $\gamma_{SLV}$ remains unknown. Examination of the drop size influence on the contact angle allows one to calculate a pseudo line tension value. On this basis, the line tension term ($\gamma_{SLV}K_{gs}$) would be replaced by a pseudo line tension term.

$$\gamma_{SLV}K_{gs}=\gamma_{SLV}^{*}(r,x_i)/r \tag{3.44}$$

$$\cos\theta=\cos\theta_{\infty}-\gamma_{SLV}^{*}(r,x_i)/r\gamma_{LV} \tag{3.45}$$

which appear to be more useful. The pseudo line tension can be verified experimentally for each system individually, whereas the geodesic curve as well as the line tension itself are difficult to

determine for real systems. Nevertheless, it is important to emphasize that the pseudo line tension is an empirical value determined experimentally and express the variation in Cosθ with 1/r. The pseudo line tension is a parameter which is equivalent to the hypothetical force which should be applied to the system to cause the observed changes in the contact angle.

Using a theoretical approach, corrugations of the three-phase contact line with local contact angles, caused by the heterogeneity of the solid surface, play an important role in the sign and in the magnitude of the pseudoline tension.

Pseudo line tension term can replace the thermodynamic line tension term which should not only be independent of drop volume but also should have a very small value, $<10^{-9}$N. This new parameter, the pseudo line tension, is not defined thermodynamically and differs from the thermodynamic line tension term. The pseudo line tension term empirically describes imperfections at the solid surfaces which affect the contact angle / drop size relationship. It can be either positive or negative. Its sign determines the direction of its action and depends on the phase through which the contact angle is measured.

### 3.4. Evaluating the Contact Angle Data

The interfacial tension $\gamma_{12}$ between two different materials 1 and 2 is one of the most important concepts in colloid and surface science

as it leads directly to a quantitative expression for the free energy of interparticle or intermolecular interaction in condensed phase systems. Interfacial tensions between two reasonably immiscible liquids can readily be measured but interfacial tensions between solids and liquids and between solids and solids cannot be determined directly. It thus becomes important to arrive at these interfacial tensions, $\gamma_{12}$, via the surface tensions $\gamma_1$ and $\gamma_2$ of the interacting materials 1 and 2. The crucial condition for achieving this goal is the availability of an appropriate combining rule. [44]

### 3.4.1. Zisman Plot

Zisman and coworkers found an empirical correlation for treating contact angle data, which allows and estimate of $\gamma_s$, the surface free energy of the solid by extrapolating value of $\gamma_L$ corresponding to $\cos\theta=1$ when a fair number of $\gamma_L$ values of different liquids are plotted vs. the $\cos\theta$ values measured with these liquids on a surface S. The value for $\gamma_s$ found was designated by Zisman as $\gamma_c$, critical surface tension. The points were found to be approximately on a straight line $\cos\theta=1-b(\gamma_L-\gamma_c)$. [21]

Fox and Zisman [45] based the interpretation of $\gamma_c$ on the premise that, as $\gamma_{LV}$ decreases toward $\gamma_{SV}$, $\gamma_{SL}$ will approach zero, and when $\gamma_{SL}$ reaches zero, $\gamma_{LV}$ will be equal to $\gamma_{SV}$. Zisman and coworkers, and many others who have followed them, have found this methodology to be very valuable for developing the classification of

surfaces and for correlation of contact angle data with other properties, such as adhesion.

Interpretation of contact angle data in chronological order is as follows:

The first important step in finding an appropriate combining rule for interfacial tension was taken by Good. [46] He studied a large number of known $\gamma_{12}$ values of organic liquid-water systems and proposed the insertion of a $\phi$ factor into a simple combining rule based on the geometric mean approach. Fowkes, [47] then showed that for apolar systems, where $\phi$=1 the geometric mean approach is the appropriate one. He also showed that in polar systems, the total surface tensions are separated into additive apolar and polar components (which he designated as dispersive and hydrogen bonding components. Fowkes established the value of the apolar surface tension component of water at 20°C as 21.8 mJ/m$^2$. He indicated, why alkanes with surface tensions less than 21.8 mJ/m$^2$ (heptane, hexane) spread on water, where as those with surface tensions greater than 21.8 mJ/m$^2$ (n-nonane, n-decane) form lenses when deposited on water. After than for a long time (about two decades), no great advances were made. Again Fowkes indicated that, in contrast to the apolar interfacial tension component, the polar (hydrogen bonding) interfacial tension component cannot be derived from the polar surface tensions via a geometric combining rule. However, the nature of the correct combining rule for polar interfacial tensions remained unclear. [48] The dilemma concerning the dipole-dipole and dipole-induced dipole varieties of van der Waals forces had actually already been resolved earlier by Lifshitz [49] for macroscopic systems and this was recognized by Chaudhury [44] who adopted Liftshitz's approach to surface of interfacial systems. This

finally allowed a much more clear-cut delineation between the apolar Liftshitz-van der Waals (LW) forces, which comprise all the electrodynamic interactions on a macroscopic scale and the polar electron acceptor-electron donor (Lewis) acid-base (AB) interactions. The rules governing interfacial AB interactions quickly became clear and the $\gamma^{LW}$ and $\gamma^{AB}$ properties and the electron acceptor ($\gamma^+$) and the electron-donor ($\gamma^-$) parameters of a variety of material were soon determined experimentally. [44,46,48-55]

The realization of pronounced asymmetry of the polar properties of all hydrophilic materials, in favor of their electron donicity gives rise to a strong AB repulsion. This led to a complete understanding of the mechanisms of hydration pressure, non-van't-Hoffian osmotic pressures in concentrated aqueous polymer solutions, polymer phase separation in aqueous media, stability of micelles of non ionic surfactants and quantitative determination of the critical micelle concentration from the molecular surface properties of the surfactant chains, microemulsion formation etc.

### 3.4.2. Molecular Theory of Contact Angles in Apolar Systems

#### 3.4.2.1. The Geometric Mean Combining Rule

It is not possible to get beyond Young's equation as an interpretation of contact angle data, without invoking molecular considerations and theories of intermolecular forces. Thus, Fox and

Zisman premise that $\gamma_{SL} \rightarrow 0$ as $\gamma_{LV} \rightarrow \gamma_{SV}$ was reasonable, but a derived analytical relation between $\gamma_{LV}$ and $\gamma_{SV}$ could not be given. The linearity of the plot of Cosθ vs. $\gamma_{LV}$ could not be trusted if there were no liquids available for which $\gamma_{LV}$ was close to $\gamma_C$. [45]

By the early 1950's it was recognized that a puzzle existed in interpreting contact angle data. First a geometric mean combining rule was introduced by which $\gamma_{SL}$ could be eliminated from Young's equation.

The hypothesis was proposed that the free energy of adhesion is equal to the geometric mean of the free energies of cohesion of the separate phases. For cases where both phases are apolar.

$$\Delta Gij^a = \sqrt{\Delta G^c{}_i \Delta G^c{}_j} = -2\sqrt{\gamma_i \gamma_j} \tag{3.46}$$

$$\Delta Gij^a = \gamma_{ij} - \gamma_i - \gamma_j \tag{3.47}$$

combining these two equations give

$$\gamma_{ij} = \gamma_i + \gamma_j - 2\sqrt{\gamma_i \gamma_j} = \left(\sqrt{\gamma_i} - \sqrt{\gamma_j}\right)^2 \tag{3.48}$$

By combining this with Young equation, below equation is obtained.

$$\gamma_s = \frac{\gamma_L (1+\cos\theta)^2}{4} \text{(for apolar solid and liquid)} \tag{3.49}$$

$$\gamma_{SV} = \gamma_{SL} + \gamma_{LV}\cos\theta \tag{3.50}$$

$$\gamma_S + \gamma_L - 2\sqrt{\gamma_S\gamma_L} = \gamma_S - \gamma_L\cos\theta \tag{3.51}$$

$$\gamma_L(1+\cos\theta) = 2\sqrt{\gamma_S\gamma_L} \tag{3.52}$$

$$\frac{\gamma^2_L(1+\cos\theta)^2}{4} = \gamma_s\gamma_L \tag{3.53}$$

$$\cos\theta = -1 + 2\sqrt{\gamma_S / \gamma_L} \tag{3.54}$$

$$\gamma_{SL} = \gamma_L\left[\frac{(1+\cos\theta)^2}{4} - \cos\theta\right] \tag{3.55}$$

The above relations support the Fox-Zisman postulate that as $\theta \rightarrow 0$ $\gamma_{sL} \rightarrow 0$ But there was an apparent conflict between the Fox-Zisman graphical method, in which Cosθ was an empirical, linear function of $\gamma_L$ and geometric mean combining rule makes Cosθ a linear of $1/(\gamma_L)^{1/2}$

Girifalco and Good proposed an equation containing an interaction parameter $\phi$ in other words $\phi$ is the correction parameter of the solid-liquid interface free energy described as a function of the geometric mean of the total surface free energy of the contacting phases [56]

$$\gamma_{SL} = \gamma_S + \gamma_L - 2\phi\sqrt{(\gamma_S\gamma_L)} \tag{3.56}$$

The utility of this equation is limited because $\phi$ is an empirical parameter whose value is not known before experiments and therefore difficult to calculate.

When Cos$\theta$ is plotted against $\gamma_L$ for apolar liquids on a solid, a straight line should be obtained over a small range of values of $\gamma_L$. $\gamma_c$ for an apolar solid obtained with apolar liquids should be the same as $\gamma_s$. When an extrapolation over more than about 1 dyne/cm in $\gamma_L$ is needed, a far more reliable method for determining $\gamma_c$ is to plot Cos$\theta$ us $1/(\gamma_L)^{1/2}$. Because plot vs. $\gamma_L$ gives to low value of $\gamma_c$ when extrapolated.

### 3.4.3. Molecular Theory of Contact Angles of Polar Liquids and Solids

#### 3.4.3.1. Fowkes Approach

In 1950's the problem was to develop a predictive theory for calculating $\phi$ for systems in which one or both phases were polar. In 1960's an approach to the problem was proposed by Fowkes. He introduced the hypothesis that the surface free energy of a liquid or solid could be subdivided into components due to the London dispersion force $\gamma^d$, to the Debye induction force $\gamma^i$, to the Keasom dipole-dipole force $\gamma^p$ and to a component due to hydrogen bonding $\gamma^h$, [57]

$$\gamma=\gamma^{d}+\gamma^{i}+\gamma^{p}+\gamma^{h} \tag{3.57}$$

However, from a practical point of view, the surface free energy is considered as a sum of the dispersion $\gamma^{d}$ and the nondispersion $\gamma^{h}$ components.

$$\gamma^{n}=\gamma^{i}+\gamma^{p}+\gamma^{h} \tag{3.58}$$

$$\gamma=\gamma^{d}+\gamma^{n} \tag{3.59}$$

or

$$\gamma=\gamma^{d}+\gamma^{AB} \tag{3.60}$$

AB referred to acid-base interaction

According to Fowkes [61], geometric mean theory is applicable to $\gamma^{d}$ but not to $\gamma^{AB}$. The difficulty with the use of geometric mean or harmonic mean combining rules for the polar surface tension components is that none of these treatments can account for the occurrence of a zero polar surface tension components. To take these phenomena into account, it is dispensable to treat the electron acceptor-electron donor interactions between two different materials as separate terms. If one of these two interactions becomes zero on account of the monopolarity of one of its components, its polarity will still be reflected in the other term for interactions between a

monopolar solid and a bipolar liquid or for interactions between a bipolar solid and a monopolar liquid. Fowkes developed an equation to find acid base component of work of adhesion from $\Delta H^{AB}$ (enthalpy of interaction, which has been derived through the four parameter equation. introduced by Drago) and the surface area fraction or the population of interaction, $n^{AB}$ in terms of bonds per unit area. [57]

$$WA^{AB}=-fn^{AB}\Delta H^{AB} \tag{3.61}$$

where f is a factor for converting the enthalpy to free energy.

### 3.4.3.2 The Acid-Base Theory of Contact Angles

Van Oss-Good Approach:

A combining rule which is not a geometric mean, for estimating $\gamma^{AB}$, was proposed by van Oss et al. [44,48] In reality, no substance is completely polar, all compounds are subject to apolar interactions, such as London dispersion forces, but only polar compounds, in addition may take part in acid-base interactions. Van Oss suggested that if a solid surface involves both Lifshitz-van der Waals and acid-base interactions, the total $\gamma$ should be the sum of two components $\gamma^{LW}$ and $\gamma^{AB}$ instead $\gamma^{d}$ and $\gamma^{AB}$ as proposed by Fowkes. Because $\gamma^{d}$ has sometimes already included the induction component $\gamma^{i}$, and generally $\gamma^{p}$ is small due to the tendency toward mutual cancellation of the

dipole field in a condensed phase. Hence, $\gamma^{LW}$ is more inclusive than $\gamma^{d}$ because it includes all long range interactions.

$$\gamma^{LW}=\gamma^{d}+\gamma^{i}+\gamma^{p} \tag{3.62}$$

$$\gamma=\gamma^{LW}+\gamma^{AB} \tag{3.63}$$

(A hydrogen bond is an example of Lewis acid (electron acceptor) and Lewis base (electron donor) interaction. Thus, hydrogen bonding is a special case of Lewis acid-base interaction.

A molecule can be both a Lewis acid and a Lewis base as water. Such substances are called bipolar. In recent years, van Oss and his coworkers splitted the asymmetric acid-base component of a bipolar system into two separate parameters: Lewis acid parameter of surface tension, $\gamma^{+}$ and Lewis base parameter of surface tension $\gamma^{-}$. These parameters enable to postulate a combining rule which can be used in treating the contribution of acidic and basic character to the adhesion across an interface and to the cohesion of a bulk phase.

First combining rule for $\gamma_{ij}^{AB}$ was suggested by Small which was derived from molecular orbital theory and is not a geometric mean[58]

$$\gamma_{ij}^{AB}=2\sqrt{\gamma_i^{+}\gamma_i^{-}}+2\sqrt{\gamma_j^{+}\gamma_j^{-}}-2\sqrt{\gamma_i^{+}\gamma_j^{-}}-2\sqrt{\gamma_i^{-}\gamma_j^{+}} \tag{3.64}$$

$$\gamma_{ij}^{AB}=2\left(\sqrt{\gamma_i^{+}}-\sqrt{\gamma_j^{+}}\right)\left(\sqrt{\gamma_i^{-}}-\sqrt{\gamma_j^{-}}\right) \tag{3.65}$$

The acid-base component $\gamma_i^{AB}$ of the surface free energy of a pure substance $\gamma_i$ is given by

$$\gamma_i^{AB} = 2\sqrt{\gamma_i^+ \gamma_i^-} \quad \text{(bipolar)} \tag{3.66}$$

$$\gamma_i^{AB} = 0 \quad \text{(monopolar or apolar)} \tag{3.67}$$

Acid-base component of work of adhesion and free energy of interaction is as follows:

$$W_{Aij}^{AB} = -G_{ij}^{AB} = 2\left[\sqrt{\gamma_i^- \gamma_j^+} + \sqrt{\gamma_i^+ \gamma_j^-}\right] \tag{3.68}$$

One of the contributions of this approach is the possibility of obtaining a negative liquid-solid interfacial tension. Negative values occur when

$$\gamma_i^+ < \gamma_j^+ \quad \text{and} \quad \gamma_i^- > \gamma_j^-$$

or when

$$\gamma_i^+ > \gamma_j^+ \quad \text{and} \quad \gamma_i^- < \gamma_j^-$$

If in addition $\left|\gamma_{ij}^{AB}\right| > \left|\gamma_{ij}^{LW}\right|$ then net interfacial free energy $\gamma_{ij}$ will be negative. A system of two liquid phases with $\gamma_{ij}<0$ cannot be mechanically stable but if one or both phases is a solid, the system may be stable.

Combining the below equations

$$\Delta G_{SL} = -(1+\cos\theta)\gamma_L \tag{3.69}$$

$$\Delta G_{SL} = 2\left(\sqrt{\gamma_S^{LW}\gamma_L^{LW}} + \sqrt{\gamma_S^{+}\gamma_L^{-}} + \sqrt{\gamma_S^{-}\gamma_L^{+}}\right) \tag{3.70}$$

the complete Young equation comprising both the apolar and polar interactions becomes

$$(1+\cos\theta)\gamma_L = 2\left(\sqrt{\gamma_S^{LW}\gamma_L^{LW}} + \sqrt{\gamma_S^{+}\gamma_L^{-}} + \sqrt{\gamma_S^{-}\gamma_L^{+}}\right) \tag{3.71}$$

As there are three unknowns in equation (3.71) pertaining to the surface properties of the solid, $\gamma_s^+$ and $\gamma_s^-$, the equation must be used three times to solve for these unknowns. This entails doing contact angle determination with at least three different completely characterized liquids of which two must be polar.

Measuring contact angles using apolar liquids on an apolar solid give the entire surface tension as for and apolar or monopolar substance.

$$\gamma_S^{LW} = \gamma_L^{LW}(\text{apolarliquid})\frac{(1+\cos\theta)^2}{4} \qquad (3.72)$$

Above equation is same as the equation obtained by geometric mean rule. The value of $\gamma_s^{LW}$ obtained in this way is valid regardless of whether there is an acid-base component of $\gamma_s$. If the solid is monopolar and if the liquid is monopolar in the same sense as the solid e.g. both being Lewis acids, then above equation still yields the correct value of $\gamma^{LW}$ for the solid.

Similarly the LW component of the surface tension of a hydrogen bonding (or polar) liquid, whose total surface tension is $\gamma_1$, can be determined by measuring the contact angle on an apolar solid whose $\gamma^{LW}$ value is known.

$$\gamma_1^{LW} = \frac{\gamma_1^2(1+\cos\theta)^2}{4\gamma_s^{LW}} \qquad (3.73)$$

To determine $\gamma^+$ and $\gamma^-$ values, one arbitrary relation involving one liquid must be introduced. It is chosen for water

$$\gamma_w^+ = \gamma_w^- \qquad (3.74)$$

Knowing $\gamma_{water}^{LW}$=21.8 and $\gamma_{water}$=72.8 $\gamma_w^+ = \gamma_w^- = 25.5$ mJ/m$^2$ is obtained. All acid-base parameters calculated are therefore relative to those of water.

After $\gamma_s^{LW}$ has been measure, it is possible to simplify the set of three equations to a set of two to solve unknowns $\gamma_s^+$ and $\gamma_s^-$.

$$\sqrt{\gamma_s^+} = \frac{AF - BD}{CF - DE} \tag{3.75}$$

$$\sqrt{\gamma_s^-} = \frac{BC - AE}{CF - DE} \tag{3.76}$$

where

$$A = \gamma_2(1+\cos\theta) - 2\sqrt{\gamma_s^{LW}\gamma_2^{LW}} \tag{3.77}$$

$$B = \gamma_3(1+\cos\theta) - 2\sqrt{\gamma_s^{LW}\gamma_3^{LW}} \tag{3.78}$$

$$C = 2\sqrt{\gamma_2^-} \tag{3.79}$$

$$D = 2\sqrt{\gamma_2^+} \tag{3.80}$$

$$F = 2\sqrt{\gamma_3^-} \tag{3.81}$$

$$G = 2\sqrt{\gamma_3^+} \tag{3.82}$$

Negative square roots may appear. $\sqrt{\gamma_s^-}$ has turned out to be negative only in very rare cases and might lead to the suspicion of experimental error. So negative $\sqrt{\gamma_s^-}$ values may be dismissed as artifacts. Negative values of $\sqrt{\gamma_s+}$ occur more often. This situation has not received a definite answer yet. It is possible that the phenomenon is physically real. In such cases above equation can be used

$$\gamma_S^{AB} = 2\sqrt{\gamma_s^+}\sqrt{\gamma_s^-} \qquad (3.83)$$

The significance of a negative square root of $\sqrt{\gamma_s+}$ is that acid character in the surface leads to a negative contribution to $\gamma_s$. An array of surface dipoles in the solid surface with even a slight preponderance of positive end out wards could account for this.

Equation of State Approach:

Equation of state approach for interfacial tensions is proposed by Neumann is 1964 and is based on macroscopic thermodynamics. The types and relative magnitudes of intermolecular forces in either phase have not been considered relevant. Neumann assumed ideal solid which is smooth, homogeneous, rigid and having no vapor pressure. [59]

He expressed the interfacial tensions by Gibbs-Duhem type equations by entropy, chemical potential, temperature and surface coverage of the absorbate. But the equations are applicable only to binary systems. Neumann stated from these thermodynamic

approaches that between surface tensions there exists a relation which is referred to as an equation of state expressed as follows

$$\gamma^{sL}=f(\gamma^{SV},\gamma^{LV}) \tag{3.84}$$

From the empirical data they derived that:

$$\gamma_{SL}=(\sqrt{\gamma_{SV}}-\sqrt{\gamma_{LV}})^2/(1-0.015\sqrt{\gamma_{SV}\gamma_{LV}}) \tag{3.85}$$

Many objections were made to the approach. But there are three broad objections to the Neumann's theory. First Morrison [60] has shown that the theory's claimed thermodynamic derivation is erroneous. Second Fowkes [61] et al. and van Oss et.al. [62] have shown that there are a great many cases of gross experimental disagreement between predictions from Neumann's equation and observed interfacial tensions between water organic liquids. Third Neumann's equation takes no account at all of hydrogen bonds or Lewis acid-base nature of polar compounds.

### 3.4.4. Two-Liquid Method

For high surface energy solids such as glass and metals the wetting is generally complete and determination of surface energy

from simple contact angle measurements becomes impossible. Murr, [63] described a standard test system for high energy surfaces involving contact angle measurements using mercury as the liquid and determining the drop shape by means of scanning electron microscopy, but because of surface contamination measurements must be taken under vacuum. For these reasons, a method consisting of the measurement of contact angle of drops of a liquid, deposited on high-surface energy solids previously immersed in another liquid, was developed of course, two immiscible liquids have to be used and therefore systems involving water in hydrocarbon media are usually chosen. This method is called two-liquid contact angle measurement.

It is also possible to apply the two-liquid-phase method to low energy solids (e.g. polymeric materials). In particular, orientation phenomena at polymer-liquid interfaces can be directly analyzed. The ability of polymeric surfaces to modify their structure in contact with liquid media, especially water, may be studied by contact angle measurements using water as the bulk liquid phase. [64,65]

First this method is applied to polymeric materials (polytetrafluoroethylene and polyethylene) by measuring the contact angle in water of organic liquids by Peper and Berch [66]. Then Tamai and coworkers [67] developed the theoretical background of the method. They determined surface energy of different metals and some polymers. Hamilton [68] also studied polymers in octane-water (bulk phase) system.

### 3.4.4.1. Principles of the Method

Assuming that Young's equation can be applied to a liquid $L_1$, liquid $L_2$ (bulk phase), solid S system, following relationship can be obtained.

$$\gamma_{SL2}=\gamma_{L1L2}\cos\theta_{SL1}+\gamma_{SL1} \qquad (3.86)$$

where $\gamma_{SL2}$, $\gamma_{LIL2}$ and $\gamma_{SL1}$ are, respectively, the interfacial free energies of S-$L_2$, $L_1$-$L_2$ and S-$L_1$ interfaces and $\theta_{SL1}$ is the contact angle of a drop of liquid L1 on solid S.

Fowkes [69] has shown that if only dispersion forces are interacting between contacting solid and liquid $L_1$, the dispersion, interaction force is approximately equal to $(\gamma_s^d\gamma_{L1}^d)^{1/2}$ on each side of the interface. Then the necessary work to create the interface $\gamma_{SL1}$ is the sum of the work to create each of the surfaces, $\gamma_S+\gamma_{L1}$, minus the amount of energy stabilized by bringing those surfaces into contact, $2(\gamma_s^d\gamma_{L1}^d)^{1/2}$

$$\gamma_{SL1}=\gamma_S+\gamma_{L1}-2(\gamma_s^d\gamma_{L1}^d)^{1/2} \qquad (3.87)$$

In the case of nondispersion forces such as electrostatic, metallic, hydrogen bonding (except London interactions) interacting at the interface another energy term $I_{SLI}$ due to the stabilization by the non dispersion forces is added. [70-71]

$$\gamma_{SL1}=\gamma_S+\gamma_{L1}-2(\gamma_S^d\gamma_{L1}^d)^{1/2}-I_{SLI} \quad (3.88)$$

$$\gamma_{SL2}=\gamma_S+\gamma_{L2}-2(\gamma_S^d\gamma_{L2}^d)^{1/2}-I_{SL2} \quad (3.89)$$

Considering again the Young-Dupre equation:

$$\gamma_{SL}=\gamma_{SL2}+\gamma_{L1L2}\cos\theta \quad (3.90)$$

and combining this equation with Fowkes equation gives

$$\gamma_{L1}-\gamma_{L2}+\gamma_{L1L2}\mathrm{Cos}\theta_{SL1}=2(\gamma_S^d)^{1/2}[(\gamma_{SL1}^d)^{1/2}-(\gamma_{SL2}^d)^{1/2}]-I_{SL1}-I_{SL2} \quad (3.91)$$

If liquid L1 is water (subscript w) and liquid L2 is a hydrocarbon (subscript H), the term $I^P_{SL2}$ may be considered equal to zero since the surface free energy of hydrocarbons consists of only the London dispersion term. So above equation can be rewritten as:

$$\gamma_W-\gamma_H+\gamma_{WH}\cos\theta_{SW}=2(\gamma_S^d)^{1/2}[(\gamma_W^d)^{1/2}-(\gamma_H^d)^{1/2}]+I_{SW}^P \quad (3.92)$$

If the contact angles of water droplets on the solid surface are measured in several hydrocarbon bulk phases the plot of $\gamma_W-\gamma_H+\gamma_{WH}\mathrm{Cos}\theta_{SW}$ versus $(\gamma_W^d)^{1/2}-(\gamma_H^d)^{1/2}$ should give a straight line with slope $2(\gamma_S^d)^{1/2}$ and intercept $I^P_{SW}$. With this method dispersive component of the surface energy of the solid and the magnitude of

the dispersive interactions between water and solid surface can be determined.

Nevertheless, this principle is based on the assumption that a water droplet can displace the hydrocarbon layer from the solid surface at contact. It is not certain to what extent this will happen and there will not remain a thin film of the nonpolar liquid between the solid and water preventing direct contact.

For water-hydrocarbon system it was shown that water is capable of displacing the hydrocarbon with the below criterion.

$$I^{P}_{SW} > 2[(\gamma_S{}^{d})^{1/2} - (\gamma_H)^{1/2}][(\gamma_H)^{1/2} - (\gamma_W{}^{d})^{1/2}]$$

By taking two points from $\gamma_W - \gamma_H + \gamma_{WH}\mathrm{Cos}\theta_{SW}$ versus $(\gamma_W{}^{d})^{1/2} - (\gamma_H)^{1/2}$ graph and writing the slope $\gamma_S{}^{d}$ value can be formulized as follows:

$$(\gamma_s{}^{d})^{1/2} = \frac{(\gamma_{H1} - \gamma_{H2}) - (\gamma_{wH_1}\cos\theta_{WH1} - \gamma_{WH2}\cos\theta_{WH_2})}{2\left[(\gamma_{H1})^{1/2} - (\gamma_{H2})^{1/2}\right]} \qquad (3.93)$$

Also van Oss approach for the interfacial tension can be adopted to the two liquid method. Considering Young-Dupre equation and van Oss equation:

$$\gamma_{SL1} - \gamma_{SL2} = \gamma_{L1L2}\cos\theta_{L1L2} \qquad (3.94)$$

$$\gamma_{SL}=\gamma_S^{LW}+\gamma_L^{LW}-2(\gamma_S^{LW}+\gamma_L^{LW})^{1/2}+2[(\gamma_S^{+})^{1/2}-(\gamma_L^{+})^{1/2}][(\gamma_S^{-})^{1/2}-(\gamma_L^{-})^{1/2}] \quad (3.95)$$

by writing equation. (3.95) for two different liquids W and D (W is the bulk phase) and substituting into equation. (3.94) below equation can be obtained:

$$\gamma_W-\gamma_D-2(\gamma_S^{LW}\gamma_W^{LW})^{1/2}-2(\gamma_S^{+}\gamma_W^{-})^{1/2}-2(\gamma_S^{-}\gamma_W^{+})^{1/2}+2(\gamma_S^{LW}\gamma_D^{LW})^{1/2}$$
$$+2(\gamma_S^{-}\gamma_D^{+})^{1/2}=\gamma_{DW}\cos\theta_{DW} \quad (3.96)$$

by writing this equation three times for different systems one can solve for $\gamma_S^{LW}$, $\gamma_S^{+}$ and $\gamma_S^{-}$.

### 3.4.4.2. Orientation and Surface Configuration Change

Surfaces of polymer solids are different from those of more rigid materials such as metals and ceramics. Because polymer molecules have much greater freedom for rearrangement they may orient themselves in response to a change in surrounding environment. Accordingly, the surface properties of a polymer solid may not be the same as the properties of the bulk. Reorientation does not necessarily require long range segmental motion or migration of large segments but can be achieved by relatively simple short range motion such as rotational motion of segments that are at the surface. [72,73]

According to the principle of surface state equilibration when a water droplet is placed on a polymeric surface in the sessile droplet

contact angle measurement or a surface is immersed into water, the surface configuration of the polymer in contact with liquid water should change following the change of surrounding medium from air to water.

The variation with time of the surface energy of the polymer in contact with an orienting polar liquid such as water can be directly studied by means of the two-liquid phase method. A plate of modified polymer is put into contact with water. At different contact times, droplets of hydrocarbons are placed at the water-polymer interface and the surface characteristics are then determined.

### 3.5. Influence of Evaporation on Contact Angle

Several sources of wetting hysteresis are known which the major ones are considered to be either chemical such as chemical attack, inhomogeneity of chemical composition of the surface, swelling, dissolution or physical such as surface roughness, local adsorption, orientation. [74-76]

Analogous effects may also be observed when there is mass transfer due to evaporation of the liquid. When a liquid is placed on the surface of a solid, it remains as a drop with the formation of a contact angle between the liquid and solid phases, provided the liquid does not wet the solid. The magnitude of the contact angle depends on the physical characteristics of both the liquid and the solid phase. A contact angle initially imposed in the advancing mode will diminish and tend towards a receding value when the liquid

constituting the meniscus starts to evaporate . The higher value of the contact angle of a given volume of a liquid always gives a thicker sessile drop with a smaller base radius. The contact angle plays therefore an important role in the rate of evaporation of the sessile drop. Therefore, complete understanding of how evaporation influences the contact angle is important in understanding the spreading process for fluids in which mass is not conserved. During evaporation from a meniscus, an initially advancing contact angle will tend toward a lower values. Saturation of the atmosphere around the drop is therefore necessary to measure a significant value of $\theta_A$.

Picknett and Bexon identified two extreme modes of evaporation. In the first which is called the constant angle mode, the contact angle is unaltered during evaporation the drop shape remaining that of a spherical cap but with diminishing area of contact between liquid and surface. This is the expected behavior for an ideal system, where there is no hysteresis. In the second, which is called constant area mode, evaporation takes place with unchanged contact are between liquid and surface, the shape remaining that of a spherical cap but with diminishing contact angle. This is the expected behavior where there is contact angle hysteresis. Evaporation follows this mode until the receding contact angle is attained, when the constant contact angle mode takes over. They pointed out a decrease of evaporation rate with increasing initial contact angle. [77]

Yekta-Fard measured contact angles of drops in different atmospheres and showed $\theta$ to vary with the surrounding phase. [78]

Birdi and Vu observed that the rate of evaporation was dependent on the radius of the solid-liquid interface and proportional to the radius rather than the liquid-vapor surface area. They also reported that for small droplets of volatile fluids on low-energy

surfaces two regimes may be observed. With $\theta>90°$ the evaporation rate was non-linear, the contact radius decreased and the contact angle remained constant. With $\theta<90°$ the evaporation rate was linear and the contact radius was constant. [79]

Peiss showed that evaporation rate vary linearly with the radius when it is small but become a curve with increasing r. [80]

Shanahan studied the evolution of contact angles of water on three polymer surfaces both with and without an environment saturated in water vapor. It was observed that in a saturated atmosphere evolution was slow and drop height and contact angle reduced while diameter remained constant. This is attributed to a slight diffusion of water into the polymer. In dry atmosphere they observed that evolution was more rapid and involved three stages. First height and contact angle reduced with constant diameter. In the second, height and diameter decreased while contact angle remained constant. In the last all (diameter, height, angle) decreased and the drop volume tended to zero. This behavior was probably related to anchoring effects of the triple on heterogeneities. [75]

During the evaporation of a liquid occasionally stick-slip behavior of the triple line is observed. First gradually the drop height, h, and contact angle, $\theta$, decrease while the contact radius, r, remains constant. This reduction of h and $\theta$ occurs smoothly over a relatively long time until $\theta$ reaches a minimal value and then, quite abruptly, motion of the triple line causes r to decrease and both $\theta$ and h to increase at essentially constant drop volume since the process is rapid. The cycle is then repeated with a relatively long period at constant but smaller r followed by a quick jump of the triple line to a still lower value of r. [81]

### 3.5.1. Theory of Evaporation of Microdroplets

When a drop of fluid is sufficiently small, the influence of gravity becomes negligible and the fluid forms a spherical cap. In the small angle limit it is then possible to obtain the time dependence of the height of the spherical cap, h, the contact radius, $r_o$, the contact angle, $\theta$, and the radius of the sphere forming the spherical cap, R.

$$R_0=R\sin\theta \tag{3.97}$$

$$h=R(1-\cos\theta) \tag{3.98}$$

$$h=r_0\tan(\theta/2) \tag{3.99}$$

For the spherical cap geometry the solid-liquid and liquid-vapor surface areas are given by

$$A_{SL}=\pi r_o^2 \tag{3.100}$$

$$A_{LV}=2\pi R^2(1-\cos\theta) \tag{3.101}$$

Volume of the spherical cap is

$$V=\frac{\pi}{3}\left(\frac{r_o}{\sin\theta}\right)^3(2-3\cos\theta+\cos^3\theta) \tag{3.102}$$

# 4. ELECTRON SPECTROSCOPY FOR CHEMICAL ANALYSIS (ESCA)

Several spectroscopic techniques such as X-ray photoelectron spectroscopy (XPS or ESCA), secondary ion mass spectroscopy (SIMS), ion scattering spectroscopy (ISS) and Fourier transformed infrared-internal reflection spectroscopy (FTIR-IRS) have been utilized to characterize surfaces. Of these, XPS seems to be the most widely used due to its versatility and comparative ease of data interpretation. [8]

ESCA (Electron Spectroscopy for Chemical Analysis) is an excellent spectroscopic tool for studying the considerable detail aspects of structure and bonding in the surface regions of polymers. The technique involves the measurement of binding energies of electrons ejected by interactions of a molecule with a monoenergetic beam of soft X-rays. The most commonly employed X-ray sources are $AlK\alpha_{1,2}$ and $MgK\alpha_{1,2}$ with corresponding photon energies of 1486.6 and 1253.7 eV, respectively. [2]

With the conventionally employed X-ray photon sources, cross-sections for core levels for most elements of the periodic table are within two orders of magnitude of that for the $C_{1s}$ levels and the technique thus has a convenient sensitivity range for all elements. Core orbitals are essentially localized on atoms and therefore have binding energies characteristic of a given element. For this reason study of core levels is emphasized in ESCA.

To maintain the integrity of the sample during the time taken for measurement and to obviate scattering of electrons entering the analyzer, samples must be maintained at pressures of $10^{-7}$ Torr or better. The relatively low sticking coefficient for most small molecules comprising the extraneous atmosphere for polymers, pressures in the range $10^{-10}$ Torr would typically be required to accommodate the sticking probabilities.

Samples may conveniently be studied as films or powders mounted on a sample probe which may be taken into the spectrometer from atmosphere via insertion lock and valves. The sample requirements are modest and the surface sensitivity of the technique is such that outermost 100 A° is analyzed from 0.2 sq. cm in area depending on the spectrometer design.

ESCA has excellent surface sensitivity and is capable of differentiating surface from subsurface. These features are a consequence of the extremely short mean free paths (escape depths) of electrons in solids. The ESCA spectrum of a given core level consists of well-resolved peaks corresponding to electrons escaping without undergoing energy losses, superimposed on a background tailing to lower kinetic energy arising from inelastically scattered electrons, as it is evident from the wide-scan spectra.

For the commonly used X-ray sources the mean free path of the photons is typically $\sim 10^4$ A° which is many orders of magnitude larger than the typical mean free paths of photoemitted electrons, therefore X-ray beam is essentially unattenuated over the range of surface thickness from which the photoelectrons emerge.

Although there are well-developed techniques for studying chemical compositions and features of structure and bonding

pertaining to the bulk of polymer samples, until the advent of ESCA information with regard to surface compositions could only be inferred rather indirectly by surface free energy measurements e.g. contact angle measurements. Contact angle determinations have been extensively used to investigate the polarity of the surfaces.

X-ray photoelectron spectroscopy (ESCA) developed by Siegbahn and coworkers allows chemical structure analysis even in polymers in a range 1000 times less deep than either ATR or soft X-ray spectroscopy. Basically this is because photoelectrons ejected from atoms deep in the sample are either self absorbed by the sample or lose part of their kinetic energy and contribute only to the spectral background. The effective escape depth varies with the electron kinetic energy and surface structure but is of the order of a few tens of angstroms. ESCA spectra exhibit small chemical shifts owing to the environment of an atom in a molecule which is related to the electron density around the molecules attached to the atom considered. [2]

ESCA involves irradiation of materials in vacuo with monoenergetic soft X-rays and sorting the emitted electrons by energy. The spectrum obtained is a plot of the number of electrons vs. kinetic energy. The kinetic energy of the emitted electrons depends on the atomic environment, the energy of the incident X-ray beam and the spectrometer work function. These variables are related through

$$KE=h\nu-BE-\phi \qquad (4.1)$$

fuction correction. Each element has a unique spectrum and the spectral peaks from a mixture are approximately the sum of the elemental peaks from the individual constituents. Since the mean free path of the electron is small the electrons that are detected originate from only the top few atomic layers. Quantitative data can be obtained from the peak heights or peak areas and identification of chemical states often can be made from the exact positions and seperations of the peaks.

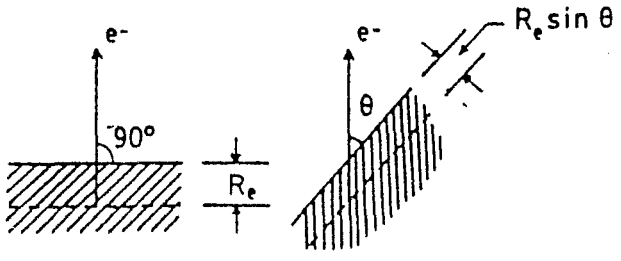


FIGURE 4.1 Angle Dependence of ESCA [16]

While contact angle measurements can clearly provide some indication of the immediate surface composition of polymer films, ESCA offers the possibility of obtaining quantitative information on compositions and structure and bonding in not only the immediate surface but also the subsurface typically to a depth of ~50 A°. The analytical depth profiling capability of the technique arises from the strong dependence on kinetic energy of the mean free path for photoemitted electrons corresponding to the elastic peaks in the ESCA spectrum. The intensity I of the signal from a given core level arising from a surface layer of thickness d is given by:

$$I=I_{\infty}(1-e^{-d/\Lambda}) \qquad (4.2)$$

where $I_{\infty}$ is the intensity observed for an infinitely thick layer and $\Lambda$ is the escape depth of the photoemitted electron. Similarly, the intensity of a signal arising from the bulk of a sample under a surface layer of thickness d is

$$I=I_{\infty}e^{-d/\Lambda} \qquad (4.3)$$

These equations form the basis for determination of the surface structure by ESCA. The primary sources of ESCA data which have been routinely utilized in the application of the technique to polymers are absolute and relative binding energies and relative peak areas.

As in a relatively crude manner, contact angle measurements can in appropriate instances provide information on the gross structure of the immediate outer boundary layer of a polymer film, a technique providing more detailed insight into the surface structure is needed. The application of the relatively new technique of ESCA to the quantitative evaluation of the surface structure of fluorinated polyethylene films by Clark et al in 1974 demonstrate the great potential of the technique in this area. Meanwhile, Clark also demonstrated the utility of ESCA for studying aspects of structure and bonding pertaining to the bulk of homogeneous samples, in

particular simple homopolymers and copolymers. He then extended his work to the copolymers which has the possibility of different bulk and surface structure and investigated the block copolymers of PDMS and polystyrene in 1976. [8]

After then studies on siloxane containing copolymers by means of ESCA technique took the interest as the difference in the surface energies of the components make their surface structure different from bulk and polysiloxane segments are accumulated or enriched, particularly, on the air-side surfaces.

Dwight, McGrath and Riffle [82] confirmed surface segregation phenomena of PDMS blocks in PDMS-polycarbonate block copolymers in 1979. McGrath et al studied surface phase separation in PDMS- polysulfone block copolymers by means of ESCA in 1988 [7]. He also studied PDMS-urethane copolymers in 1983. Inoue and his coworkers studied the block copolymers of PDMS-polymethylmethacylate in 1988 [9].

Chen and Gardella [83] repeated the surface characterization of PDMS-polystyrene block copolymers by ESCA and ATR-FTIR in 1992 as no systematic studies of the effects of block length and architecture of block copolymers on surface morphology have been reported by Clark in previous study. In 1992 Pertsin and Gorelova used ESCA to compare the surface behavior in various binary systems of PDMS with polybisphenol A sulfone polybisphenol A carbonate and also blends of PDMS-polycarbonate block copolymers in PVC and found pronounced surface enrichment in siloxane. [12]

Tezuka et al [84] characterized polyurethane-siloxane block copolymers in 1991 and polyvinyl alcohol- PDMS in 1986 by ESCA. Surface characterization of siloxane- urethane block copolymers was

also made by Nelson [13] in 1993 by ESCA and he noticed the difference in silicon amount between the air and glass side of the polymer films. Chen, Gardella and Cohen [3] measured the surface composition of solution cast film of diblock copolymers of PDMS and nylon-6 by using angle dependent ESCA in 1994. They detected segregation of PDMS in the free surface region of the block copolymers. Chen and Gardella also determined the surface composition of a series of segmented poly(siloxane-urea-urethane)s by angle and energy dependent ESCA in 1995 [15].

In all of the above studies of surface characterization of siloxane containing block copolymers by means of ESCA it was concluded that surface is enriched or covered by the lower surface energy component PDMS. [1-17]

# 5. PROPERTIES OF POLYDIMETHYLSILOXANE AND ITS COPOLYMERS

Polysiloxanes, especially polydimethylsiloxanes are unusual macromolecular amphiphile composed of pendant organic methyl groups along the siloxane backbone and extremely interesting materials since they posses unique combination of properties which are not shown by any other polymeric materials, with the exception of some highly fluorinated polymers. These properties include extremely low glass transition temperatures (~-120°C the lowest recorded for any polymer), very high chain flexibility, large free volume, low boiling and freezing points, insolubility in water, good oxidative, thermal and UV stability, hydrophobicity (water repellancy), physiological inertness (biocompatibility), high gas permeability, surface activity(low surface energy), good wetting and spreading, high compressibility and dampening action, small temperature variation of physical constants, excellent atomic oxygen and oxygen plasma resistance, low reactivity, toxicity, combustibility and low environmental hazard.

Four structural characteristics of PDMS account for these attributes and are the link between the structure, properties and uses of PDMS are low intermolecular forces between methyl groups, unique flexibility of siloxane backbone, high energy of siloxane bond and partial ionic nature of siloxane bond.

Despite their many unique properties pure polydimethylsiloxanes are mechanically too weak to be used directly as a polymer and they show cold flow even at very high molecular

weights (Mn 500,000 g/mol). One major route to make useful products from these polymers is by filling them with high surface silica and then crosslinking by using various methods to obtain silicone rubbers. However, they also display fair mechanical properties and low tear strengths. In addition, crosslinking process limits the broader use of these systems since they cannot be processed from solution or melt which are offered by many thermoplastic elastomers. [6,7]

One method to overcome these difficulties is by the synthesis of siloxane containing multiphase, block, segmented or graft copolymers. Due to their multiphase morphology, the novel systems produced display the interesting properties of siloxanes in addition to the desirable mechanical properties of the organic polymers they are combined with.

## 5.1. Surface Properties of Siloxane Containing Copolymers

Surface properties of polymers play critical roles in many applications. These include paints and protective coatings (surface finish, gloss, friction coefficient, weatherability and water resistance), biomaterials (interaction with blood), textile fibers, photoresists. Some of the most interesting and unique features of siloxane containing copolymers are associated with their surface morphology and the resultant surface properties which distinguish them from other polymeric systems. Due to their very large molar volumes, low cohesive energy densities (intermolecular interactions) and high chain flexibility, polydimethylsiloxanes have extremely low surface tension, surface energies and very low solubility parameters. This

leads to their widespread use as stabilizers in polyurethane foams and as emulsifiers.

The most familiar surface characteristic of PDMS is its low liquid surface tension ranging from 16 to 21 dyn/cm depending on molecular weight. This is at least 10 dyn/cm lower than that of many other organic polymers, such as polystyrene (30-34 dyn/cm), PMMA (38-40 dyn/cm), PU (35-45 dyn/cm), PET (40-43 dyn/cm). One major advantage offered by siloxane polymers is their solubility. PDMS is extremely nonpolar and has very low experimental solubility parameter ($\delta$=7.5 $(cal/cm^3)^{1/2}$). This leads to the thermodynamic incompatibility with almost all other organic polymer systems. This low surface tension and incompatibility account for the tendency of PDMS containing materials to accumulate at air-substrate surfaces. E.g. air-polymer surfaces of blends of various organic polymers with siloxane containing copolymers are dominated by the low surface energy siloxane. (At condensed interfaces, such as that between organic oils and water, the same surface tension driving force does not exist for PDMS to accumulate at the interface.) the thermodynamic driving force behind this process is the minimization of the interfacial and/or surface energy. It has been clearly shown in the literature that even at very low levels of bulk siloxane content (0.5-5 % by weight), the resultant blends display completely silicone like surface properties.

Surface modification of conventional polymers through the addition of small amounts of siloxane containing copolymers was first reported by Zisman and coworkers in 1964[21]. The surface properties that can be modified or improved by this blending technique include biocompatibility, hydrophobicity, surface finish and gloss, release properties, reduction in friction and atomic oxygen resistance. Two major advantages of this approach are the possibility of changing the surface properties of organic polymers without

affecting their bulk properties and ease of compounding, which can be obtained either through solution or melt blending.

In surface modification of conventional polymers through the addition of siloxanes, pure polydimethylsiloxanes have very little use due to their extreme incompatibility with almost all organic base polymers, which leads to their exuclation from the system over a period of time. Therefore, siloxane homopolymers can at best provide a temporary surface modification to the blend. An effective way of achieving permanent surface modification in such blends is through the use of siloxane containing multiphase, block, segmented or graft copolymers. In these systems the organic component of the siloxane copolymer provides miscibility with the base polymer while siloxane segments migrate to the air-polymer surface. Therefore, in essence, these organic segments act as anchoring groups for the siloxane blocks and thereby provide permanent surface modification.

Surface composition and morphology of copolymeric systems are usually studied by contact angle (wettability) and surface tension measurements and by x-ray photoelectron spestroscopy (XPS or ESCA). Other techniques that are also used include surface sensitive FT-IR (Attenuated Total Reflactance ATR). While contact angle and ESCA provide information on surface thickness ranging from 5 to 50 A, ATR-IR provides from 20000-30000 A.

### 5.1.1. Interaction of PDMS with Substrates

PDMS can interact with substrates both through London dispersion forces from the induced dipoles in the methyl groups and

through permanent dipoles in the partially polar siloxane backbone. At the polymer-air surface, configuration that maximize the packing of methyl groups at the surface are adopted, but at other interfaces, the backbone dipole assumes a more important role, because interaction energies involving permanent dipoles are stronger than dispersion forces associated with methyl groups. Thus, in general, with significantly polar substrates, PDMS will interact through its siloxane backbone with polar entities on the substrate surfaces, whereas with predominantly nonpolar substrates interaction will be through methyl groups by London dispersion forces. The main consequence of the low surface tension of PDMS resulting from dominant London dispersion force interaction of methyl groups is that this liquid polymer should spread over any high surface energy substrate. [85]

## 5.2. Applications of PDMS and its Copolymers

Due to their unique combination of properties - explained in preceding sections - siloxane containing systems offer a wide range of specialty applications in many diverse fields. Some of these are as follows:

One of the major uses of siloxane containing copolymers, particularly the polysiloxane-poly(alkylene oxide) systems, is in the stabilization of rigid polyurethane foams. The basic requirements for the block copolymer surfactants to form well-defined, controllable foams are the high surface activity and low surface energy for the

nucleation, formation and stabilization of the cells and good emulsifying abilities for the raw materials. Reduction of surface tension reduces the work needed to form a new surface, hence affording the foam formation much more easily. Siloxane containing copolymeric surfactants also find applications as surfactants in paints and personal care products such as shampoos.

Siloxane-urethane segmented copolymers, which have very good mechanical, fatique and surface properties or their blends with conventional polyurethanes have been successfully used in the production of blood pumps and artificial hearts. Polysiloxane based block copolymers have also been examined wrt. Their transport properties as they are of special interest as membranes in biomedical applications. The combination of good mechanical, dielectric, permeation properties of siloxane-carbonate segmented copolymers have led to their use as blood oxygenation and dialysis membranes. Other well-established application of siloxane copolymers is in soft contact lenses because of their high permeability to gases. The oxygen required by the eye for its metabolic process must be obtained by inward diffusion from the air rather than through blood vessels. PDMS is ideal for such lenses as it has high permeability to oxygen.

Experiments on various Space Shuttle Missions have shown that polydimethylsiloxanes and siloxane-imide copolymers are much more resistant to the atomic oxygen attack encountered in the Low Earth Orbit environment than many other polymeric systems including aromatic polyimides and fiber reinforced epoxy composites.

Organofunctionally terminated siloxane oligomers have been used to improve the water repellancy of nylon, polyester and cotton-polyester fabrics because of their low surface tension. Although water

repellancy is very prominent for a polysiloxane surface, these polymers are, nevertheless, highly permeable to water vapor and have been used for protecting textiles or leather, while still allowing substrate " breathing " (the passage of air and water vapor through the coating). Thin coatings of polycarbonate-PDMS segmented copolymers have provided good ice-releasing properties to various substrates, such as aluminum and concrete.

Organofunctionally terminated siloxane oligomers and siloxane containing copolymers are used in the formulations of magnetic recording media (tapes and hard disks) to improve the lubricity and abrasion resistance of the base materials, which are usually PET, PVC polyurethane/phenoxy resin blends. Siloxane-imide copolymers possess very good thermal resistance and hydrophobic surface properties therefore they are reported to be excellent passivation and/or protective coatings for semiconductor devices.

# 6. EXPERIMENTAL

## 6.1. Materials and Chemicals

The samples characterized in this work are the homopolymer polycaprolactone (PCL) from Polysciences and two grades of commercial α,ω-hydroxy terminated polycaprolactone-polydimethylsiloxane-polycaprolactone (PCL_PDMS_PCL) triblock copolymers differing only in the molecular weights of PCL end blocks supplied from Goldschmidt. The copolymers are designated as H-Si 6440 and H-Si 6460 by the supplier. The molecular weight of PCL is ~33000 g/mol. The properties of the copolymers are given below:

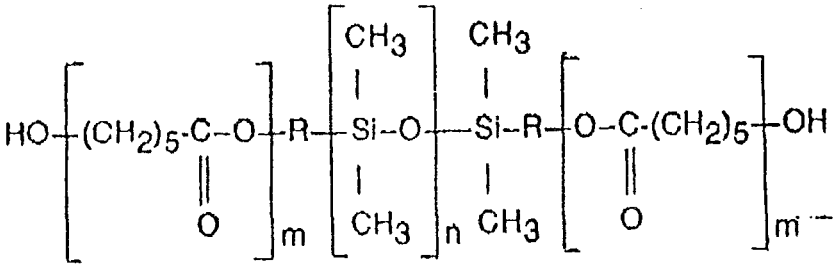

TABLE 6.1. Properties of the copolymers

| | H-Si 6440 | H-Si 6460 |
|---|---|---|
| Functionality | 2 | 2 |
| n/m calculated | 30/18 | 30/27 |
| Mn | 6500±600 | 8500±800 |
| Melting point | 54 | 57 |

The samples were designated according to the increasing siloxane content as P1,P2,P3.

TABLE 6.2. PDMS content of the samples

| | Name | % wt PDMS | % mol PDMS |
|---|---|---|---|
| P1 | PCL | 0 | 0 |
| P2 | H-Si 6460 | 26.9 | 36.5 |
| P3 | H-Si 6440 | 35.5 | 46.3 |

## 6.2. Sample Preparation

Both the PCL and the copolymers were taken in pellet form from the suppliers. For contact angle studies smooth surfaces are desired. By solvent casting it was impossible to obtain smooth surfaces because of the crystallinity of PCL. Therefore, films were prepared by melting the pellets on glass slides at ~60°C and then by cooling. The glass sides of the samples were used for measurements because air sides had some roughness.

Chemicals used in the measurements were distilled water, formamide, ethyleneglycol, glycerol and paraffin.

## 6.3. Equipment

Contact angle measurements were made by a Kernco type goniometer. It has the accessories of high temperature cuvette with temperature control system (0-300°C), special motorized tilt stage for determining advancing and receding angles and a glass cuvette is available for special applications such as measuring the contact angle of a liquid against a solid when both the liquid and solid are immersed in a second liquid (two-liquid method). The experiments were performed in the laboratories of TUBITAK Marmara Research Center, Gebze-Kocaeli.

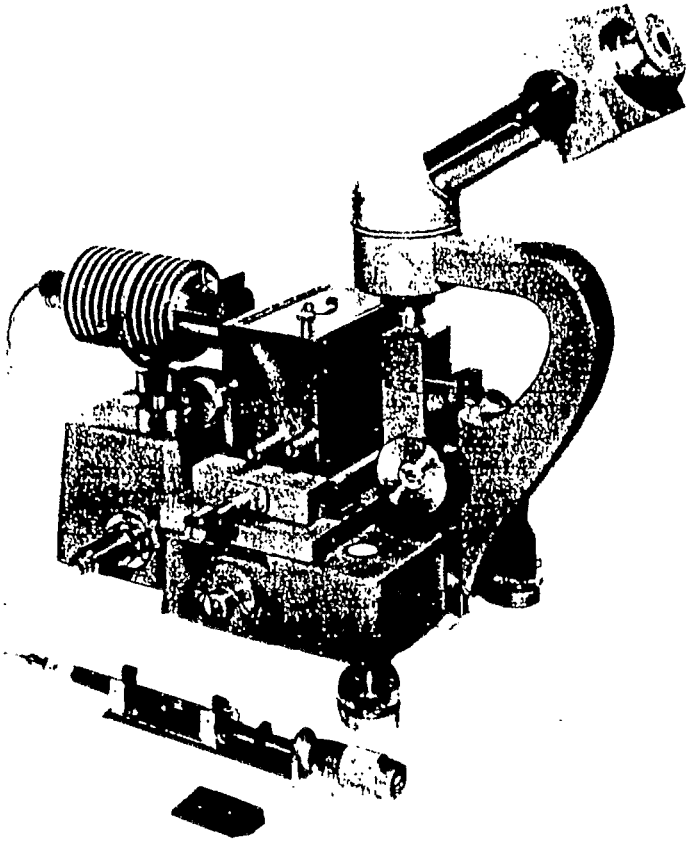

FIGURE 6.1. Contact Angle Goniometer

XPS measurements were performed on a KRATOS ES 300 spectrometer using $AlK_{\alpha}$ excitation ($h\nu$=1486.3 eV) under ultra high vacuum $10^{-9}$ Torr. The samples used in ESCA measurements were in pellet form. (Not in film form prepared by melting). The spectra were taken in the laboratories of Bilkent University, Ankara.

## 6.4. Characterization of the Samples

When a liquid droplet is set on a smooth horizontal solid surface, it spreads infinitely or it reaches equilibrium making a contact angle to the solid surface. The contact angle is the angle between the tangent line at the contact point and the horizontal line of the solid surface. This angle can be measured by using the protactor scale of the meter. The contact angle can also be found indirectly by calculation from equation (3.9) and called as $\theta$theo. The height and radius of the droplet can be measured by using the micrometer contained in the same ocular piece as the protractor. Three unit of the scale is equal to the one milimeter. The droplet is settled on the test surface by using a microburette.

Drop size dependence of the contact angles was investigated by measuring the diameter, height and angle of drops of water, formamide, ethyleneglycol, glycerol and paraffin different in size.

Time dependence of the contact angles were studied by measuring the contact angle with time until the angle became constant or disappeared.

The critical surface tension of the samples were found from the Zisman plots. Surface tension components of the polymers were calculated from contact angles of paraffin, water, formamide, ethyleneglycol and glycerol using different approaches of one liquid method. The surface tension components of the testing liquids used in the calculations are given in the following table:

TABLE 6.3. Surface tension components of the testing liquids

| | $\gamma_L$ | $\gamma^{LW}$ | $\gamma^{AB}$ | $\gamma^{+}$ | $\gamma^{-}$ |
|---|---|---|---|---|---|
| water | 72.8 | 21.8 | 51 | 25.5 | 25.5 |
| glycerol | 64 | 34 | 30 | 3.92 | 57.4 |
| formamide | 58 | 39 | 19 | 2.28 | 39.6 |
| ethylene glycol | 48 | 29 | 19 | 1.92 | 47 |
| paraffin | 28.9 | 28.9 | 0 | 0 | 0 |

Surface tension components of the polymers were also calculated from two liquid method data. Contact angles of water, formamide and ethyleneglycol drops in paraffin bulk phase and contact angles of paraffin drop in water, formamide and ethyleneglycol bulk phases were measured. The interfacial surface tensions of the two immiscible phases used are as follows

TABLE 6.4. Interfacial surface tension components

| Water-paraffin | ethyleneglycol-paraffin | formamide-paraffin | glycerol-paraffin |
|---|---|---|---|
| 52 | 17.5 | 26 | 28 |

To investigate the effect of evaporation on time dependence of contact angles the measurements of water drop contact angles on P1 were taken in a closed box in saturated medium. Saturation was obtained by putting water in small pans in the closed box and heating to 50°C. After cooling to room temperature, it was set to room temperature.

# 7. RESULTS AND DISCUSSION

## 7.1. Determination of Surface Tension Components

During measurements of the contact angles of different liquids, the drop size dependence was recognized. But obtaining drops with equal diameters was difficult. Therefore, the drop size dependence of the contact angles of each liquid ($H_2O$, formamide, ethylene glycol, glycerol) on each sample ($P_1$, $P_2$, $P_3$) was determined. The dependence was expressed as $\cos\theta$ vs 1/r graphs given in Appendix A.

The data points when plotted were found to be very scattered. Therefore, it was difficult to derive a generalized common conclusion from the trends of the linear regression lines. But when the data points of the three samples were compared at same 1/r values, it can be concluded that for water, formamide and glycerol drops $\cos\theta P_1 > \cos\theta P_2 > \cos\theta P_3$. This order could not be observed for paraffin and ethylene glycol drops. For paraffin the reason might be its nonpolarity but for ethylene glycol $\cos\theta P_3 > \cos\theta P_2 > \cos\theta P_1$ and for ethylene glycol $\cos\theta P_3 > \cos\theta P_1 > \cos\theta P_2$ order was obtained. The order for the angles values are just the opposite of the cosine values of them.

As the diameters of the measured contact angles were around 4-5 unit (corresponding to 1/r=0.4-0.5). 1/r values set to 0.45 and the angles corresponding this 1/r value were determined from drop size dependence ($\cos\theta$ vs 1/r graphs). These contact angle values at set

diameter can be used in surface tension calculations as they were normalized with respect to each other by eliminating drop size dependence.

TABLE 7.1. Contact angle values at 1/r=0.45

| θ | $H_2O$ | formamide | ethylene glycol | glycerol | paraffin |
|---|---|---|---|---|---|
| $P_1$ | 85 | 63 | 68 | 72 | 33 |
| $P_2$ | 93 | 81 | 77 | 86 | 26 |
| $P_3$ | 88 | 69 | 64 | 73 | 25 |

Comparison of the water contact angles of the samples can be give an idea about the surface properties of the polymers (e.g. polarity of the surface). It is known that PDMS exhibits excellent hydrophobicity and give water contact angles higher than 90° . It would be expected that PDMS segments occupy the outermost surfaces of the copolymers due to its low surrface energy. It can be said that higher water contact angles indicate the presence of a more complete overlayer of PDMS at the surface.

The critical surface tension for spreading defines the wettability of a solid surface by noting the lowest surface tension $\gamma_L$ a liquid can have and still exhibit a contact angle greater than zero degrees on that solid and it is a characteristic for each solid surface. The values of $\gamma_C$ for a given solid is determined by observing the spreading behavior and the angle θ of a series of liquids of decreasing $\gamma_L$ . A rectilinear relation exists between cosθ and $\gamma_L$, the intercept of this line with cosθ=1 line gives the value of $\gamma_C$ and it is independent of the nature of the test liquids.The data and cosθ vs $\gamma_L$ graphs for the

samples were given in the appendix B. The calculated $\gamma_c$ values are given in the below table.

TABLE 7.2. Critical surface tensions

| | $P_1$ | $P_2$ | $P_3$ |
|---|---|---|---|
| $\gamma_c$ | 21.28 | 21.06 | 22.64 |

The $\gamma_c$ value of P1 homopolymer PCL is very small. Its value must be higher than the $\gamma_c$ values of the copolymers or at least they must be equal. When $\gamma_c$ value is smaller it can be said that the PDMS content is higher. Therefore, P2 has higher PDMS content than P3 although its bulk PDMS content is less. As this method does not give distinguishable results, it is not efficient.

### 7.1.1. One Liquid Method

The surface free energy components of a solid are $\gamma^{LW}$ due to the apolar Lifshitz - Van der waals forces comprising all the electrodynamic interactions on a macroscopic scale; $\gamma^{AB}$ due to polar electron acceptor, electron donor acid base interactions ($\gamma^+$ (electron acceptor) and $\gamma^-$ (electron donor) components of $\gamma^{AB}$ ). As there are three unknowns $\gamma^{LW}$, $\gamma^+$, and $\gamma^-$ ($\gamma^{AB}$ can be obtained from $\gamma^+$ and $\gamma^-$ components) Fowkes- van Oss - Good equation must be written for three different liquids.

$$(1+\cos\theta)\gamma_L = 2\left(\sqrt{\gamma_S{}^{LW}\gamma_L{}^{LW}} + \sqrt{\gamma_S{}^{+}\gamma_L{}^{-}} + \sqrt{\gamma_S{}^{-}\gamma_L{}^{+}}\right)$$

The three liquids can be chosen either as one apolar and two polar or all three polar liquids. In the first case $\gamma_s^{LW}$ was evaluated using an apolar liquid (the eqn reduces to only one unknown as $\gamma_L^+=\gamma_L^-=0$ for apolar liquid), then the remaining two unknowns were solved simultaneously using the two polar liquids. In the second case as all liquids are polar the unknowns were determined by solving the three equations simultaneously by Mathematica. As the contact angles of four polar liquids were measured, all the double, triple combinations were taken and the results were averaged. But in the combinations one liquid must always be water. So double combinations were water formamide, water - ethylene glycol and water glycerol. Triple ones were water - ethylene glycol - formamide, water - ethylene glycol - glycerol, water - formamide - glycerol.

In solving the equations negative square roots of the $\gamma_s^+$ and $\gamma_s^-$ may appear. Negative $\sqrt{\gamma_s^-}$ values are considered as experimental error and dismissed. For negative $\sqrt{\gamma_s^+}$ values, it is possible that the phenomenon is physically real, then instead of writing

$$\gamma_s^{AB} = 2\sqrt{\gamma_s^+\gamma_s^-}$$

it must be written as

$$\gamma_s^{AB} = 2\sqrt{\gamma_s^+}\sqrt{\gamma_s^-}$$

In the calculations negative $\sqrt{\gamma_s^+}$ values were encountered for water - formamide and water - ethylene glycol pairs for P2

The significance of a negative square root of $\gamma^+$ is that acid character in the surface leads to a negative contribution to $\gamma_s$. An

array of surface dipoles in the solid surface, with even a slight preponderance of positive end outwards could account for this.

The result were given in the tables

TABLE 7.3. one apolar and two polar liquid combination

| | $\gamma_s^+$ | $\gamma_s^-$ | $\gamma_s^{LW}$ | $\gamma_s^{AB}$ | $\gamma_s^{tot}$ |
|---|---|---|---|---|---|
| P1 | 0.753 | 6.466 | 24.426 | 4.413 | 28.839 |
| P2 | 0.046 | 5.143 | 26.05 | 0.973 | 27.023 |
| P3 | 0.402 | 4.372 | 26.256 | 2.65 | 28.907 |

TABLE 7.4. Three polar liquid combination.

| | $\gamma_s^+$ | $\gamma_s^-$ | $\gamma_s^{LW}$ | $\gamma_s^{AB}$ | $\gamma_s^{tot}$ |
|---|---|---|---|---|---|
| P1 | 0.678 | 3.914 | 29.63 | 3.258 | 32.888 |
| P2 | 0.04 | 5.686 | 21.08 | 0.954 | 22.034 |
| P3 | 0.07 | 4.29 | 30.65 | 1.096 | 31.746 |

Then the results of this two cases were averaged.

TABLE 7.5. Averaged values of Table 7.3. and Table 7.4.

| | $\gamma_s^+$ | $\gamma_s^-$ | $\gamma_s^{LW}$ | $\gamma_s^{AB}$ | $\gamma_s^{tot}$ |
|---|---|---|---|---|---|
| P1 | 0.716 | 5.19 | 27.028 | 3.836 | 30.864 |
| P2 | 0.043 | 5.414 | 23.565 | 0.964 | 24.528 |
| P3 | 0.236 | 4.331 | 28.453 | 1.873 | 30.326 |

The order of the magnitude of the $\gamma_S^{tot}$ values were same with the order of the water contact angles of the samples. The surface tension of the pure PDMS is known as 21-22 dynes/cm. Therefore, it can be concluded that the surface of the sample P2 is enriched with the PDMS segments. But as the surface tension of P3 is higher than P2 and even near to $\gamma_S^{tot}$ value of pure PCL (P1) the PDMS content at the surface of P3 is less than P2 altough its bulk PDMS content is higher. Also comparison of $\gamma_S^{AB}$ values gives the same conclusion.

### 7.1.2. Two Liquid Method

From Fowkes equation $\gamma_s^d$ and $I_s^p$ values of the solid can be found graphically

$$\gamma_1-\gamma_2+\gamma_{12}\cos\theta_{s1}=2(\gamma_s^d)^{1/2}\{(\gamma_1^d)^{1/2}-(\gamma_2^d)^{1/2}\}+I_{s1}^p$$

1 denotes the liquid drop and 2 denotes the bulk phase. Then the plot of $\gamma_1-\gamma_2+\gamma_{12}\cos\theta_{s1}$ vs. $(\gamma_1^d)^{1/2}-(\gamma_2^d)^{1/2}$ should give a straight line with slope $2(\gamma_s^d)^{1/2}$ and intercept $I_{s1}^p$ .

The measurements were separated into two parts as water, formamide, ethyleneglycol drops in paraffin bulk phase and paraffin drop in water, formamide, ethyleneglycol bulk phases. The contact angles measured were given in the following tables.

TABLE 7.6 Contact angles of paraffin drop in given medium

| In | P1 | P2 | P3 |
|---|---|---|---|
| water | 51 | 38 | 30 |
| ethyleneglycol | 77 | 50 | 36 |
| formamide | 57 | 36 | 28 |

TABLE 7.7. Contact Angles of Given Drops in Paraffin Bulk Phases

| Drop | P1 | P2 | P3 |
|---|---|---|---|
| water | 125 | 136 | 140 |
| ethyleneglycol | 104 | 131 | 135 |
| formamide | 114 | 131 | 136 |

The surface tension components obtained from graphs by linear regression were as follows

TABLE 7.8. For paraffin bulk phase case

| | $l_s^p$ | $\gamma_s^d$ |
|---|---|---|
| P1 | 15.658 | 2.062 |
| P2 | 8.514 | 3.193 |
| P3 | 6.833 | 4.051 |

TABLE 7.9. For Paraffin Drop Case

| | $l_s^p$ | $\gamma_s^d$ |
|---|---|---|
| P1 | 13.627 | 1.324 |
| P2 | 6.099 | 2.503 |
| P3 | 3.059 | 5.087 |

In both cases (paraffin as bulk and drop) $l_s^p$ values are decreasing and $\gamma_s^d$ values increasing with the increasing PDMS content in the bulk indicating that hydrophobicity is increasing. This shows that PDMS surface concentration is in the same order as in the bulk. P3 did not violate the expected order as in the one liquid method results. This might be due to the restriction of reorientation of the surface. Values of two liquid method are smaller than the values of one liquid method because there is no spreading pressure effect contrubuting in two liquid method.

This method may also give a measure of hysteresis whereby the advancing water contact angle is obtained from measurements of water drop in paraffin and the receding angle from measurements of paraffin drop in water. Paraffin bulk and water bulk measurements were called as dry and hydrated respectively. As the amount of bulk PDMS content increases, the degree of hysteresis increases. $\gamma_s^d$ values in the dry state were higher than in the hydrated state as expected. Because in air or immersed in paraffin the hydrophobic PDMS groups are at the surface, in polar medium more PCL will become exposed and reoriente themselves to interact with the polar liquid. This conformational changes at the surface is to minimize the interfacial free energy. It is known that mobile interfaces will organize or restructure themselves to achieve the lowest possible interfacial energy with the surrounding phase.

The two liquid graphical method does not allow us to calculate the total surface free energy since there is no way to adequately calculate the nondispersive force component and therefore nothing can be said about the kind of intermolecular interactions being responsible for the nondispersive component. Such information can be obtained from van Oss approach. For paraffin bulk phases following equation can be written for three cases and solved simultaneously for the three unknowns

$$\gamma_p+\gamma_B-2(\gamma_s^{LW}\gamma_p^{LW})^{1/2}+2(\gamma_s^{LW}\gamma_B^{LW})^{1/2}+2(\gamma_s^{+}\gamma_B^{-})^{1/2}-2(\gamma_s^{-}\gamma_B^{+})^{1/2}=\gamma_{PB}\cos\theta_{BP}$$

P refers to paraffin and B refers to polar liquid. Results were as follows

TABLE 7.10. Van Oss Approach

| | $\gamma_s^+$ | $\gamma_s^-$ | $\gamma_s^{LW}$ | $\gamma_s^{AB}$ | $\gamma_s^{tot}$ |
|---|---|---|---|---|---|
| P1 | 0.827 | 0.719 | 6.761 | 1.542 | 8.303 |
| P2 | 0.186 | 0.360 | 7.658 | 0.516 | 8.174 |
| P3 | 0.18 | 0.096 | 5.608 | 0.263 | 5.871 |

Except $\gamma_s^{AB}$ values the others are not reasonable but the source of error was not known.

## 7.2. ESCA Study

ESCA technique gives a quantitative analysis in surface characterization of polymers.

The peaks of the ESCA spectra for the samples are given below:

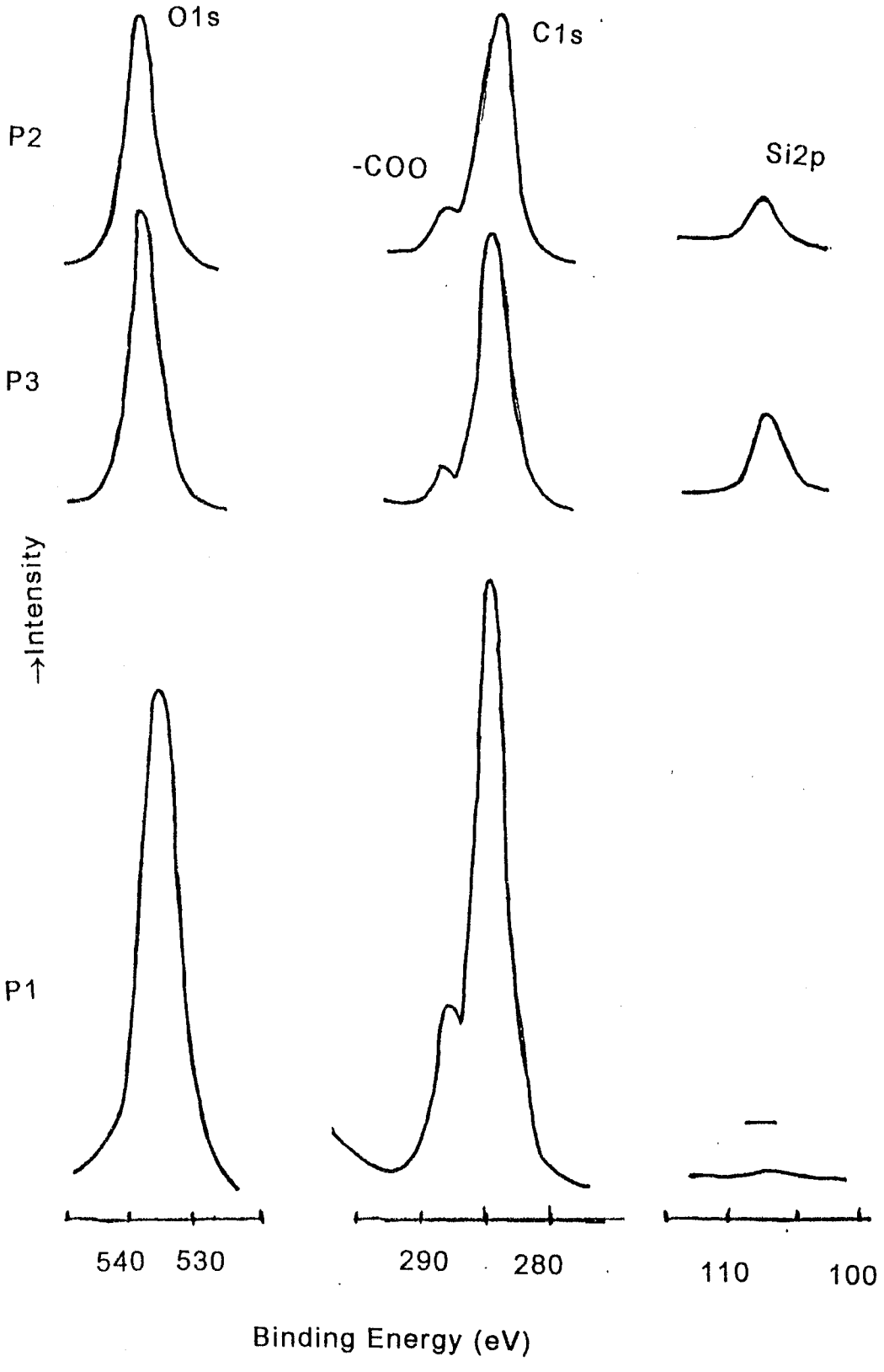


FIGURE 7.1. ESCA spectra of the samples

ESCA spectra of homopolymer PCL was taken to identify the characteristics on ESCA spectra of one of the components of copolymers. PCL gives two peaks in the C1s region around 285-290 eV. The main peak at lower binding energy corresponds to the saturated carbon atoms (5 in each repeat unit of PCL in bulk). The smaller peak higher binding energy arises from the unsaturated carbons (1 in each repeat unit of PCL in bulk). But the peak area ratio of the main peak to the small peak was found as 4/1. The existance of an unsaturated carbon atom peak in the C1s region is one way to monitor the amount of PCL in the surface region, since only PCL component in the copolymers has unsaturated carbon atoms. The % of the peaks are given in the below table:

TABLE 7.11. ESCA peak ratios of the elements of the samples

| | % Si2p | % C1s | % -COO | % O1s |
|---|---|---|---|---|
| P1 | - | 60.8 | 15.8 | 23.4 |
| P2 | 11.1 | 52.8 | 10.0 | 26.1 |
| P3 | 15.0 | 51.9 | 6.2 | 26.9 |

The surface compositions of PDMS-PCL copolymers can be calculated from the peak area ratios of Si2p to C1s. Carbon to silicon ratios of both bulk (from stoichometric calculations) and surface (from ESCA peaks) are given in the below table

TABLE 7.12. % mol PDMS in the bulk and surface

| | %mol PDMS (bulk) | C/Si (bulk) | C/Si (ESCA) | %mol PDMS (surface) |
|---|---|---|---|---|
| P2 | 36.47 | 12.45 | 6 | 60 |
| P3 | 46.27 | 8.97 | 4 | 75 |

The silicon concentration on the surface increased with the increase in the % mol PDMS bulk concentration of the copolymer. Si concentration on the surface is %11 and %15 for P2 and P3 respectively. As C/Si ratios of the surface are lower than the bulk it can be concluded that Si composition is higher on the surface than in the bulk. Or in other words the surface concentrations of PDMS of both copolymers are higher than the bulk values values. PDMS surface phase separation can be attributed to the lower surface energy of the PDMS segments at the polymer-air interface as compared with that of the polar hard segment PCL.

The average molecular weights for the soft PDMS segments are same in two copolymers but the average lengths for the hard segment are different. It appears that the surface concentration of PDMS decreases as the length of the hard segment increases.

PDMS surface phase separation can also be observed from the ratio of higher (saturated) peak to smaller (unsaturated) C peak. In PCL ratio is 4/1, in copolymer P2 it is 5/1 and 9/1 in P3. Increase in the ratio with increasing PDMS bulk content is an indication of PDMS phase separation. Because saturated C % increases with the contribution of saturated carbons of PDMS.

## 7.3. Time Dependence of Contact Angles

Time dependence of contact angles of the samples were represented in Figures 7.2-7.5 graphically. All the testing liquids

except paraffin showed a time dependence of contact angles. This might be an indication of surface reorientation. Because, in air medium the PDMS enrichement of the surface of the copolymers were expected due to the minimization of the surface free energy. In other words, apolar groups were expected to exist on the surface of the copolymers. When a polar liquid was dropped, surface reorientation might occur and polar PCL blocks tried to come to the surface in order to minimize the surface interfacial energy.

From the time dependence graphs of formamide, ethyleneglycol and glycerol it was observed that initially contact angles of P2 and P3 were close but with time P3 showed sharper change in contact angle and become closer to the contact angle values of PCL. This was also an indication of orientation of PCL blocks to the surface when the sample encounters with a polar medium. In P2 the change in contact angles with time was significantly less than in P3. This might be due to the difficulty of orientation of PCL blocks because of its higher length.

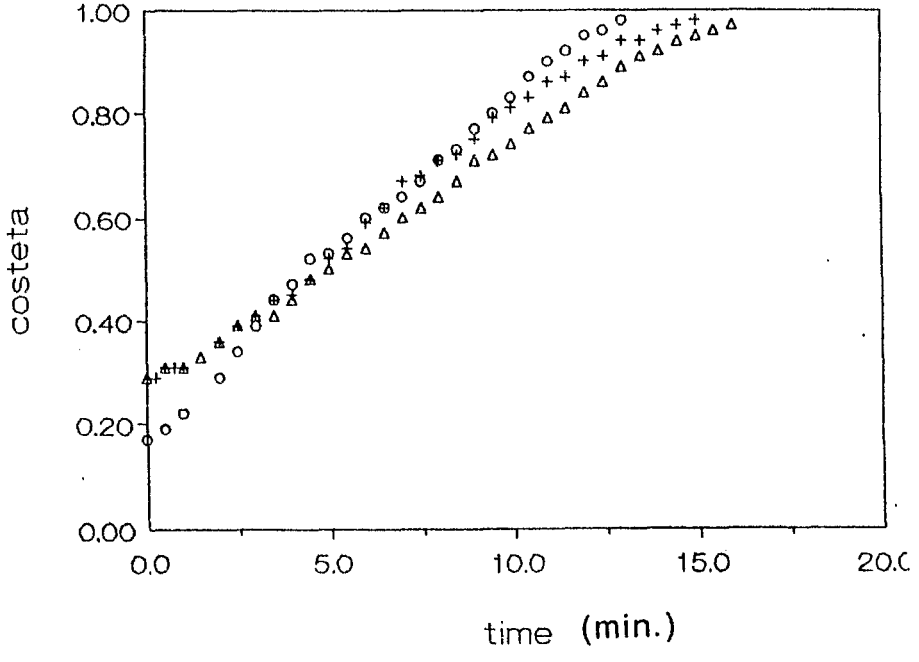


FIGURE 7.2. cosθ vs time for water drop (+→P1, Δ→P2, o→P3)

With water time dependency was different than with other polar drops. In formamide, ethyleneglycol and glycerol the contact angles changed with time and then settled at a constant value. But in water drops the contact angles were changed with time until the drop disappeared. Also PCL showed change in contact angles with time. This gave the idea that with water another effect, probably evaporation in addition to reorientation caused the change with time.

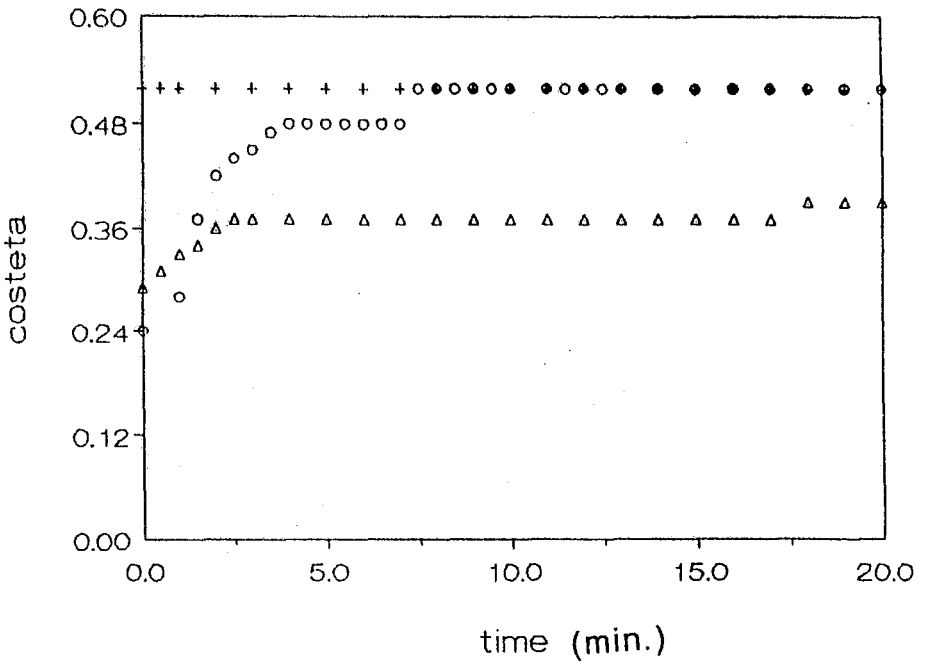


FIGURE 7.3. cosθ vs time graph for formamide drop
(+→P1, Δ→P2, o→P3)

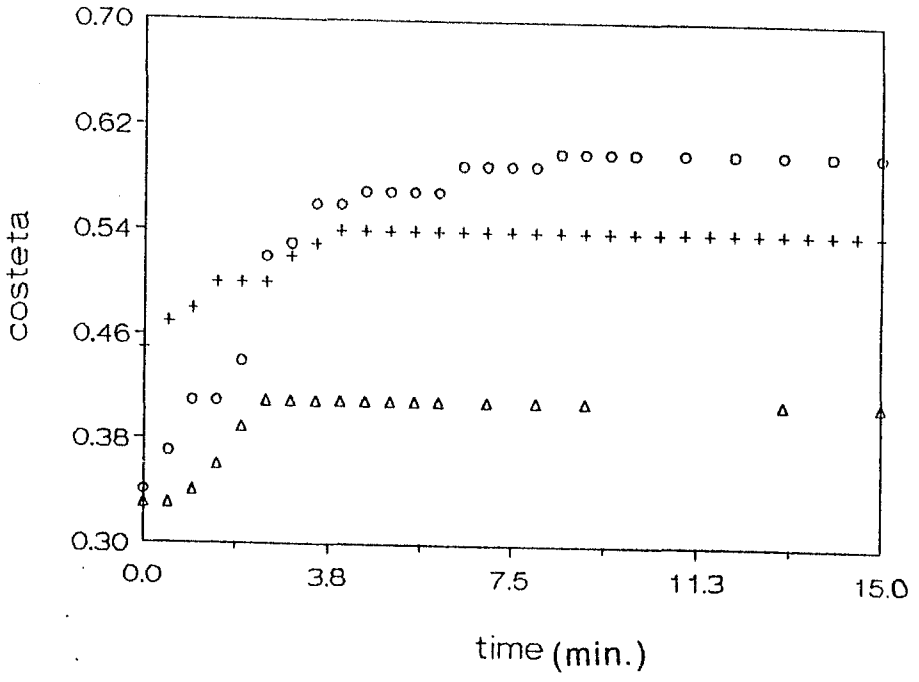


FIGURE 7.4. cosθ vs time graph for ethyleneglycol drop
(+→P1, Δ→P2, o→P3)

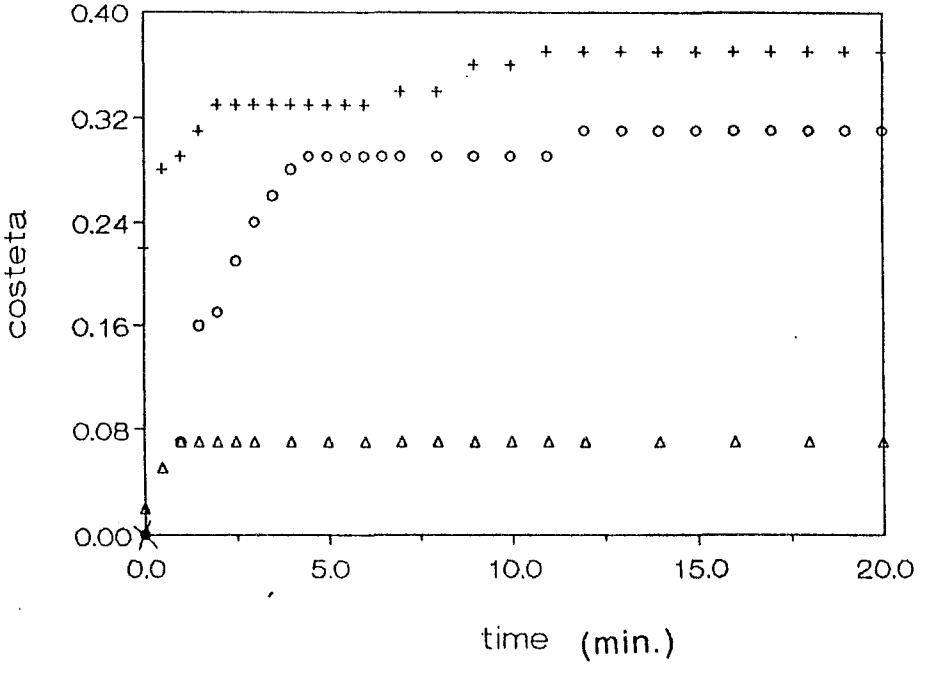


FIGURE 7.5. cosθ vs time graph for glycerol drop
(+→P1, Δ→P2, o→P3)

In contact angle values of one liquid method, it was recognized that with polar liquids the contact angles of P3 were smaller than the contact angles of P2. This indicates that PDMS content at the surface was higher in P2 altough its bulk PDMS content was less than P3. This observation also strengthens the immediate orientation of PCL blocks in P3.

Effect of evaporation is significant for water drops because water is the liquid having the lowest boiling point among the testing liquids. While bp of water is 100°C, it is 193°C for formamide, 197°C for ethyleneglycol and 289°C for glycerol.

The effect of evaporation of water was studied in closed saturated (with the vapor of water) medium. Because during evaporation from a meniscus an initially advancing contact angle will tend toward a lower value. Saturation of the atmosphere around the drop is therefore necessary to measure a significant value of $\theta$. Only water contact angles on PCL was measured because in copolymers reorientation effect was mixed with evaporation effect.

From $\theta$ and diameter vs time graphs two modes were observed. First constant diameter (contact area of the liquid with the solid) and decreasing $\theta$ region and then constant $\theta$ and decreasing diameter region occuring in cycle. This can be explained by the stick-slip behavior of the triple line. The angle first decrease to receding value for that contact area value then quite abruptly motion of the triple line causes diameter to decrease.

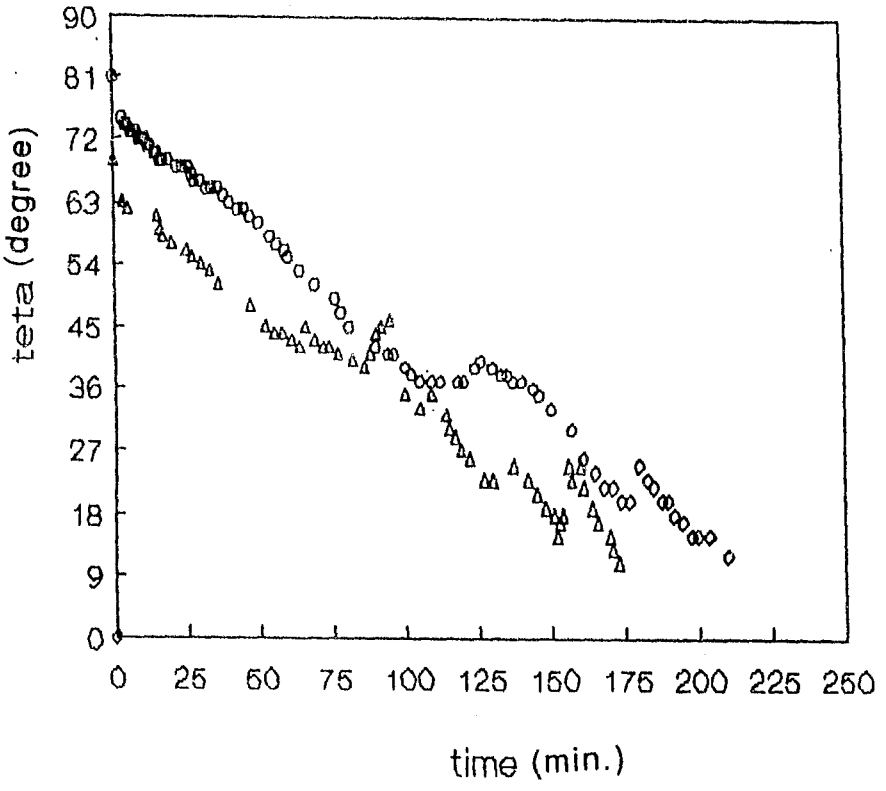


FIGURE 7.6. θ vs time for P1-water drop in saturated medium
(o→1st sample, Δ→2nd sample)

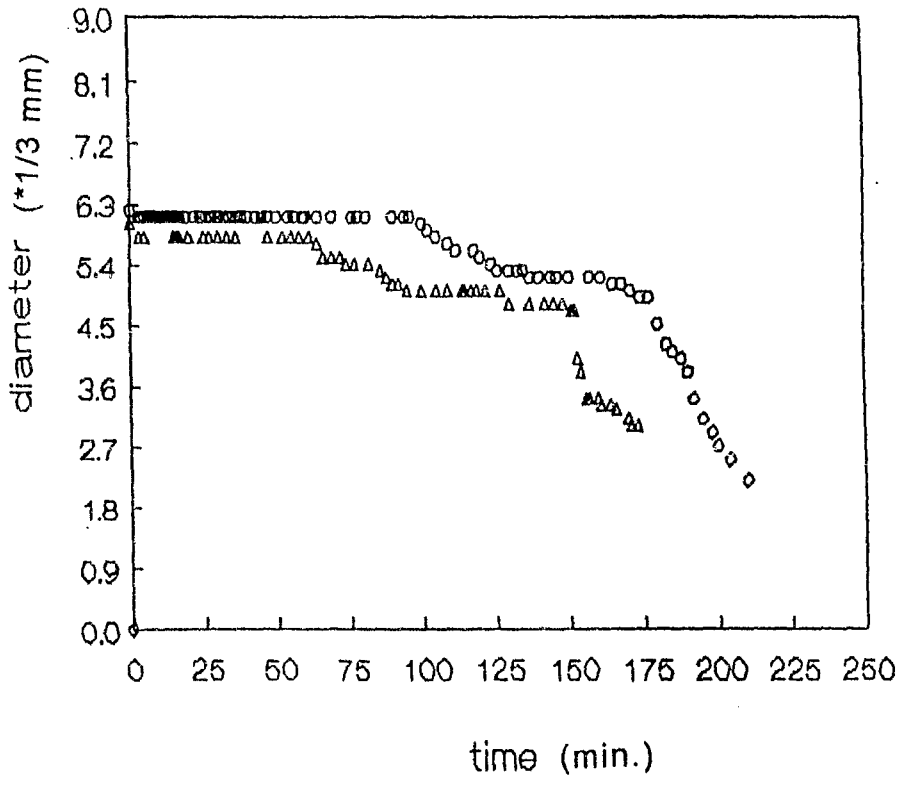


FIGURE 7.7. d vs time graph for P1-water drop in saturated medium
(o→1st sample, Δ→2nd sample)

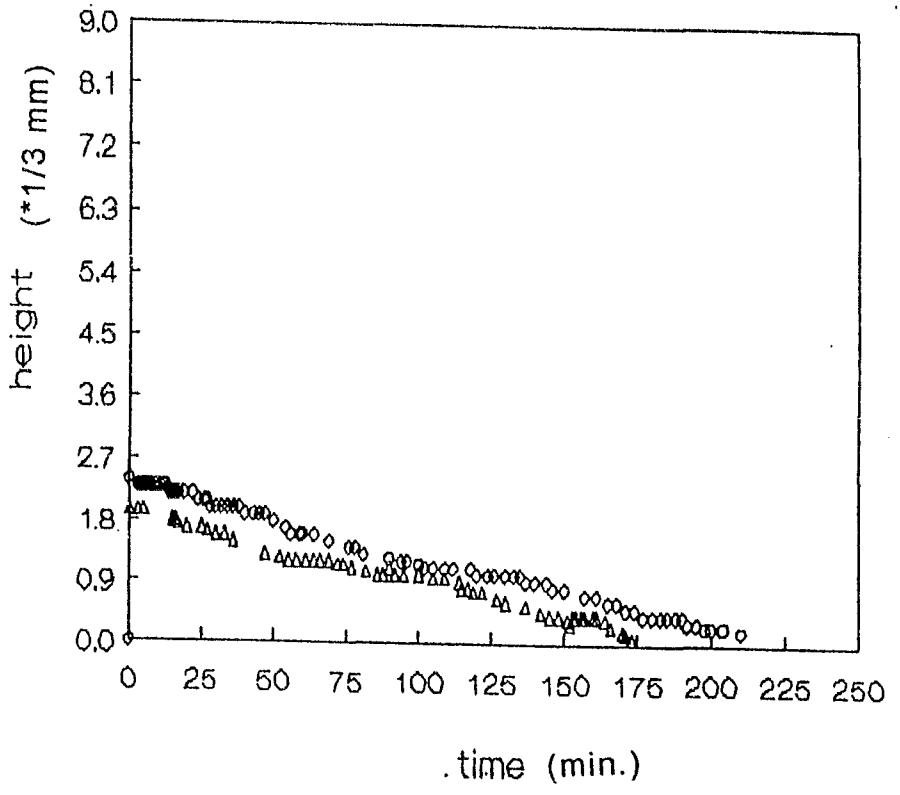


FIGURE 7.8. h vs time graph for P1-water in saturated medium
(o→1st sample, Δ→2nd sample)

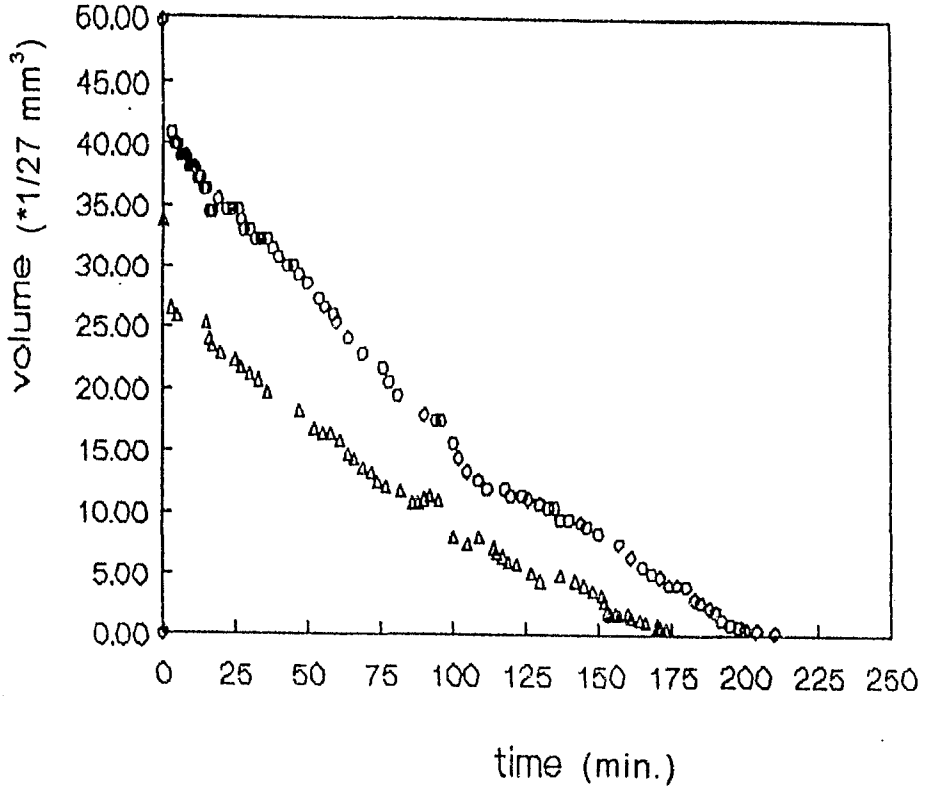


FIGURE 7.9. Volume vs time graph for P1-water in saturated medium
(o→1st sample, Δ→2nd sample)

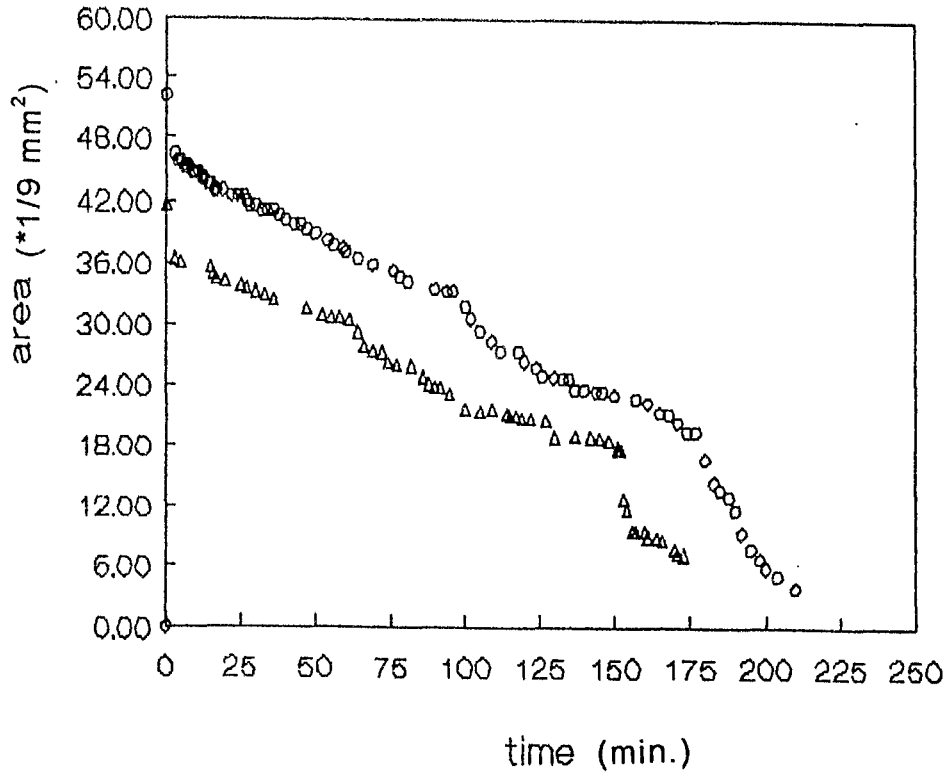


FIGURE 7.10. Area vs time graph for P1-water in saturated medium

Volume change of the samples were linear with time. But area was not a linear function of time. At constant angle and decreasing diameter modes, area was constant with time altough it is proportional to the square of the radius at constant angle.

There were two different drops that were observed. The conditions of the medium and the sample were same. Their initial contact angles were different altough their initial diameter and height values were very close. Their disappearance periods were different but the time passed for one degree decrease in contact angles were nearly equal. (210/81≅173/69 210 and 173 are the disappearance periods, 81 and 69 are the initial contact angles). The θ, diameter, height, volume and area vs. Time graphs of the samples were qualitatively similar. When the graphs of the sample with smaller initial contact angle were shifted 30 min., all of them coincide with the graphs of the other sample. This observation is also an indication of the stick-slip behavior. As the drop evaporates, it would prefer to

maintain the equilibrium value of contact angle $\theta_0$ thus minimizing its free energy for its volume at a given moment but when a critical value of volume is reached a sudden decrease in diameter disturbs the equilibrium and then a new equilibrium is set.

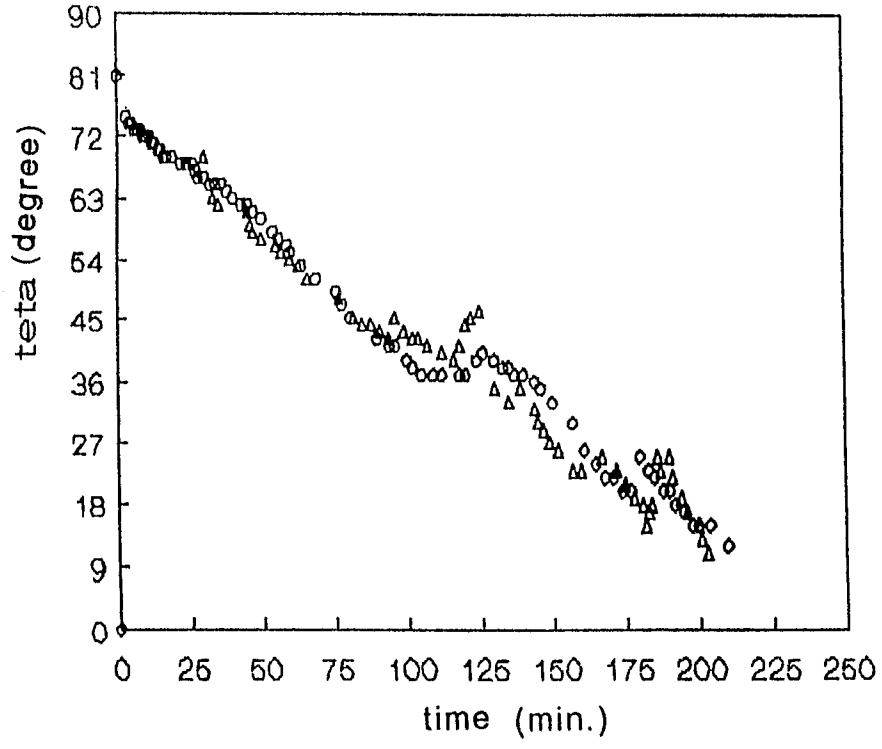


FIGURE 7.10 θ vs time graph shifted 30 min.

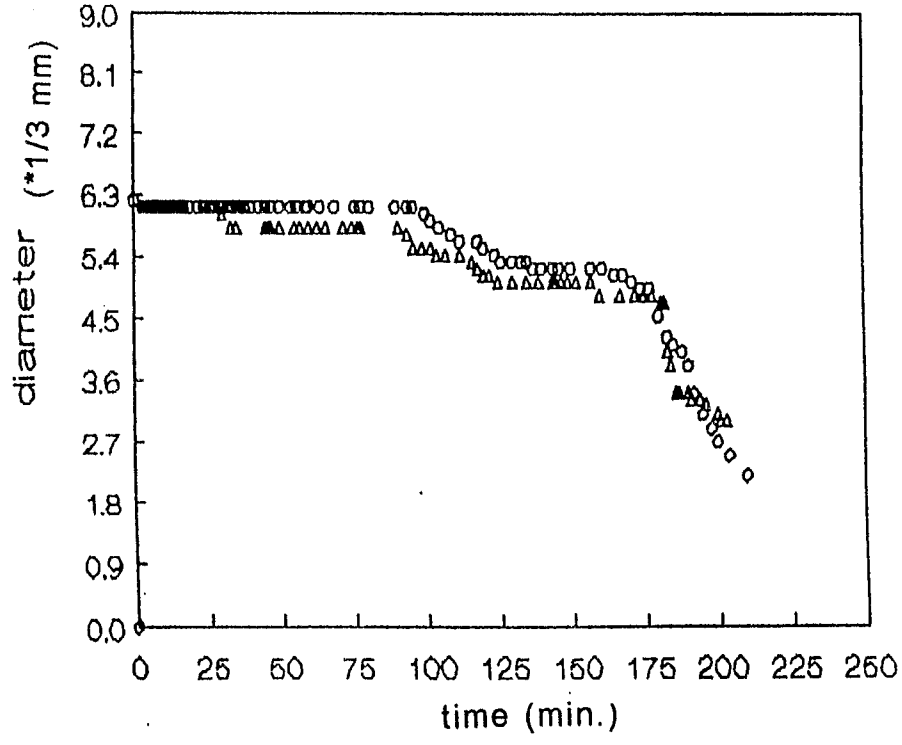


FIGURE 7.11. d vs time graph shifted 30 min.

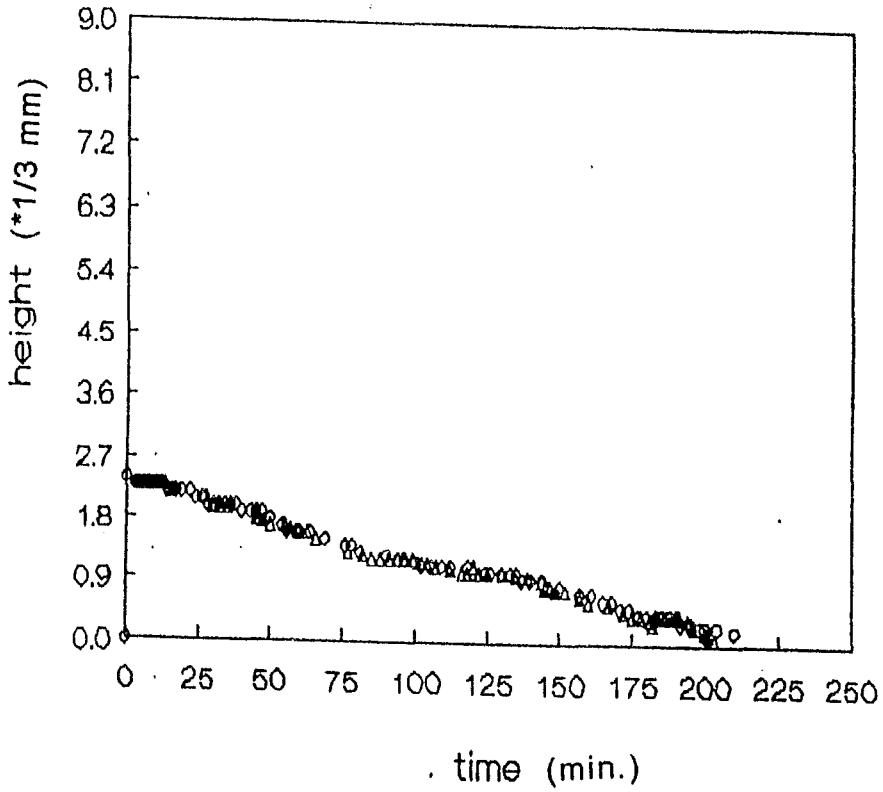


FIGURE 7.12. h vs time graph shifted 30 min.
(o→1st sample, Δ→2nd sample)

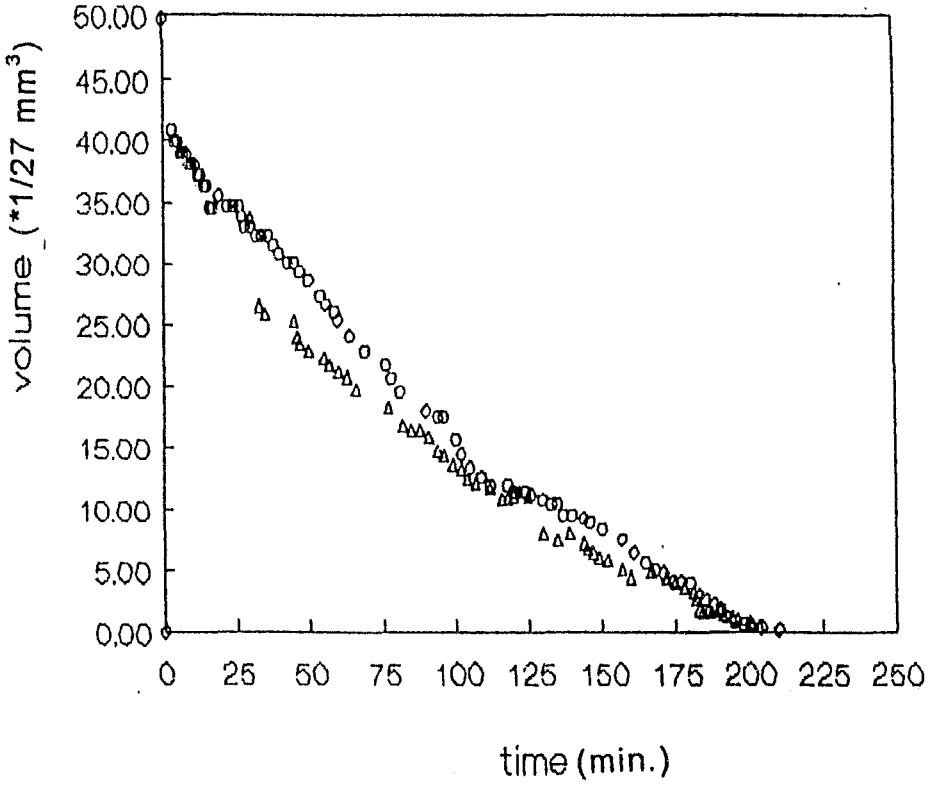


FIGURE 7.13. volume vs time graph shifted 30 min.
(o→1st sample, Δ→2nd sample)

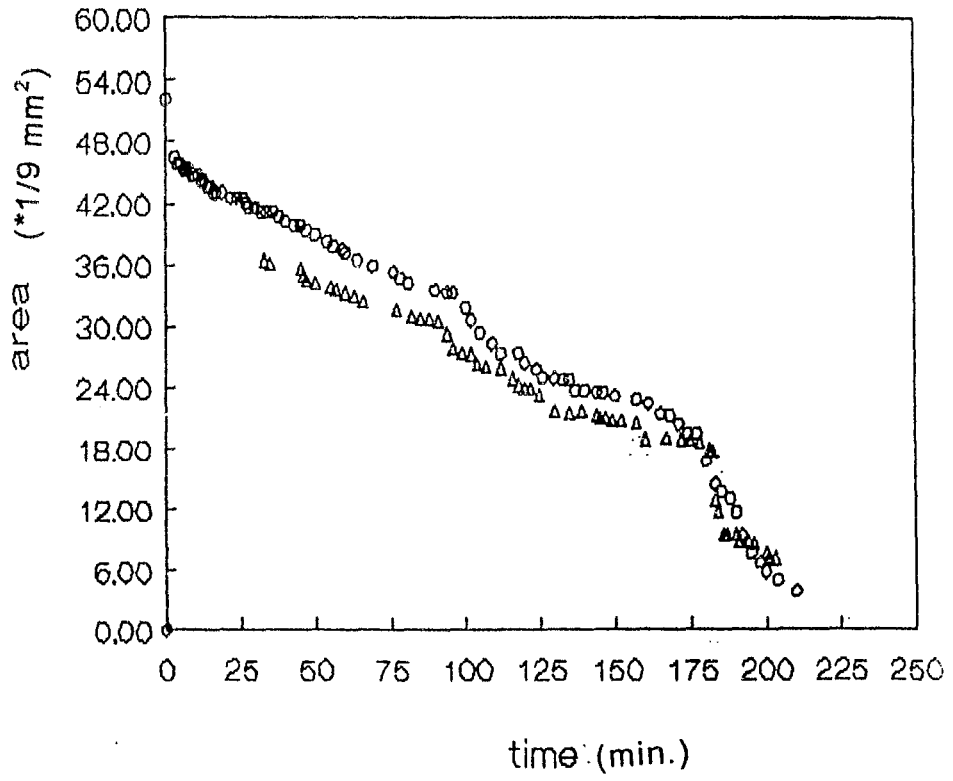


FIGURE 7.14. area vs time graph shifted 30 min.
(o→1st sample, Δ→2nd sample)

# 8. CONCLUSIONS AND RECOMMENDATIONS

The conclusions that can be drawn from the experimental findings of this work can be summarized as follows

Triblock copolymers of PCL-PDMS-PCL were studied. They had the same length of PDMS segments but differing in the length of PCL blocks.

It is known that PDMS gives water contact angles higher than 90°. Higher contact angles indicate the presence of a more complete overlayer of PDMS at the surface of silicon containing systems. So from the comparison of the water contact angles of the samples it can be concluded that P2 shows higher PDMS content at the surface than P3 altough its bulk PDMS content is less.

From the critical surface tension evaluations comparable results could not be obtained. From the one liquid method calculations total surface tension of the sample P2 was obtained close to the literature value of pure PDMS. But the surface tension of P3 was closer to the surface tension of homopolymer PCL. Acid-base component of surface tension indicates the amount of polar groups at the surface. Lowest $\gamma_s^{AB}$ value for P2 showed that it had higher amount of PDMS at the surface than P3.

From the graphical calculations of two liquid method it was obtained that $l_s^n$ values were decreasing and $\gamma_s^d$ values were increasing with the incresing PDMS content in the bulk indicating that

hydrophobicity is increasing. This shows that PDMS surface concentration increased with the increase in the bulk PDMS content.

XPS analysis showed the phase separation of PDMS (due to its lower surface energy) in copolymers quantitatively. % mol PDMS at the surface were higher than the bulk values and they increased with the increasing % bulk PDMS content of the copolymers.

With time contact angles of the polar testing liquids on the samples especially copolymers' were changing and then they became constant at another $\theta$ value. This might be due to reorientation of PCL blocks to come to the surface in order to minimize the surface interfacial energy.

Change of water contact angles with time continued until the drop disappeared indicating that reorientation effect was mixed with the evaporation effect due to the lower boiling point of water than other testing liquids.

In evaporation study of water drops on PCL in closed saturated medium, stick-slip behavior of the triple line was observed. The angle first decrease to receding value for that contact area value, then quite abruptly motion of the triple line causes the diameter to decrease.

As recommendations for future studies followings can be said

To minimize the effect of time on initial measurements of contact angles photographs of the drops can be taken to read the angle and dimensions.

Surface characterization of the blends of these copolymers can be studied. To investigate the effect of PCL block length on reorientation, more copolymer differening in PCL block legths can be investigated. Effect of evaporation on the copolymers can be analysed.

In order to observe the change in siloxane composition with depth, angle dependent study can be made. XPS sampling depth decreases with the decrease in the electron take-off angle.

Upon hydration surface rearrangement was observed in contact angle studies . To understand this effect qualitatively, ESCA spectra of the hydrated samples can be taken.

# APPENDIX A

## Drop Size Dependence of Contact Angles

TABLE A.1 Data of cosθ vs. 1 / r Graph for P1-$H_2O$ drop

| Diameter | Height | Angle | $\theta_{theo}$ | cosθ | 1/r |
|---|---|---|---|---|---|
| 2.8 | 1.0 | 68 | 71 | 0.37 | 0.71 |
| 3.6 | 1.3 | 73 | 72 | 0.29 | 0.56 |
| 4.0 | 1.5 | 76 | 74 | 0.24 | 0.50 |
| 5.3 | 2.0 | 74 | 74 | 0.28 | 0.38 |
| 5.6 | 2.2 | 80 | 75 | 0.17 | 0.35 |
| 6.0 | 2.3 | 78 | 75 | 0.21 | 0.33 |
| 6.4 | 2.4 | 74 | 74 | 0.28 | 0.31 |
| 6.6 | 2.6 | 75 | 76 | 0.26 | 0.30 |
| 7.1 | 2..6 | 78 | 72 | 0.21 | 0.28 |
| 7.6 | 2.85 | 75 | 74 | 0.26 | 0.26 |

In all cosθexp vs. 1/R graphs r was measured in units from the scale of the goniometer. 3 unit=1mm

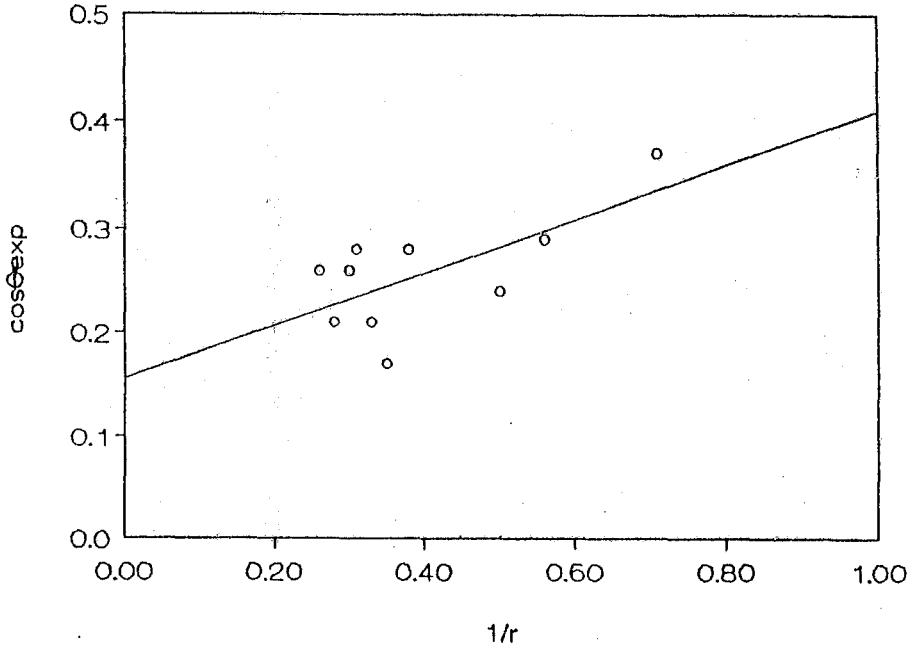


FIGURE A.1. cosθ vs. 1/ r for P1-water drop

TABLE A.2 Data of cosθ vs. 1 / r Graph for P2-$H_2O$ drop

| Diameter | Height | Angle | $\theta_{theo}$ | cosθ | 1/r |
|---|---|---|---|---|---|
| 2.2 | 0.9 | 81 | 79 | 0.16 | 0.91 |
| 2.4 | 1.2 | 90 | 88 | 0.00 | 0.83 |
| 3.1 | 1.3 | 81 | 80 | 0.16 | 0.64 |
| 3.8 | 1.6 | 80 | 80 | 0.17 | 0.53 |
| 4.2 | 2.0 | 90 | 87 | 0.00 | 0.48 |
| 4.7 | 2.1 | 84 | 84 | 0.10 | 0.43 |
| 5.0 | 2.3 | 86 | 84 | 0.07 | 0.40 |
| 5.4 | 2.6 | 84 | 89 | 0.10 | 0.37 |
| 6.0 | 2.8 | 83 | 86 | 0.12 | 0.33 |
| 6.3 | 3.2 | 85 | 91 | 0.09 | 0.32 |
| 7.0 | 3.3 | 81 | 87 | 0.16 | 0.28 |
| 7.3 | 3.5 | 91 | 88 | -0.02 | 0.27 |

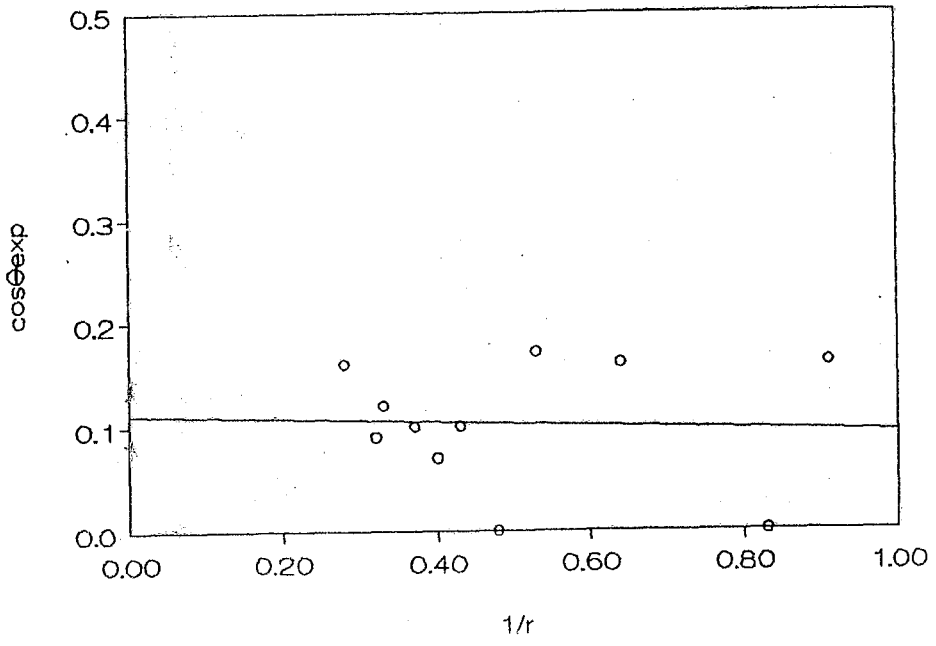


FIGURE A.2. cosθ vs. 1/ r for P2-water drop

TABLE A.3 Data of cosθ vs. 1 / r Graph for P3-$H_20$ drop

| Diameter | Height | Angle | $\theta_{theo}$ | cosθ | 1/r |
|---|---|---|---|---|---|
| 3.0 | 1.2 | 85 | 80 | 0.09 | 0.67 |
| 3.9 | 1.7 | 84 | 82 | 0.10 | 0.51 |
| 4.8 | 2.0 | 79 | 80 | 0.19 | 0.42 |
| 5.8 | 2.4 | 81 | 79 | 0.16 | 0.35 |
| 6.2 | 2.6 | 82 | 80 | 0.14 | 0.32 |
| 6.7 | 2.7 | 79 | 78 | 0.19 | 0.30 |
| 7.6 | 3.1 | 83 | 78 | 0.12 | 0.26 |

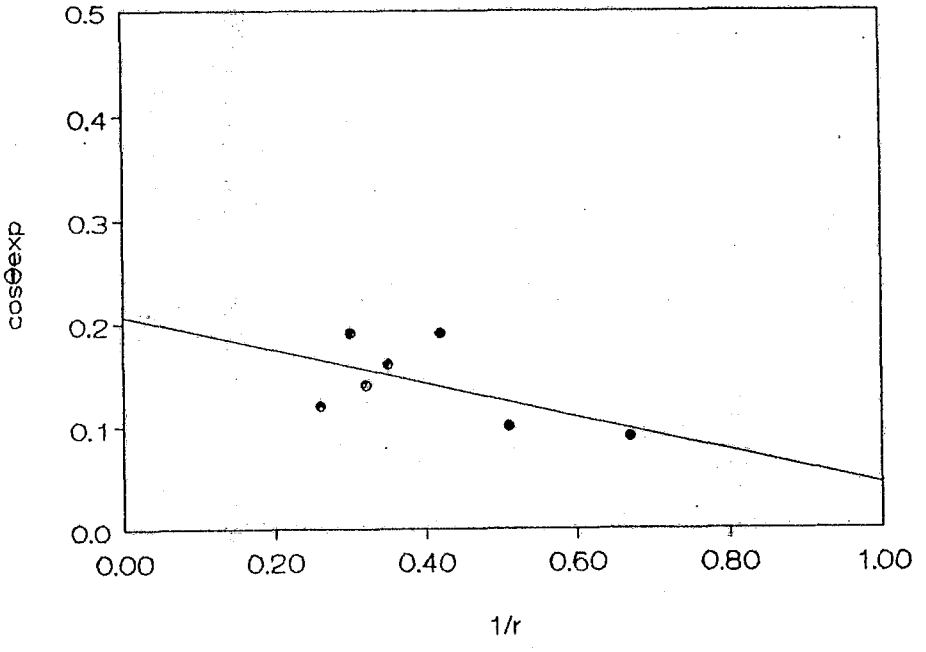


FIGURE A.3. cosθ vs. 1/ r for P3-water drop

TABLE A.4 Data of cosθ vs. 1 / r Graph for P1-Formamide drop

| Diameter | Height | Angle | $\theta_{theo}$ | cosθ | 1/r |
|---|---|---|---|---|---|
| 2.8 | 0.9 | 60 | 65 | 0.50 | 0.71 |
| 3.5 | 1.2 | 59 | 69 | 0.52 | 0.57 |
| 4.3 | 1.6 | 64 | 73 | 0.44 | 0.47 |
| 5.3 | 2.0 | 64 | 74 | 0.44 | 0.38 |
| 6.0 | 2.1 | 64 | 70 | 0.44 | 0.33 |
| 6.7 | 2.3 | 64 | 69 | 0.44 | 0.30 |
| 7.8 | 2.6 | 60 | 67 | 0.50 | 0.26 |

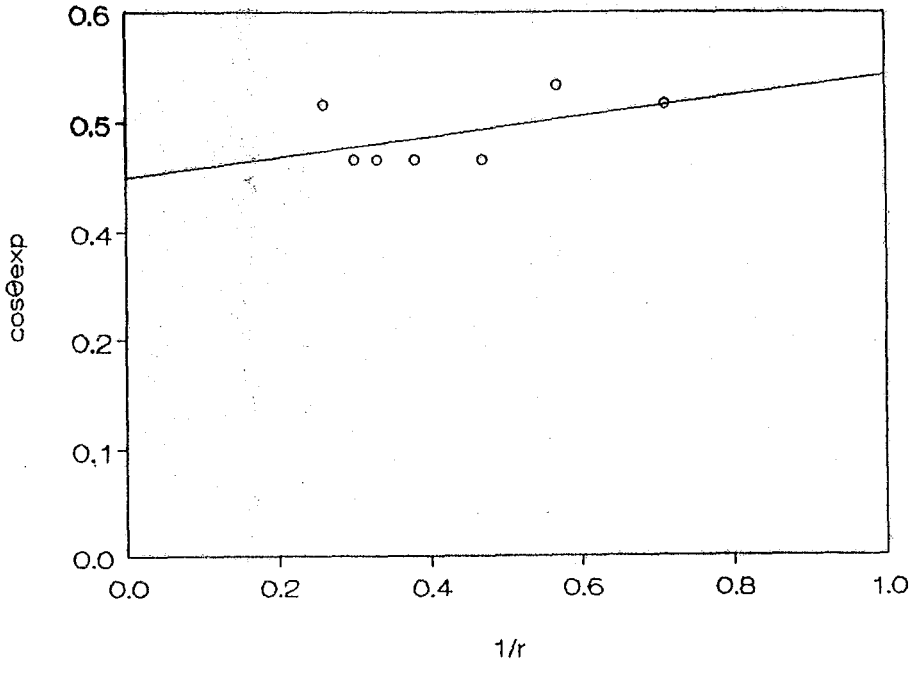


FIGURE A.4. cosθ vs. 1/ r for P1-formamide drop

TABLE A.5 Data of cosθ vs. 1 / r Graph for P2-formamide drop

| Diameter | Height | Angle | $\theta_{theo}$ | cosθ | 1/r |
|---|---|---|---|---|---|
| 2.6 | 1.2 | 85 | 85 | 0.09 | 0.77 |
| 3.9 | 1.7 | 80 | 82 | 0.17 | 0.51 |
| 4.5 | 2.0 | 83 | 83 | 0.12 | 0.44 |
| 5.1 | 2.2 | 80 | 83 | 0.17 | 0.39 |
| 5.9 | 2.5 | 77 | 80 | 0.22 | 0.34 |
| 6.8 | 2.9 | 79 | 81 | 0.19 | 0.29 |
| 7.6 | 3.1 | 78 | 78 | 0.21 | 0.26 |

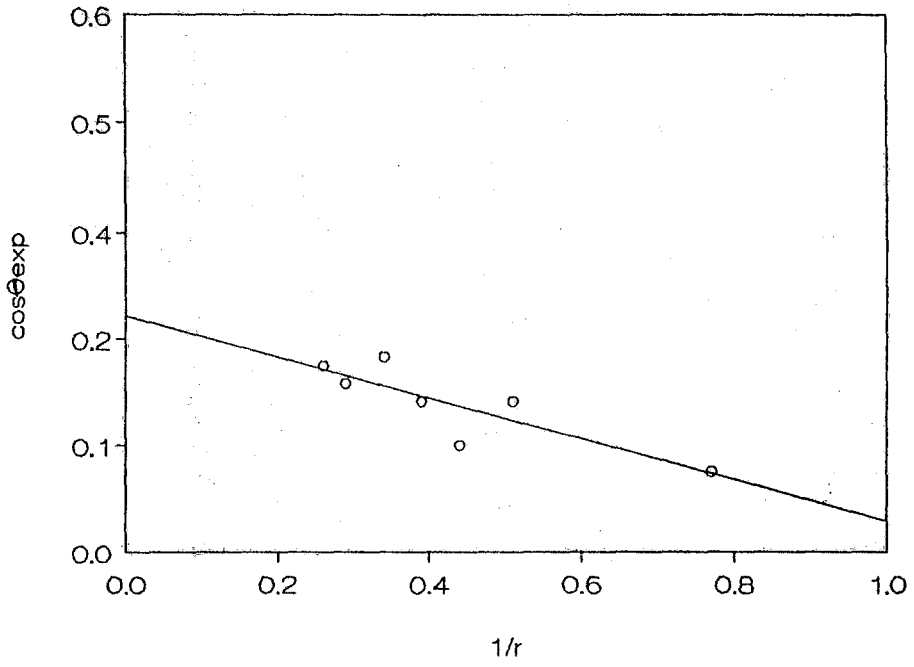


FIGURE A.5. cosθ vs. 1/ r for P2-formamide drop

TABLE A.6 Data of cosθ vs. 1 / r Graph for P3-formamide drop

| Diameter | Height | Angle | $\theta_{theo}$ | cosθ | 1/r |
|---|---|---|---|---|---|
| 2.8 | 1.0 | 68 | 71 | 0.37 | 0.71 |
| 4.0 | 1.6 | 71 | 77 | 0.33 | 0.50 |
| 5.0 | 1.8 | 69 | 73 | 0.36 | 0.40 |
| 6.0 | 2.1 | 70 | 70 | 0.34 | 0.33 |
| 7.0 | 2.3 | 67 | 67 | 0.39 | 0.29 |
| 8.0 | 2.7 | 62 | 68 | 0.47 | 0.25 |

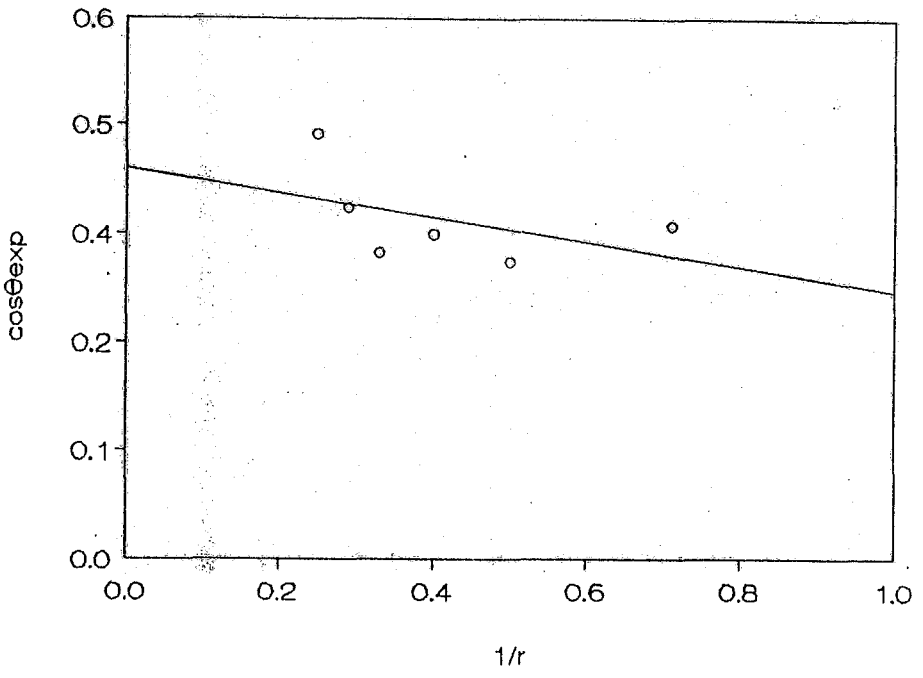


FIGURE A.6. cosθ vs. 1/ r for P3-formamide drop

TABLE A.7 Data of cosθ vs. 1 / r Graph for P1-ethyleneglycol drop

| Diameter | Height | Angle | $\theta_{theo}$ | cosθ | 1/r |
|---|---|---|---|---|---|
| 3.9 | 1.8 | 74 | 85 | 0.28 | 0.51 |
| 5.0 | 2.1 | 73 | 80 | 0.29 | 0.40 |
| 6.0 | 2.4 | 70 | 77 | 0.34 | 0.33 |
| 7.0 | 2.9 | 71 | 79 | 0.33 | 0.29 |
| 8.0 | 3.1 | 70 | 76 | 0.34 | 0.25 |

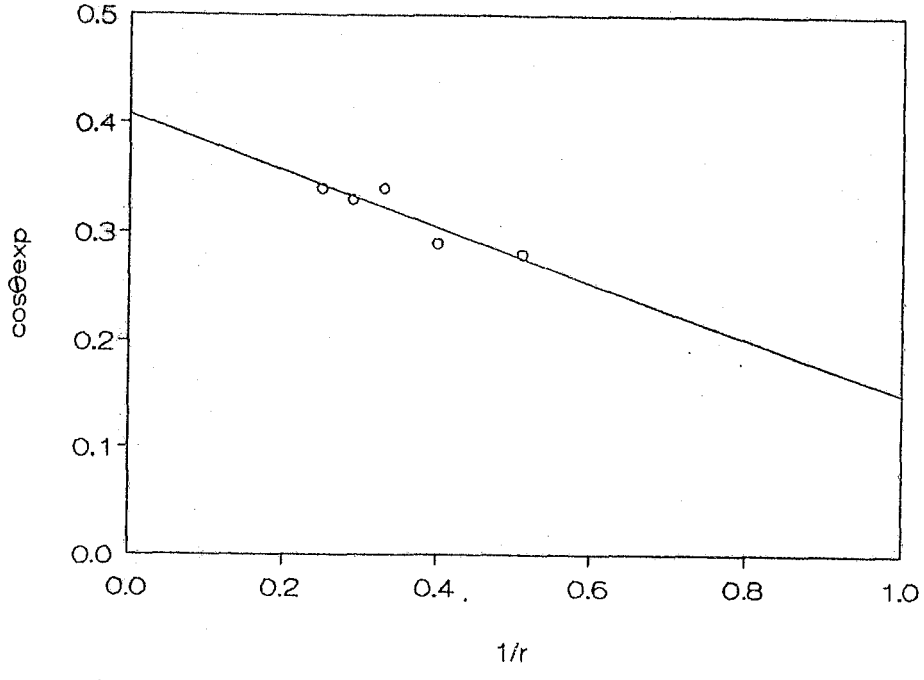


FIGURE A.7. cosθ vs. 1/ r for P1-ethyleneglycol drop

TABLE A.8 Data of cosθ vs. 1 / r Graph for P2-ethyleneglycol drop

| Diameter | Height | Angle | $\theta_{theo}$ | cosθ | 1/r |
|---|---|---|---|---|---|
| 3.9 | 1.8 | 80 | 85 | 0.17 | 0.51 |
| 4.8 | 2.1 | 75 | 82 | 0.26 | 0.42 |
| 5.7 | 2.2 | 74 | 75 | 0.28 | 0.35 |
| 7.2 | 3.0 | 76 | 80 | 0.24 | 0.28 |
| 8.0 | 3.2 | 78 | 77 | 0.21 | 0.25 |

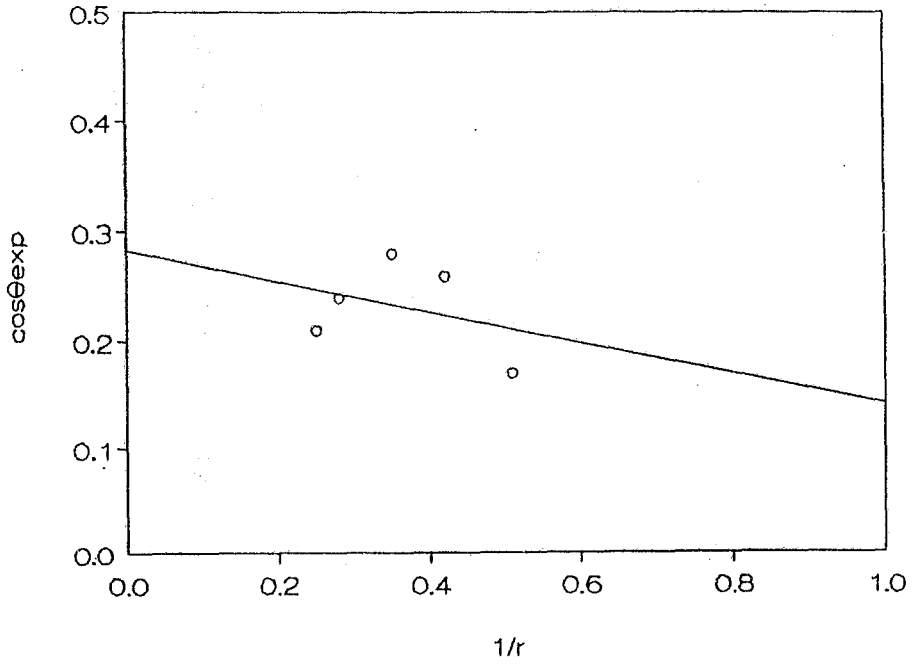


FIGURE A.8. cosθ vs. 1/ r for P2-ethyleneglycol drop

TABLE A.9 Data of cosθ vs. 1 / r Graph for P3-ethyleneglycol drop

| Diameter | Height | Angle | $\theta_{theo}$ | cosθ | 1/r |
|---|---|---|---|---|---|
| 4.7 | 1.8 | 64 | 75 | 0.44 | 0.43 |
| 6.0 | 2.1 | 66 | 70 | 0.41 | 0.33 |
| 7.0 | 2.7 | 70 | 75 | 0.34 | 0.29 |
| 8.3 | 2.8 | 63 | 68 | 0.45 | 0.24 |

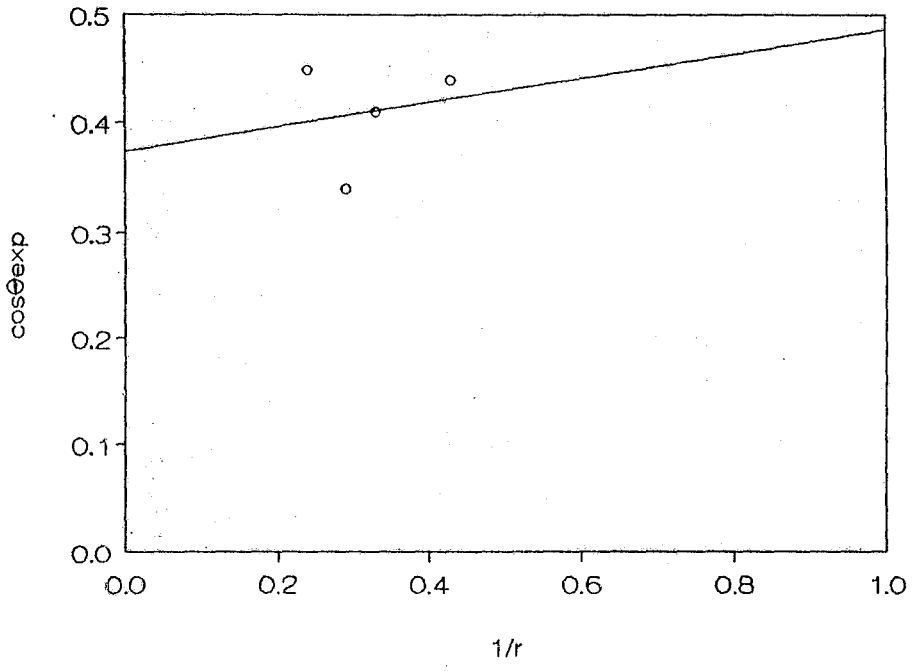


FIGURE A.9. cosθ vs. 1/ r for P3-ethyleneglycol drop

TABLE A.10 Data of cosθ vs. 1 / r Graph for P1-glycerol drop

| Diameter | Height | Angle | $\theta_{theo}$ | cosθ | 1/r |
|---|---|---|---|---|---|
| 2.8 | 1.4 | 87 | 90 | 0.05 | 0.71 |
| 3.8 | 1.8 | 84 | 88 | 0.10 | 0.53 |
| 5.2 | 2.3 | 75 | 83 | 0.26 | 0.38 |
| 6.6 | 3.1 | 86 | 86 | 0.07 | 0.30 |
| 7.5 | 3.2 | 78 | 81 | 0.21 | 0.27 |

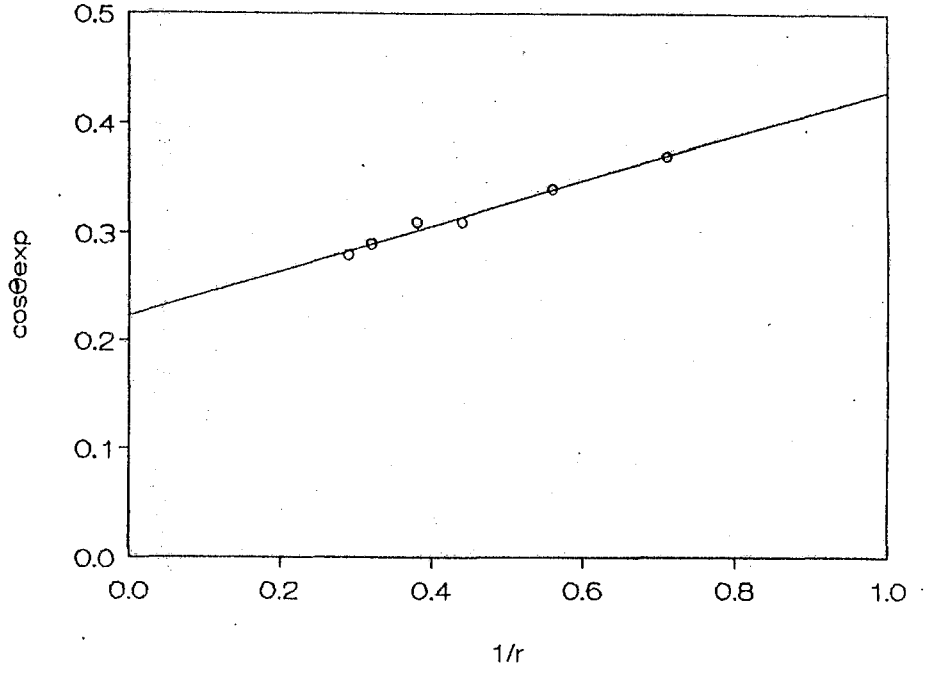


FIGURE A.10 cosθ vs. 1/ r for P1-glycerol drop

TABLE A.11 Data of cosθ vs. 1 / r Graph for P2-glycerol drop

| Diameter | Height | Angle | $\theta_{theo}$ | cosθ | 1/r |
|---|---|---|---|---|---|
| 3.8 | 1.9 | 87 | 90 | 0.05 | 0.53 |
| 5.0 | 2.4 | 84 | 88 | 0.10 | 0.40 |
| 6.3 | 2.9 | 85 | 85 | 0.09 | 0.32 |
| 7.0 | 3.3 | 87 | 87 | 0.05 | 0.29 |

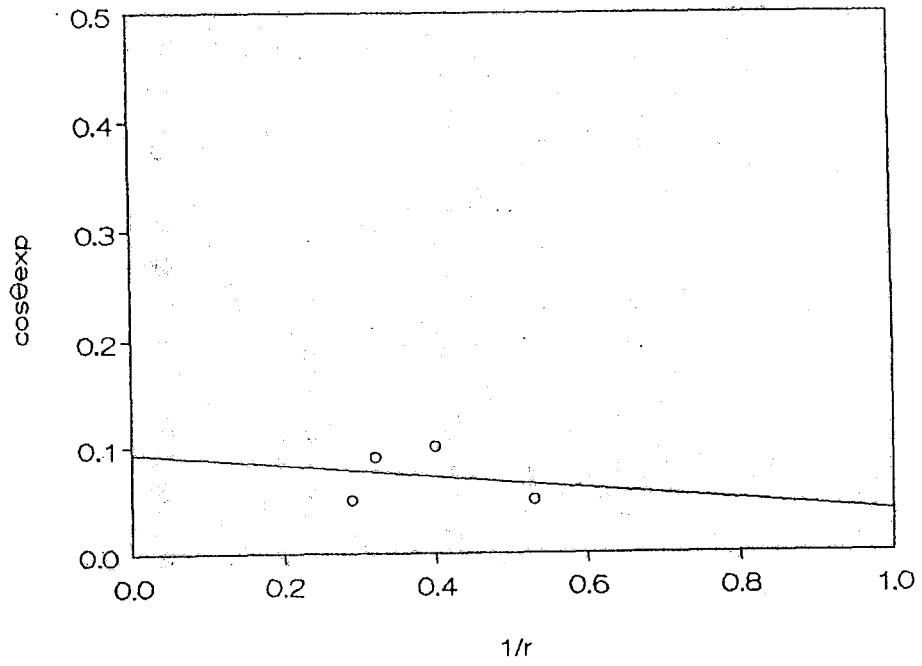


FIGURE A.11 cosθ vs. 1/ r for P2-glycerol drop

TABLE A.12 Data of cosθ vs. 1 / r Graph for P3-glycerol drop

| Diameter | Height | Angle | $\theta_{theo}$ | cosθ | 1/r |
|---|---|---|---|---|---|
| 3.7 | 1.5 | 77 | 78 | 0.22 | 0.54 |
| 5.5 | 2.5 | 80 | 84 | 0.17 | 0.36 |
| 6.7 | 2.8 | 77 | 80 | 0.22 | 0.30 |
| 8.0 | 3.1 | 75 | 76 | 0.26 | 0.25 |

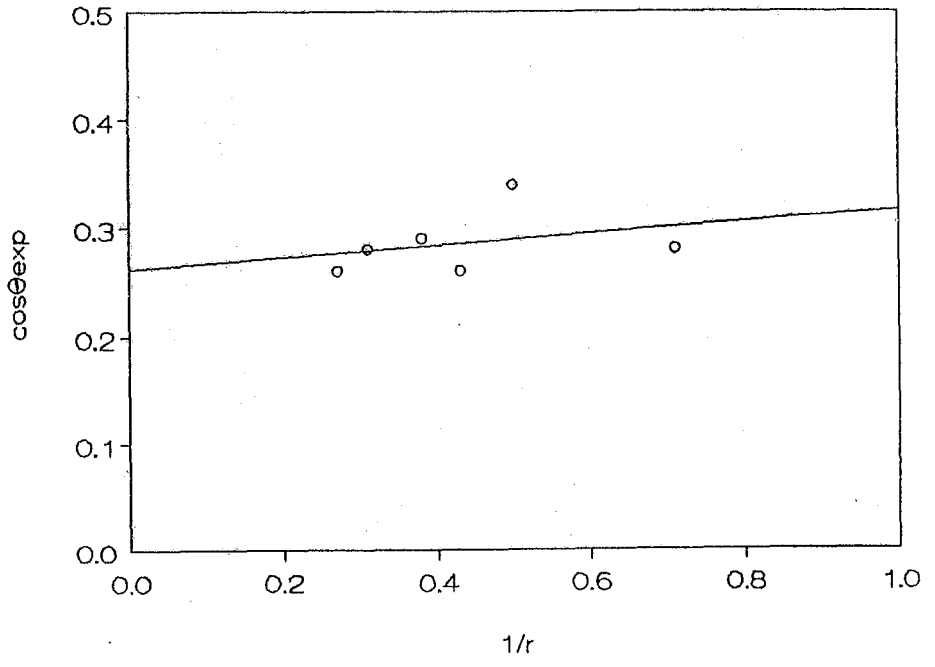


FIGURE A.12 cosθ vs. 1/ r for P3-glycerol drop

TABLE A.13 Data of cosθ vs. 1 / r Graphs for P1,2,3-paraffin drop

| P1 | | P2 | | P3 | |
|---|---|---|---|---|---|
| cosθ | 1/r | cosθ | 1/r | cosθ | 1/r |
| 0.766 | 0.364 | 0.788 | 0.714 | 0.906 | 0.800 |
| 0.829 | 0.328 | 0.961 | 0.667 | 0.891 | 0.408 |
| 0.799 | 0.282 | 0.914 | 0.370 | 0.921 | 0.333 |
| 0.777 | 0.204 | 0.839 | 0.333 | 0.899 | 0.227 |
| - | - | 0.829 | 0.250 | - | - |

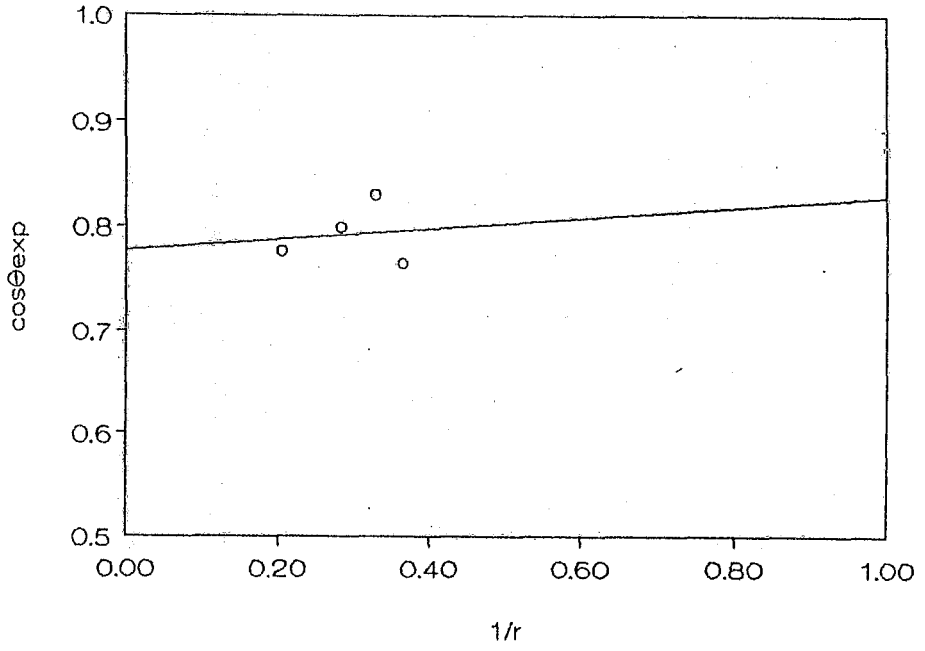


FIGURE A.13 cosθ vs. 1/ r for P1-paraffin drop

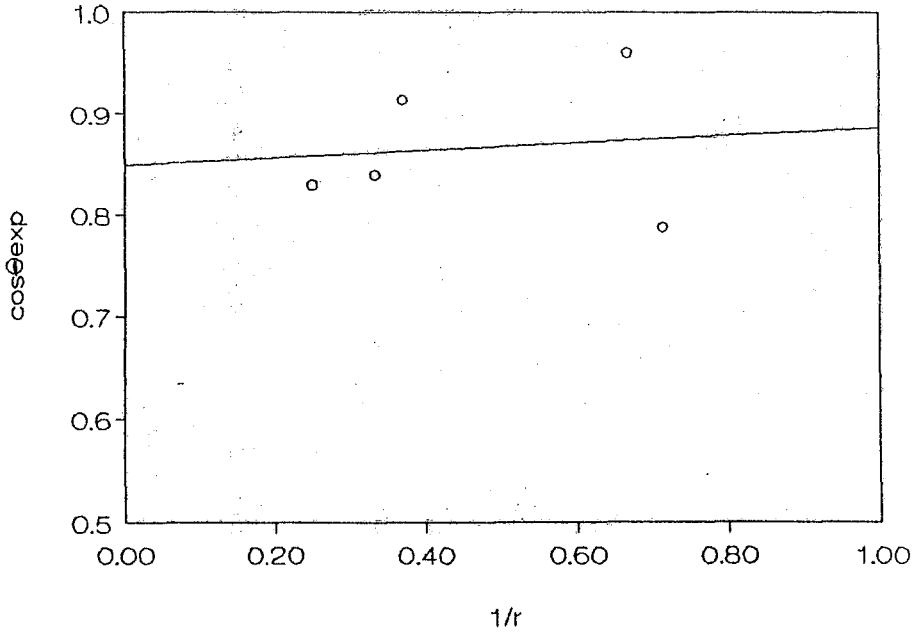


FIGURE A.14. cosθ vs. 1/ r for P2-paraffin drop

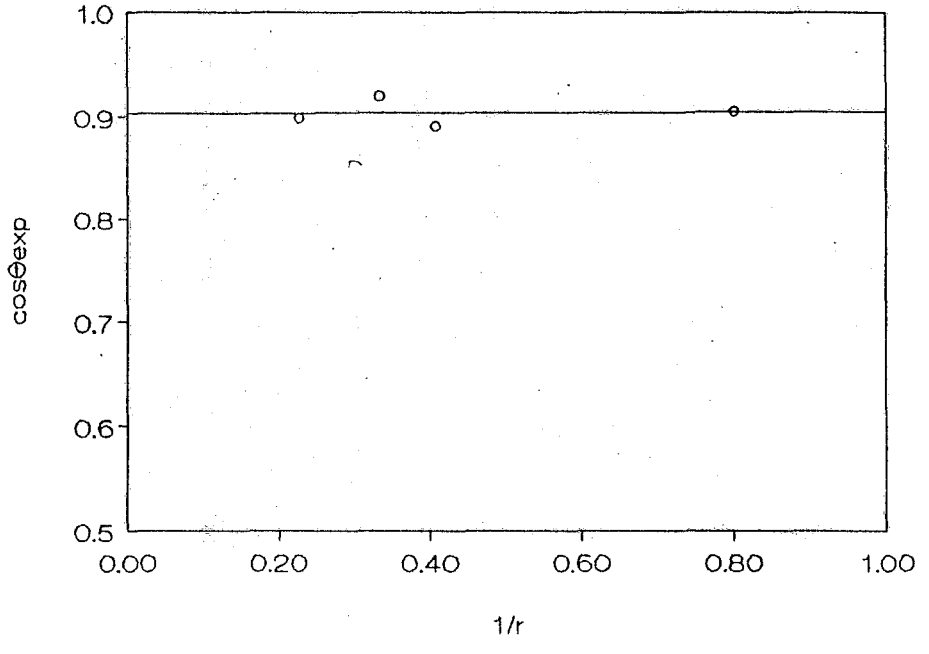


FIGURE A.15. cosθ vs. 1/ r for P3-paraffin drop

# APPENDIX B

## Evaluation of Contact Angles by One Liquid Method

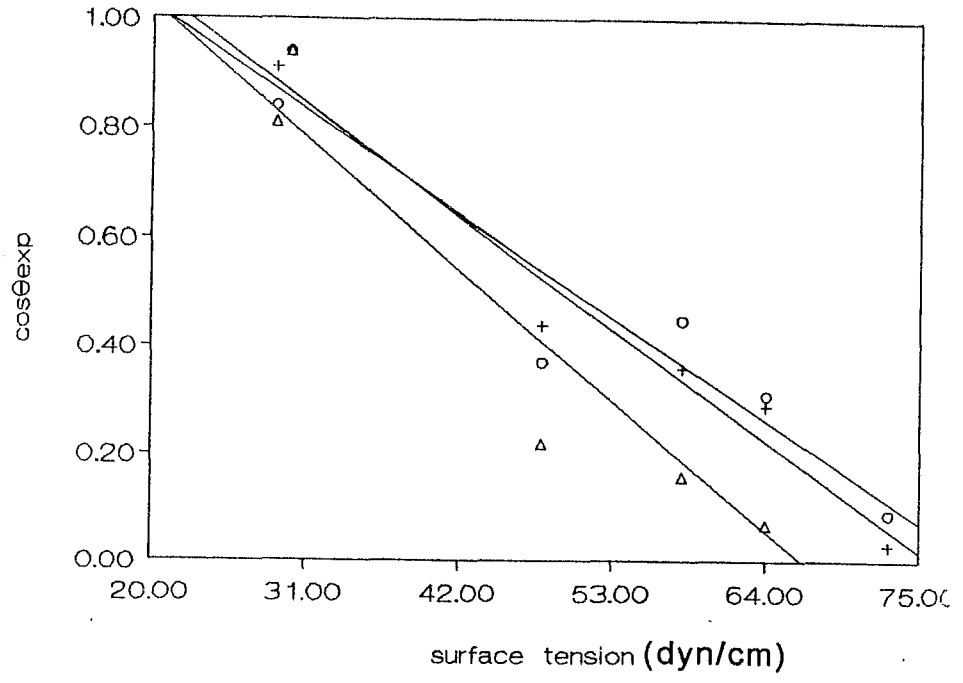


FIGURE B.1. Zisman Plot

One Liquid Method:

One apolar liquid (paraffin) was used to solve $\gamma_S^{LW}$ (first eqn) and two polar liquids were used to solve for $\gamma_S^+$ and $\gamma_S^-$ (second eqn)

$$(1+\cos\theta)\gamma_L = 2(\gamma_S^{LW}\gamma_{par}^{LW})^{1/2}$$

$$E = C(\gamma_S^+)^{1/2} + D(\gamma_S^-)^{1/2}$$

TABLE B.1. E values for one liquid calculations

| E | water | formamide | ethylene glycol | glycerol |
|---|---|---|---|---|
| P1 | 32.994 | 22.603 | 12.75 | 26.141 |
| P2 | 21.33 | 3.325 | 3.827 | 8.943 |
| P3 | 27.492 | 14.786 | 13.854 | 22.955 |

TABLE B.2. Coefficients of one liquid method eqn

| | B | C | D |
|---|---|---|---|
| water | 9.34 | 10.1 | 10.1 |
| formamide | 12.49 | 12.59 | 3.02 |
| ethylene glycol | 10.77 | 13.71 | 2.77 |
| glycerol | 11.66 | 15.15 | 3.96 |

With three polar liquids following eqn was solved by Mathematica

$$A=B(\gamma_S^{LW})^{1/2}+C(\gamma_S^{+})^{1/2}+D(\gamma_S^{-})^{1/2}$$

$$A=\gamma_L(1+\cos\theta) \qquad B=2(\gamma_L^{LW})^{1/2} \qquad C=(\gamma_L^{-})^{1/2} \qquad D=(\gamma_L^{+})^{1/2}$$

TABLE B.3. A values used in one liquid method

| A | P1 | P2 | P3 |
|---|---|---|---|
| water | 79.14 | 68.99 | 75.34 |
| formamide | 84.33 | 67.07 | 78.78 |
| ethylene glycol | 65.98 | 58.8 | 69.04 |
| glycerol | 83.78 | 68.46 | 82.71 |

# APPENDIX C

## Evaluation of Contact Angles by Two Liquid Method

Two Liquid Method:

$y=\gamma_P-\gamma_B+\gamma_{PB}\cos\vartheta_{SP}$ $x=2\{(\gamma_P^d)^{1/2}-(\gamma_B^d)^{1/2}$

$l_s^n$ and $\gamma_s^d$ was found from the intercept and slope of y versus x graphs respectively. (Only y changes with the sample)

For paraffin bulk phase:

TABLE C.1. Data for paraffin bulk phase

| drop | x | y(P1) | y(P2) | y(P3) |
|---|---|---|---|---|
| water | -1.414 | 14.074 | 6.494 | 4.066 |
| ethylene glycol | 0.019 | 14.866 | 7.619 | 6.726 |
| formamide | 1.738 | 18.525 | 12.042 | 10.397 |

For paraffin drop:

TABLE C.2. Data for paraffin drop

| bulk | x | y(P1) | y(P2) | y(P3) |
|---|---|---|---|---|
| water | -1.414 | 11.175 | 2.923 | -1.133 |
| ethylene glycol | 0.019 | 15.163 | 7.851 | 4.942 |
| formamide | 1.738 | 14.939 | 8.066 | 6.143 |

# APPENDIX D

## Time Dependence of Contact Angles

TABLE D.1. Data for Time Dependence of Water Drops

| P1/$H_2O$ drop | | P2/$H_2O$ drop | | P3/$H_2O$ drop | |
|---|---|---|---|---|---|
| θ | t | θ | t | θ | t |
| 74 | 0sec | 73 | 0sec | 80 | 0sec |
| 73 | 15sec | 72 | 30sec | 79 | 30sec |
| 72 | 30sec | 72 | 60sec | 77 | 60sec |
| 72 | 45sec | 71 | 1.30 | 73 | 2.0 |
| 72 | 60sec | 69 | 2.0 | 70 | 2.30 |
| 69 | 2.0 | 67 | 2.30 | 67 | 3.0 |
| 67 | 2.30 | 66 | 3.0 | 64 | 3.30 |
| 66 | 3.0 | 66 | 3.30 | 62 | 4.0 |
| 64 | 3.30 | 64 | 4.0 | 59 | 4.30 |
| 63 | 4.0 | 61 | 4.30 | 58 | 5.0 |
| 61 | 4.30 | 60 | 5.0 | 56 | 5.30 |
| 59 | 5.0 | 58 | 5.30 | 53 | 6.0 |
| 57 | 5.30 | 57 | 6.0 | 52 | 6.30 |
| 54 | 6.0 | 55 | 6.30 | 50 | 7.0 |
| 52 | 6.30 | 53 | 7.0 | 48 | 7.30 |
| 48 | 7.0 | 52 | 7.30 | 45 | 8.0 |
| 47 | 7.30 | 50 | 8.0 | 43 | 8.30 |
| 45 | 8.0 | 48 | 8.30 | 40 | 9.0 |
| 44 | 8.30 | 45 | 9.0 | 37 | 9.30 |
| 41 | 9.0 | 44 | 9.30 | 34 | 10.0 |
| 38 | 9.30 | 42 | 10.0 | 30 | 10.30 |
| 36 | 10.0 | 40 | 10.30 | 26 | 11.0 |
| 34 | 10.30 | 38 | 11.0 | 23 | 11.30 |
| 31 | 11.0 | 36 | 11.30 | 18 | 12.0 |
| 29 | 11.30 | 33 | 12.0 | 15 | 12.30 |
| 26 | 12.0 | 31 | 12.30 | 12 | 13.0 |
| 24 | 12.30 | 27 | 13.0 | | |
| 24 | 13.0 | 25 | 13.30 | | |
| 20 | 13.30 | 23 | 14.0 | | |
| 17 | 14.0 | 20 | 14.30 | | |
| 14 | 14.30 | 18 | 15.0 | | |
| 12 | 15.0 | 16 | 15.30 | | |
| | | 13 | 16.0 | | |

TABLE D.2. Data for Time Dependence of Ethyleneglycol Drops

| P1/eth.gly | | P2/eth.gly | | P3/eth.gly | |
|---|---|---|---|---|---|
| θ | t | θ | t | θ | t |
| 63 | 0sec | 71 | 0sec | 70 | 0sec |
| 62 | 30sec | 71 | 30sec | 68 | 30sec |
| 61 | 60sec | 70 | 60sec | 66 | 60sec |
| 60 | 1.30 | 69 | 1.30 | 64 | 1.30 |
| 60 | 2.0 | 67 | 2.0 | 61 | 2.0 |
| 60 | 2.30 | 66 | 2.30 | 59 | 2.30 |
| 59 | 3.0 | 66 | 3.0 | 58 | 3.0 |
| 58 | 3.30 | 66 | 4.0 | 56 | 3.30 |
| 58 | 4.0 | 66 | 5.0 | 56 | 4.0 |
| 58 | 4.30 | 66 | 6.0 | 55 | 4.30 |
| 57 | 5.0 | 66 | 7.0 | 55 | 5.0 |
| 57 | 5.30 | 66 | 8.0 | 55 | 6.0 |
| 57 | 6.0 | 66 | 9.0 | 54 | 6.30 |
| 56 | 6.30 | 66 | 10.0 | 54 | 7.0 |
| 56 | 7.0 | 66 | 11.0 | 54 | 8.0 |
| 56 | 7.30 | 66 | 12.0 | 53 | 8.30 |
| 56 | 8.0 | 66 | 13.0 | 53 | 9.0 |
| 56 | 8.30 | 66 | 14.0 | 53 | 10.0 |
| 56 | 9.0 | 66 | 15.0 | 53 | 11.0 |
| 56 | 9.30 | | | 53 | 12.0 |
| 56 | 10.0 | | | 53 | 13.0 |
| 56 | 11.0 | | | 53 | 14.0 |
| 56 | 12.0 | | | 53 | 15.0 |
| 56 | 13.0 | | | | |
| 56 | 14.0 | | | | |
| 56 | 15.0 | | | | |

TABLE D.3. Data for Time Dependence of Formamide Drops

| P1/formamide | | P2/formamide | | P3/formamide | |
|---|---|---|---|---|---|
| θ | t | θ | t | θ | t |
| 59 | 0 | 73 | 0 | 76 | 0 |
| 59 | 0.5 | 72 | 0.5 | 74 | 1 |
| 59 | 1 | 71 | 1 | 68 | 1.50 |
| 59 | 2.0 | 70 | 2.0 | 65 | 2.0 |
| 59 | 4.0 | 69 | 3.0 | 64 | 2.50 |
| 59 | 6.0 | 68 | 5.0 | 63 | 3.0 |
| 59 | 8.0 | 68 | 6.0 | 62 | 3.50 |
| 59 | 10.0 | 68 | 8.0 | 61 | 4.0 |
| 59 | 12.0 | 68 | 10.0 | 61 | 5.0 |
| 59 | 14.0 | 68 | 12.0 | 60 | 6.0 |
| 59 | 16.0 | 68 | 14.0 | 60 | 7.0 |
| 59 | 18.0 | 68 | 16.0 | 59 | 8.0 |
| 59 | 20.0 | 67 | 17.0 | 59 | 10.0 |
| | | 67 | 18.0 | 59 | 12.0 |
| | | 67 | 19.0 | 59 | 14.0 |
| | | 67 | 20.0 | 59 | 16.0 |
| | | | | 59 | 18.0 |
| | | | | 59 | 20.0 |

TABLE D.4. Data for Time Dependence of Glycerol Drops

| P1/Glycerol | | P2/ Glycerol | | P3/ Glycerol | |
|---|---|---|---|---|---|
| θ | t | θ | t | θ | t |
| 77 | 0sec | 89 | 0sec | 90 | 0sec |
| 74 | 30sec | 87 | 30sec | 86 | 60sec |
| 73 | 60sec | 86 | 60sec | 81 | 1.30 |
| 72 | 1.30 | 86 | 2.0 | 80 | 2.0 |
| 71 | 2.0 | 86 | 3.0 | 78 | 2.30 |
| 71 | 3.0 | 86 | 4.0 | 76 | 3.0 |
| 71 | 4.0 | 86 | 6.0 | 75 | 3.30 |
| 71 | 5.0 | 86 | 8.0 | 75 | 4.0 |
| 71 | 6.0 | 86 | 10.0 | 74 | 5.0 |
| 70 | 7.0 | 86 | 12.0 | 73 | 6.0 |
| 70 | 8.0 | 86 | 14.0 | 73 | 8.0 |
| 69 | 9.0 | 86 | 16.0 | 73 | 10.0 |
| 69 | 10.0 | 86 | 18.0 | 73 | 11.0 |
| 68 | 11.0 | 86 | 20.0 | 72 | 12.0 |
| 68 | 12.0 | | | 72 | 14.0 |
| 68 | 14.0 | | | 72 | 16.0 |
| 68 | 16.0 | | | 72 | 18.0 |
| 68 | 18.0 | | | 72 | 20.0 |
| 68 | 20.0 | | | | |

# APPENDIX E

## Time Dependence of Contact Angles of Water on P1 in Saturated Medium

TABLE E.1. Data for 1. P1-water drop in saturated medium

| θ | t | d | h | V | A |
|---|---|---|---|---|---|
| 81 | 0 | 6.2 | 2.4 | 49.68 | 52.21 |
| 75 | 3 | 6.1 | 2.3 | 40.91 | 46.43 |
| 74 | 4 | 6.1 | 2.3 | 39.94 | 45.82 |
| 74 | 5 | 6.1 | 2.3 | 39.94 | 45.82 |
| 73 | 6 | 6.1 | 2.3 | 39.00 | 45.23 |
| 73 | 7 | 6.1 | 2.3 | 39.00 | 45.23 |
| 73 | 8 | 6.1 | 2.3 | 39.00 | 45.23 |
| 72 | 9 | 6.1 | 2.22 | 38.08 | 44.65 |
| 72 | 10 | 6.1 | 2.22 | 38.08 | 44.65 |
| 72 | 11 | 6.1 | 2.22 | 38.08 | 44.65 |
| 71 | 12 | 6.1 | 2.18 | 37.18 | 44.09 |
| 71 | 13 | 6.1 | 2.18 | 37.18 | 44.09 |
| 70 | 14 | 6.1 | 2.2 | 36.31 | 43.55 |
| 70 | 15 | 6.1 | 2.2 | 36.31 | 43.55 |
| 69 | 16 | 6.1 | 2.2 | 34.45 | 43.03 |
| 69 | 17 | 6.1 | 2.2 | 34.45 | 43.03 |
| 69 | 19 | 6.1 | 2.2 | 34.45 | 43.03 |
| 68 | 22 | 6.1 | 2.2 | 34.62 | 42.52 |
| 68 | 24 | 6.1 | 2.1 | 34.62 | 42.52 |
| 68 | 26 | 6.1 | 2.1 | 34.62 | 42.52 |
| 67 | 26 | 6.1 | 2.1 | 34.62 | 42.52 |
| 67 | 27 | 6.1 | 2.1 | 33.81 | 42.03 |
| 66 | 28 | 6.1 | 2 | 33.01 | 41.55 |
| 66 | 30 | 6.1 | 2 | 33.01 | 41.55 |
| 65 | 32 | 6.1 | 2 | 32.23 | 41.08 |
| 65 | 34 | 6.1 | 2 | 32.23 | 41.08 |
| 65 | 36 | 6.1 | 2 | 32.23 | 41.08 |
| 64 | 38 | 6.1 | 2 | 31.47 | 40.64 |
| 63 | 40 | 6.1 | 1.9 | 30.73 | 40.20 |
| 62 | 43 | 6.1 | 1.9 | 30.00 | 39.78 |
| 62 | 45 | 6.1 | 1.9 | 30.00 | 39.78 |
| 61 | 47 | 6.1 | 1.9 | 29.29 | 39.36 |
| 60 | 50 | 6.1 | 1.8 | 28.59 | 38.97 |
| 58 | 54 | 6.1 | 1.7 | 27.23 | 38.20 |
| 57 | 56 | 6.1 | 1.6 | 26.58 | 37.84 |
| 56 | 59 | 6.1 | 1.6 | 25.93 | 37.49 |
| 55 | 60 | 6.1 | 1.6 | 25.30 | 37.14 |
| 53 | 64 | 6.1 | 1.6 | 24.06 | 36.49 |
| 51 | 69 | 6.1 | 1.5 | 22.87 | 35.87 |

| | | | | | |
|---|---|---|---|---|---|
| 47 | 78 | 6.1 | 1.4 | 20.60 | 34.75 |
| 45 | 81 | 6.1 | 1.3 | 19.52 | 34.24 |
| 42 | 90 | 6.1 | 1.25 | 17.95 | 33.53 |
| 41 | 94 | 6.1 | 1.2 | 17.44 | 33.31 |
| 41 | 96 | 6.1 | 1.2 | 17.44 | 33.31 |
| 39 | 100 | 6.0 | 1.15 | 15.65 | 31.82 |
| 38 | 102 | 5.9 | 1.1 | 14.43 | 30.58 |
| 37 | 105 | 5.8 | 1.1 | 13.30 | 29.38 |
| 37 | 109 | 5.7 | 1.1 | 12.62 | 28.37 |
| 37 | 112 | 5.6 | 1.1 | 11.97 | 27.39 |
| 37 | 118 | 5.6 | 1.1 | 11.97 | 27.39 |
| 37 | 120 | 5.5 | 1.0 | 11.34 | 26.42 |
| 39 | 124 | 5.4 | 1.0 | 11.41 | 25.77 |
| 40 | 126 | 5.3 | 1.0 | 11.12 | 24.98 |
| 39 | 130 | 5.3 | 1.0 | 10.78 | 24.83 |
| 38 | 133 | 5.3 | 1.0 | 10.46 | 24.68 |
| 38 | 135 | 5.3 | 1.0 | 10.46 | 24.68 |
| 37 | 137 | 5.2 | 0.9 | 9.58 | 23.61 |
| 37 | 140 | 5.2 | 0.9 | 9.58 | 23.61 |
| 36 | 144 | 5.2 | 0.9 | 9.29 | 23.48 |
| 35 | 146 | 5.2 | 0.8 | 8.99 | 23.35 |
| 33 | 150 | 5.2 | 0.8 | 8.42 | 23.10 |
| 30 | 157 | 5.2 | 0.7 | 7.57 | 22.76 |
| 26 | 161 | 5.2 | 0.7 | 6.49 | 22.37 |
| 24 | 165 | 5.1 | 0.6 | 5.62 | 21.35 |
| 22 | 168 | 5.1 | 0.6 | 5.13 | 21.20 |
| 22 | 171 | 5.0 | 0.5 | 4.83 | 20.38 |
| 20 | 174 | 4.9 | 0.5 | 4.12 | 19.44 |
| 20 | 177 | 4.9 | 0.4 | 4.12 | 19.44 |
| 25 | 180 | 4.5 | 0.4 | 4.03 | 16.68 |
| 23 | 183 | 4.2 | 0.4 | 3.00 | 14.43 |
| 22 | 185 | 4.1 | 0.4 | 2.66 | 13.70 |
| 20 | 188 | 4.0 | 0.4 | 2.24 | 12.96 |
| 20 | 190 | 3.8 | 0.4 | 1.92 | 11.69 |
| 18 | 192 | 3.4 | 0.3 | 1.23 | 9.31 |
| 17 | 195 | 3.1 | 0.3 | 0.88 | 7.72 |
| 15 | 198 | 2.9 | 0.25 | 0.63 | 6.72 |
| 15 | 200 | 2.7 | 0.25 | 0.51 | 5.82 |
| 15 | 204 | 2.5 | 0.25 | 0.41 | 4.99 |
| 12 | 210 | 2.2 | 0.2 | 0.22 | 3.84 |

TABLE E.2. Data for 2. P1-water drop in saturated medium

| θ | t | d | h | V | A |
|---|---|---|---|---|---|
| 63 | 0 | 6 | 1.95 | 33.7 | 41.63 |
| 63 | 3 | 5.8 | 1.95 | 26.42 | 36.34 |
| 62 | 5 | 5.8 | 1.95 | 25.79 | 35.96 |
| 61 | 15 | 5.8 | 1.8 | 25.18 | 35.59 |
| 59 | 16 | 5.8 | 1.8 | 23.99 | 34.88 |
| 58 | 17 | 5.8 | 1.75 | 23.41 | 34.54 |
| 57 | 20 | 5.8 | 1.7 | 22.84 | 34.21 |
| 56 | 25 | 5.8 | 1.7 | 22.29 | 33.89 |
| 55 | 27 | 5.8 | 1.65 | 21.74 | 33.58 |
| 54 | 30 | 5.8 | 1.6 | 21.21 | 33.28 |
| 53 | 33 | 5.8 | 1.6 | 20.68 | 32.99 |
| 51 | 36 | 5.8 | 1.5 | 19.66 | 32.43 |
| 48 | 47 | 5.8 | 1.3 | 18.18 | 31.66 |
| 45 | 52 | 5.8 | 1.25 | 16.78 | 30.95 |
| 44 | 55 | 5.8 | 1.2 | 16.32 | 30.73 |
| 44 | 58 | 5.8 | 1.2 | 16.32 | 30.73 |
| 43 | 61 | 5.8 | 1.2 | 15.87 | 30.52 |
| 42 | 64 | 5.7 | 1.2 | 14.64 | 29.28 |
| 45 | 66 | 5.5 | 1.2 | 14.31 | 27.83 |
| 43 | 69 | 5.5 | 1.2 | 13.53 | 27.44 |
| 42 | 72 | 5.5 | 1.15 | 13.16 | 27.26 |
| 42 | 74 | 5.4 | 1.15 | 12.45 | 26.28 |
| 41 | 77 | 5.4 | 1.1 | 12.10 | 26.10 |
| 40 | 82 | 5.4 | 1.05 | 11.75 | 25.94 |
| 39 | 86 | 5.3 | 1 | 10.78 | 24.83 |
| 41 | 88 | 5.2 | 1 | 10.80 | 24.20 |
| 44 | 90 | 5.1 | 1.1 | 11.1 | 23.76 |
| 45 | 92 | 5.1 | 1 | 11.41 | 23.93 |
| 46 | 95 | 5 | 1 | 11.04 | 23.17 |
| 35 | 100 | 5 | 1 | 8.0 | 21.59 |
| 33 | 105 | 5 | 0.95 | 7.48 | 21.36 |
| 35 | 109 | 5 | 0.95 | 8.0 | 21.59 |
| 33 | 105 | 5 | 0.95 | 7.48 | 21.36 |
| 35 | 109 | 5 | 0.95 | 8.0 | 21.59 |
| 32 | 114 | 5 | 0.90 | 7.23 | 21.25 |
| 30 | 115 | 5 | 0.8 | 6.73 | 21.04 |
| 29 | 117 | 5 | 0.8 | 6.49 | 20.95 |
| 27 | 119 | 5 | 0.75 | 6 | 20.77 |
| 26 | 122 | 5 | 0.75 | 5.77 | 20.68 |
| 23 | 127 | 5 | 0.65 | 5.06 | 20.45 |
| 23 | 130 | 4.8 | 0.6 | 4.48 | 18.84 |

TABLE E.2. cont

| | | | | | |
|---|---|---|---|---|---|
| 25 | 137 | 4.8 | 0.55 | 4.89 | 18.98 |
| 23 | 142 | 4.8 | 0.45 | 4.48 | 18.84 |
| 21 | 145 | 4.8 | 0.4 | 4.07 | 18.72 |
| 19 | 148 | 4.8 | 0.4 | 3.67 | 18.60 |
| 18 | 151 | 4.7 | 0.35 | 3.26 | 17.78 |
| 15 | 152 | 4.7 | 0.3 | 2.7 | 17.65 |
| 17 | 153 | 4 | 0.4 | 1.89 | 12.85 |
| 18 | 154 | 3.8 | 0.4 | 1.72 | 11.62 |
| 25 | 156 | 3.4 | 0.4 | 1.74 | 9.52 |
| 23 | 157 | 3.4 | 0.4 | 1.59 | 9.46 |
| 25 | 160 | 3.4 | 0.4 | 1.74 | 9.52 |
| 22 | 161 | 3.3 | 0.4 | 1.39 | 8.88 |
| 19 | 164 | 3.3 | 0.35 | 1.19 | 8.79 |
| 17 | 166 | 3.25 | 0.25 | 1.01 | 8.48 |
| 15 | 170 | 3.1 | 0.2 | 0.77 | 7.68 |
| 13 | 171 | 3 | 0.15 | 0.61 | 7.16 |
| 11 | 173 | 3 | 0.1 | 0.51 | 7.13 |

# REFERENCES

1. Inoue H., A. Matsumoto, K. Matsuwaka, A. Ueda and S. Nagai "Surface Characteristics of Polydimethylsiloxane-Polymethylmethacrylate Block Copolymers and Their PMMA Blends," *J. Applied Polymer Science,* 41, pp.1815-1829, 1990

2. Clark D.T. "The Investigation of Polymer Surfaces by means of ESCA," in D. Clark (Ed.), *Polymer Surfaces*, pp. 309-351, John Wiley and Sons, 1978

3. Chen X., J.A. Gardella, R.E. Cohen "Surface Study of Diblock Copolymers of Polydimethylsiloxane and Nylon-6 by Electron Spectroscopy for Chemical Analysis," *Macromolecules,* 27, 2206-2210, 1994

4. Chen X., J.A. Gardella "Surface Modification of Polymers by Blending Siloxane Block Copolymers," *Macromolecules,* 27, 3363-3369, 1994

5. Lovinger A.J., B.J. Han, F.J. Padden "Morphology and Properties of Polycaprolactone-Polydimethylsiloxane-Polycaprolactone Triblock Copolymers," *J. Polymer Science, Polymer Physics Ed.,* 31, pp.115-123, 1993

6. Yılgör I., W.P. Steckle, E. Yılgör, R.G. Freelin, J.S. Riffle "Novel Triblock Siloxane Copolymers: Synthesis, Characterization, and Their Use as Surface Modifiying Additives," *J Polymer Science, Polymer Chemistry Ed.*, 27, pp.3673-3690, 1989

7. Yılgör I., J. McGrath "Polysiloxane Containing Copolymers: A Survey of Recent Developments," *Advances in Polymer Science,* 86, pp.1-86, 1988

8. Clark D.T. and J. Peeling "Application of ESCA to Polymer Chemistry," *J. Polymer Science, Polymer Chemistry Ed.,* 14, pp.543-551, 1976

9. Inoue H., A. Ueda and S. Nagai "Block Copolymers Derived From Azobiscyanopentanoic Acid, Properties of Silicone-PMMA Block Copolymers," *J. Applied Polymer Science,* 35, pp.2039-2051, 1988

10. Smith S.D., J.M. DeSimone, D.W. Dwight, J.E. McGrath "Synthesis and Characterization of Polymethylmethacrylate-Polydimethylsiloxane Copolymers," *Macromolecules,* 25, pp.2575-2581, 1992

11. Chen X., J.A. Gardella, P.L. Kumler "Fourier Transform Infrared and Electron Spectroscopy for Chemical Analysis Studies of Block Copolymers of Styrene and Dimethylsiloxane," *Macromolecules,* 25, pp.6621-6630, 1992

12. Pertsin A.J., M.M. Gorelova, V.Y. Levin, L.I. Makarova "An XPS Study of the Surface-Bulk Compositional Differences in Siloxane Containing Block Copolymers and Polymer Blends," J. *Applied Polymer Science,* 45, pp.1195-1202, 1992

13. Benrashid R., G.L. Nelson, J.H. Linn, K.H. Hanley, W.R. Wade "Surface Characterization of Segmented Siloxane-Urethane Block Copolymers," *J. Applied Polymer Science,* 49, pp.523-537, 1993

14.Lewis K.B., B.D. Ratner "Observation of Surface Rearrangement of Polymers Using ESCA," *J. Colloid and Interface Science,* 159, pp.77-85, 1993

15.Chen X., J.A. Gardella, T. Ho, K.J. Wynne "Surface Composition of a Series of Dimethylsiloxane-Urea-Urethane Segmented Copolymers Studied by ESCA," *Macromolecules,* 28, pp.1635-1642, 1995

16.Lopez L.C., D.W. Dwight "Preferential Enrichment of Chemistry at Polymer Surfaces," *J. Applied Polymer Science,* 36, pp.1404-1415, 1988

17.Pertsin A.J., M.M. Gorelova, V.Y. Levin, L.I. Makarova, L.V. Filimonova " An XPS Study of the Surface-Bulk Compositional Differences in Siloxane Containing Block Copolymers and Polymer Blends," *J. Applied Polymer Science,* 45, pp.2075-2078, 1992

18.Adamson A.W. in *Physical Chemistry of Surfaces,* 5th ed., Wiley Interscience, New York, 1990

19.Young T., "Contact Angle Phenomena in Surface Chemistry," *Trans. R. Soc. London,* 95, pp.65, 1805

20.Dupre A., "Surface Tension Determination by Contact Angle," *Theorie Mechanique de la Chaleur,* pp. 369, Gauthier-Villars, Paris, 1869

21.Zisman W.A. in *Contact Angle, Wettability and Adhesion Advances* in Chemistry Series, no 43 (American Chemical Society, Washington, D.C.) 1964

22.Bikerman J.J., *Surface Chemistry,* 2nd edn., Academic Press, New York, 1958

23.Marmur A. "Contact Angle Hysteresis on Heterogeneous Surfaces," *J. Colloid and Interface Science,* 168, pp.40-46, 1994

24.Lin F.Y.H., D. Li, A.W. Neumann "Effect of Surface Roughness on the Dependence of Contact Angles on Drop Size," *J. Colloid and Interface Science,* 159, pp.86-95, 1993

25.Drelich J., J.D. Miller "Modification of Cassie Equation," *Langmuir,* 9, pp.619, 1993

26.Drelich J., J.D. Miller "The Effect of Solid Surface Heterogeneity and Roughness on the Contact Angle/Drop Size Relationship," *J. Colloid and Interface Science,* 164, pp.252-259, 1994

27.Wenzel R.N., "Resistance of Solid Surfaces to Wetting by Water," *Ind. Eng. Chem.*, 28, pp.988-994, 1936

28.Dettre R.H., R.E. Johnson, "Contact Angle Hysteresis," *J. Phys. Chem.*, 668, pp.1744, 1964

29.Eick J.D., R.J. Good, A.W. Neumann, "Effect of Energy Barriers on Contact Angle Hysteresis," *J. Colloid Interface Sci.*, 53, pp.235, 1975

30.Huh C., S.G. Mason, "Effect of Surface Roughness on Wetting," *J. Colloid Interface Sci.*, 60, pp.11, 1977

31.Duncan D., D. Li, A.W. Neumann "Correlation of Line Tension and Solid-Liquid Interfacial Tension from the Measurement of Drop Size

Dependence of Contact Angles," *J. Colloid and Interface Science,* 169, pp.256-261, 1995

32.Cassie A.B.D., "Contact Angles," *Discuss. Faraday Soc.*, 3, pp.11-16, 1948

33.Drelich J., J.D. Miller "The Line/Pseudo-Line Tension in Three Phase Systems," *Particulate Science and Technology,* 10, pp.1-20, 1992

34.Boruvka L., A.W. Neumann, "Generalization of the Classical Theory of Capillarity," *J. Colloid Interface Sci.*, 65, pp.315, 1978

35.Harkins W.D., "Linear or Edge Energy and Tensions as Related to the Energy of Surface Formation," *J. Chem. Phys.*, 5, pp.135-140, 1937

36.Rowlinson J.S., B.Widom, *Molecular Theory of Capillarity* pp. 233-247, Oxford Science Publications, New York, 1984

37.Scheludko A., "Role of Line Tension in Heterogeneous Phase Formation," *Colloids Surf.*, 1, pp.191-196, 1980

38.Schultze H.J., *Physicochemical Elementary Processes in Flotation,* 253, pp.163-165, Elsevier, Oxford, 1984

39.Leja J., G.W. Poling, "Interpretation of Contact Angle," *Proc. Intern. Mineral Congress,* pp.325-341, London, 1960

40.Good R.J., M.N. Koo, "The Effect of Drop Size on Contact Angle," *J. Colloid Interface Sci.*, 71, pp.283, 1979

60.Morrison I.D., "Advancing, Receding and Equilibrium Contact Angles," *Langmuir,* 5, pp.540, 1989

61.Fowkes F.M., F.L. Riddle, A.L. Weber, "Model for Contact Angle Hysteresis," *Colloids Surfaces,* 43, pp.367-387, 1990

62.Van Oss C.J., R.J. Good, "Surface Thermodynamics of Acid-Base Interactions," *J. Dispersion Sci. Technol.*, 12, pp.273, 1991

63.Murr L.E., "Determination of Surface Energy of Solids by Two-Liquid-Phase Method," *Mater. Res. Sci.*, 14, pp.107, 1981

64.Schultz J., M. Nardin *Modern Approaches to Wettability Theory and Applications,* Plenum Press, New York, 1992

65.Matsunaga T., Y. Ikeda " Dispersive Component of Surface Free Energy of Hydrophilic Polymers," *J. Colloid and Interface Science,* 84, pp.8, 1981

66.Peper H., J. Berch, "Intermolecular Forces and Their Effects on Contact Angle," *J. Phys. Chem.*, 68, pp.1586, 1964

67.Tamai Y., K. Makuuchi, M. Suzuki, "Experimental Analysis of Interfacial Forces at the Plane Surface of Solids," *J. Phys. Chem.*, 71, pp.4176, 1967

68.Hamilton W.C. "Donor-Acceptor Approach to Molecular Interactions," *J. Colloid Interface Sci.*, 40, pp.219, 1972

69.Fowkes F.M., *162nd ACS Meeting, Div. Org. Coat. Plast. Chem.*, pp.11, 1971

70.Janczuk B., W. Wojcik, A. Zdziennicka "Determination of the Galena Surface Free Energy Components from Contact Angle Measurements," *Materials Chemistry and Physics,* 31, pp.235-241, 1992

71.Wang J.H., P.M. Claesson, J.L. Parker, H. Yasuda "Dynamic Contact Angles and Contact Angle Hysteresis of Plasma Polymers," *Langmuir,* 10, pp.3887, 1994

72.Yasuda H., A. Sharma "Effect of Orientation and Mobility of Polymer Molecules at Surfaces on Contact Angle and Its Hysteresis," *J. Polymer Science: Polymer Physics ed.*, 19, pp.1285-1291, 1981

73.Toussaint A.F., P. Luner "The Wetting Properties of Grafted Cellulose Films," in K.L. Mittal (ed.), *Contact Angle, Wettability and Adhesion*, pp.383-396, VSP, 1993

74.Shanahan M.E.R. "Simple Theory of Stick-Slip Wetting Hysteresis," *Langmuir,* 11, 1041, 1995

75.Shanahan M.E.R., C. Bourges-Monnier "Influence of Evaporation on Contact Angle," *Langmuir,* 11, 2820, 1995

76.Rowan S.M., M.I. Newton, G. McHale "Evaporation of Microdroplets and the Wetting of Solid Surfaces," *J. Physical Chemistry,* 99, 13268, 1995

77.Picknett R.G., R. Bexon "Evaporation of Sessile and Pendant Drops in Still Air," *J. Colloid and Interface Science,* 61, 336, 1977

59.Neumann A.W., "Equation of State Approach for Determination of Interfacial Surface Tensions," *Z. Phys. Chem,* 41, pp.339-352, 1964

60.Morrison I.D., "Advancing, Receding and Equilibrium Contact Angles," *Langmuir,* 5, pp.540, 1989

61.Fowkes F.M., F.L. Riddle, A.L. Weber, "Model for Contact Angle Hysteresis," *Colloids Surfaces,* 43, pp.367-387, 1990

62.Van Oss C.J., R.J. Good, "Surface Thermodynamics of Acid-Base Interactions," *J. Dispersion Sci. Technol.*, 12, pp.273, 1991

63.Murr L.E., "Determination of Surface Energy of Solids by Two-Liquid-Phase Method," *Mater. Res. Sci.*, 14, pp.107, 1981

64.Schultz J., M. Nardin *Modern Approaches to Wettability Theory and Applications,* Plenum Press, New York, 1992

65.Matsunaga T., Y. Ikeda " Dispersive Component of Surface Free Energy of Hydrophilic Polymers," *J. Colloid and Interface Science,* 84, pp.8, 1981

66.Peper H., J. Berch, "Intermolecular Forces and Their Effects on Contact Angle," *J. Phys. Chem.*, 68, pp.1586, 1964

67.Tamai Y., K. Makuuchi, M. Suzuki, "Experimental Analysis of Interfacial Forces at the Plane Surface of Solids," *J. Phys. Chem.*, 71, pp.4176, 1967

68.Hamilton W.C. "Donor-Acceptor Approach to Molecular Interactions," *J. Colloid Interface Sci.*, 40, pp.219, 1972

69.Fowkes F.M., *162nd ACS Meeting, Div. Org. Coat. Plast. Chem.*, pp.11, 1971

70.Janczuk B., W. Wojcik, A. Żdziennicka "Determination of the Galena Surface Free Energy Components from Contact Angle Measurements," *Materials Chemistry and Physics,* 31, pp.235-241, 1992

71.Wang J.H., P.M. Claesson, J.L. Parker, H. Yasuda "Dynamic Contact Angles and Contact Angle Hysteresis of Plasma Polymers," *Langmuir,* 10, pp.3887, 1994

72.Yasuda H., A. Sharma "Effect of Orientation and Mobility of Polymer Molecules at Surfaces on Contact Angle and Its Hysteresis," *J. Polymer Science: Polymer Physics ed.*, 19, pp.1285-1291, 1981

73.Toussaint A.F., P. Luner "The Wetting Properties of Grafted Cellulose Films," in K.L. Mittal (ed.), *Contact Angle, Wettability and Adhesion*, pp.383-396, VSP, 1993

74.Shanahan M.E.R. "Simple Theory of Stick-Slip Wetting Hysteresis," *Langmuir,* 11, 1041, 1995

75.Shanahan M.E.R., C. Bourges-Monnier "Influence of Evaporation on Contact Angle," *Langmuir,* 11, 2820, 1995

76.Rowan S.M., M.I. Newton, G. McHale "Evaporation of Microdroplets and the Wetting of Solid Surfaces," *J. Physical Chemistry,* 99, 13268, 1995

77.Picknett R.G., R. Bexon "Evaporation of Sessile and Pendant Drops in Still Air," *J. Colloid and Interface Science,* 61, 336, 1977

78.Yekta-Fard M., A.B. Ponter " Influences of Vapor Environment and Temperature on Contact Angle-Drop Size Relationship," *J. Colloid and Interface Science,* 126, pp.134, 1988

79.Birdi K.S., D.T. Vu, A. Winter "Study on the Evaporation Rates of Small Water Drops Placed on a Solid Surface," *J. Physical Chemistry,* 93, 3702, 1989

80.Peiss N., "Evaporation of Small Water Drops Maintained at Constant Volume," *J. Appl. Phys.*, 65, pp.12, 1989

81.Shanahan M.E.R., C. Bourges-Monnier "Effects of evaporation on Contact Angles on Polymer Surfaces," *International Journal of Adhesion and Adhesives,* 14, 201, 1994

82.Dwight D.W., J.E. McGrath, J.S. Riffle, "Bulk and Surface Characterization of Siloxane Containing Copolymers," *Polymer Prepr. Am. Chem. Soc. Div. Poly. Chem.*, 20, pp.702, 1979

83.Chen X., J.A. Gardella, J. Kumlar, "Synthesis and Characterization of Surface Functionalized Polybutadiene," *Macromolecules,* 25, pp.6631, 1982

84.Tezuka Y., A. Fukushima, S. Matsu, K. Imai, "Time Dependent Contact Angle Analysis of Poly(dimethylsiloxane-urethane-urea) Copolymers," *J. Colloid Interface Sci.*, 114, pp.16, 1986

85.Owen M.J. "Siloxane Surface Activity," in J.M. Zeigler and F.W. Gordon Fearon (Eds.), *Silicon Based Polymer Science*, pp. 705-709, Washington, American Chemical Society, 1990